Compensation technique for nonlinear distortion in RF circuits for multi-standard wireless systems

Kasturi Chakrabarty

Faculty of Science and Technology

COMPENSATION TECHNIQUE FOR NONLINEAR DISTORTION IN RF CIRCUITS FOR MULTI-STANDARD WIRELESS SYSTEMS

Kasturi Chakrabarty

A thesis submitted in partial fulfilment of the
requirements of the University of Westminster
for the degree of Doctor of Philosophy

May 2014

ABSTRACT

Recent technological advances in the RF and wireless industry has led to the design requirement of more sophisticated devices which can meet stringent specifications of bandwidth, data rate and throughput. These devices are required to be extremely sensitive and hence any external interference from other systems can severely affect the device and the output.

This thesis introduces the existing problem in nonlinear components in a multi-standard wireless system due to interfering signals and suggests potential solution to the problem. Advances in RF and wireless systems with emerging new communication standards have made reconfigurablility and tunability a very viable option. RF transceivers are optimised for multi-standard operation, where one band of frequency can act as an interfering signal to the other band. Due to the presence of nonlinear circuits in the transceiver chains such as power amplifiers, reconfigurable and tunable filters and modulators, these interfering signals produce nonlinear distortion products which can deform the output signal considerably. Hence it becomes necessary to block these interfering signals using special components.

The main objective of this thesis is to analyse and experimentally verify the nonlinear distortions in various RF circuits such as reconfigurable and tunable filters and devise ways to minimize the overall nonlinear distortion in the presence of other interfering signals. Reconfigurbality and tunablity in filters can be achieved using components such as varactor diodes, PIN diodes and optical switches. Nonlinear distortions in such components are measured using different signals and results noted.

The compensation method developed to minimize nonlinear distortions in RF circuits caused due to interfering signals is explored thoroughly in this thesis. Compensation method used involves the design of novel microstrip bandstop filters which can block the interfering signals and hence give a clean output spectrum at the final stage. Recent years have seen the emergence of electronic band gap technology which has “band gap” properties meaning that a bandstop response is seen within particular range of frequency. This concept was utilised in the design of several novel bandstop filters using defected

microstrip structure. Novel tunable bandstop filters has been introduced in order to block the unwanted signal. Fixed single-band and dual-band filters using DMS were fabricated with excellent achieved results. These filters were further extended to tunable structures. A dual-band tunable filter with miniaturized size was developed and designed.

The designed filters were further used in the compensation technique where different scenarios showing the effect of interfering signals in wireless transceiver were described. Mathematical analysis proved the validation of the use of a bandstop filter as an inter-stage component. Distortion improvements of around 10dB have been experimentally verified using a power amplifier as device under test. Further experimental verification was carried out with a transmitter which included reconfigurable RF filters and power amplifier where an improvement of 15dB was achieved.

ACKNOWLEDGEMENTS

Firstly, I would like to express my heartfelt thanks to the director of studies, Dr Djuradj Budimir for his continuous support and help throughout my entire PhD work. He has not only given me valuable and sound advice but always steered me in the right direction when things became difficult.

Secondly, I would like to express my heartiest thanks to Dr Andrzej Tarczynski who has been a great source of inspiration throughout my academic life in the University of Westminster and has helped me in every way possible.

I would also like to express my sincere thanks to my examiners Dr Zhirun Hu, Dr Vassilis Kodogiannis and my chair Dr Taj Khesavarz for taking the time to go through the entire thesis and giving me valuable comments and feedback.

My special thanks and gratitude goes to University of Westminster for the financial support, which helped me sponsor my studies and living costs in the United Kingdom. I am extremely grateful for their help as without that I would not have been able to pursue and finish my studies.

I would like to sincerely thank my Gurudev, my late father, my mother and my brother who have been responsible for helping and motivating me and guiding me on the right path. Lastly I would like to thank the rest of my family and friends who have been a constant source of inspiration, support system and guidance and without whom this work would not have been possible.

KASTURI CHAKRABARTY

23, SEPTEMBER, 2013

AUTHOR’S DECLARATION

I declare that all materials contained in this thesis are my own work.

Table of Contents

Chapter 1 Introduction

Chapter 2 Background

Chapter 3 Nonlinear Distortion in Passive RF Reconfigurable Circuits

Chapter 4 Compact Microstrip Bandstop Filters

Chapter 5 Compensation of Nonlinear Distortion using Novel Bandstop Filters

Chapter 6 Conclusion

List of Figures and Tables

Chapter 1

Chapter 2

Chapter 3

Chapter 4

Chapter 5

Chapter 1

Chapter 3

Chapter 4

List of Acronyms

1G First-generation

2G Second-generation

3G Third-generation

4G Fourth-generation

ACPR Adjacent channel power ratio

AMPS Advanced mobile phone system

BPF Bandpass filter

BRF Band reject filter

BSF Bandstop filter

CDMA Code division multiple access

CW Continuous wave

dB Decibel

DGS Defected ground structure

DMS Defected microstrip structures

DPD Digital pre-distortion

EBG Electromagnetic band gap

EER Envelope elimination and restoration

GPS Global positioning system

GHz Gigahertz

IMD Intermodulation distortion

IMD3 Third order intermodulation product

LINC Linear amplification using nonlinear components

LO Local oscillator

LTE Long term evolution

MEMS Micro-electro-mechanical systems

MIC Microwave integrated circuit

MIMO Multiple input multiple output

mm Millimetre

MMIC Monolithic microstrip integrated circuit

OFDM Orthogonal frequency division multiplexing

PA Power amplifier

PBG Photonic band gap

PSS Photoconductive silicon switches

PSTN Public switched telephone network

QAM Quadrature amplitude modulation

QPSK Quadrature phase shift keying

RF Radio frequency

Rx Receiver

TDMA Time division multiple access

Tx Transmitter

UMTS Universal mobile telecommunication system

UWB Ultra wide band

WLAN Wireless local area network

WPAN Wireless personal area network

WMAN Wireless metropolitan area network

Chapter 1 Introduction

The wireless industry has seen a massive technological revolution with the introduction of better standards providing excellent data rates, multi-standard systems and throughput. This has led to the increasing demand for better and more efficient subsystems which can be integrated easily and are cost effective. New devices requiring the use of various standards in the same system has led to an increased concern about interferences and subsequent nonlinear distortion products in the output spectrum. Before further discussions about the circuits which contribute to this nonlinearity, the wireless system is briefly introduced. Wireless systems can be broadly classified as the following [1.1]-[1.3]:

1. Cellular and fixed wireless
2. Wireless local area networks (WLANs)
3. Wireless personal area networks (WPANs)
4. Wireless metropolitan area networks (WMANs)

The history of cellular networks goes back to the introduction of the first-generation (1G) system, followed by the more potent digital second-generation (2G) and then the third-generation (3G) Universal Mobile Telecommunication System (UMTS) which is based on hybrid time and code division multiple access (TDMA/CDMA) technology. The more recent development is the 3GPP long term evolution (LTE) system or the fourth-generation (4G) system which is based on Multiple Input Multiple Output (MIMO) and Orthogonal Frequency Division Multiplexing (OFDM). LTE provides a common platform for wireless carriers and creates a commonality by covering the seventeen LTE FDD bands and eight LTE TDD bands [1.4].

Fixed wireless networks provide connection from one fixed point such as Public Switched Telephone Network (PSTN) to homes or business [1.5]-[1.7]. WLAN system comprises the IEEE 802.11 and HiperLAN standards. The standards vary according to the chosen operating frequency, data rate and range covered. WPAN systems include devices such as mobile phones, laptops, bluetooth etc while WMAN includes WiMAX [1.2]-[1.3]. All these systems such as HSPA, 3GPP LTE, and mobile WiMAX require radio

transceivers which can support high data rates and throughput. The development of more sophisticated systems has led to a massive demand in having glitch free, cost effective and miniaturized circuits. Hence, a primary requirement for such advanced system is to have distortion free outputs.

Transceivers in wireless systems are a key component with which signals are transmitted and received. In literature there are several structures of transceivers used according to the system and specifications, but speaking broadly, a simple transceiver consists of a baseband digital signal processing (DSP) block, mixers, amplifiers and filters. The role of the filter is to selectively pass or reject certain signals. The amplifier is used to bring the signal to the appropriate power level for transmission or receiving. The baseband signals are encoded or decoded onto a high frequency carrier. The mixers help in converting the frequency of the signals to an appropriate level for transmission and receiving. A simple block diagram of a duplex superheterodyne single conversion stage transceiver is shown below in Figure 1-1 [1.8]-[1.10].

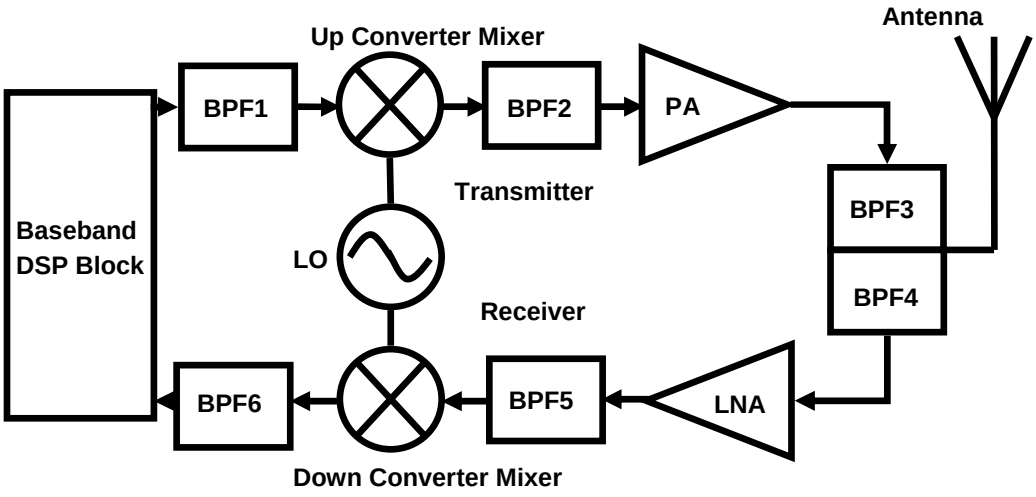

Figure 1-1: Block diagram of the super heterodyne transceiver.

From Figure 1-1, it can be seen that the transmitter (Tx) consists of bandpass filters (BPF1-3), power amplifier (PA) and the up-converter mixer. The signal after being processed in the DSP block is filtered in order to get rid of unwanted signals such as noise etc and is then up-converted to a particular RF frequency with the help of the local oscillator (LO). This signal is further filtered in order to remove the by-products of up-conversion and passed through a

power amplifier, which amplifies the power level of the signal to the required level. The receiver (Rx) receives the high frequency signal and is then passed through a low noise amplifier (LNA) which amplifies the weak received signal to the appropriate level and is further filtered (BPF5-6) and down-converted to the baseband signal. The filtering stages helps in removing unwanted signals and hence helps in conservation of power and gives a clean output without glitches. The local oscillator provides the offset frequency which when mixed with the incoming signal in the mixer produces RF signal for transmission. A similar operation is performed in the receiver part where the incoming RF frequency is down-converted to baseband signal [1.11].

Most components in the RF front-end are nonlinear in nature. The RF front-end mostly comprises of units such as PA, mixer, LNA and reconfigurable/tunable filters which can cause considerable distortions when signals are passed through them. Modulation and cross-modulation distortions are very common in such transceivers. The filters used can filter some of the unwanted signals, but sometimes the intermodulation products are formed in such ways that they appear very close to the main signal. Hence it becomes very difficult to filter out such unwanted signals. The primary requirement for an advanced system is to have distortion free outputs. In a transmitter chain, PA is a nonlinear circuit and hence when the PA works near the saturation region to get maximum power efficiency, nonlinear distortion becomes a major problem. In recent years, there has been a rapid improvement in tunable RF filters. Due to the presence of nonlinear tuning elements in these filters such as PIN diode, varactor diode and optical switch, nonlinear distortion contribution in the overall transceiver chain has increased. Therefore it has become a vital requirement to suppress and compensate nonlinear distortions in wireless transmitters [1.12]-[1.13].

With recent advancements of different standards as mentioned above, it is very common to use multi-standard systems. It is predicted that such systems will play a major role in the 900-5200MHz frequency range. A simple example can be a mobile phone, which uses Global Positioning System (GPS), 3G or 4G and Wi-Fi all together at the same time. Some cellular phone standards operate at 900MHz and 1.8GHz bands; GPS operates at 1.5GHz band while wireless LANs operates at 2.4/5GHz band [1.14]-[1.15]. Combining all of them into a

single chip is a difficult task. Hence, careful design methods need to be devised in order to design multi-standard systems. A typical block diagram of a multi-standard system is shown below in Figure 1-2.

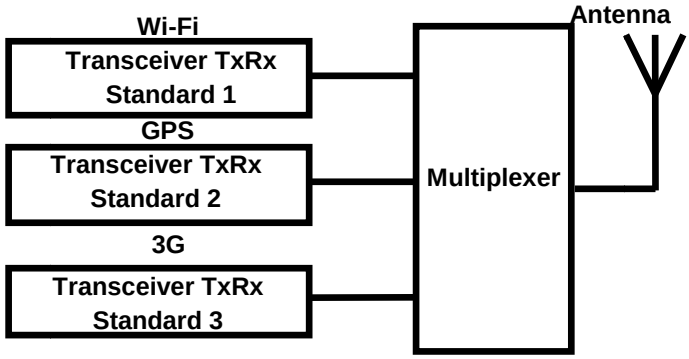

Figure 1-2: Block diagram of a multi-standard system.

Figure 1-2 shows a simple block diagram of a multi-standard system. Such systems are cost effective, compact but also complex. A major downside of such systems can be the interferences caused due to other standards. Signal leakage can be a common problem in such cases. Due to the presence of nonlinear elements in the transceiver chains of each standard any other interfering high power signal at the input can produce additional intermodulation distortion (IMD) thereby making it more difficult to obtain the desired output. To illustrate this, a block diagram of multi band transmitter is shown in Figure 1-3.

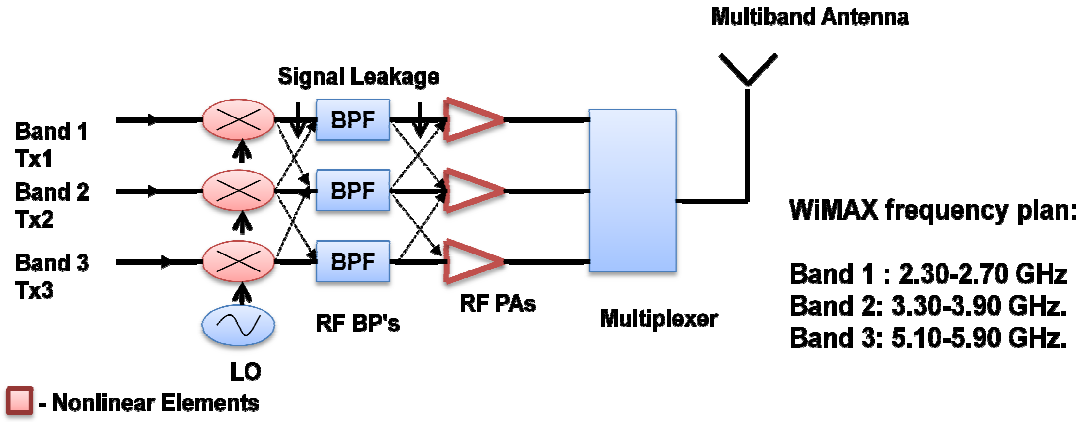

Figure 1-3: Block diagram of a multi-band transmitter system.

Figure 1-3 illustrates the problem in the case of WiMAX signals, where Band 1 which operates at 2.5GHz, acts as an interfering signal for the transmitters in Band 2 or Band 3. Due to the nonlinear elements in Tx2/Tx3 such as a PA, the interfering signal causes additional nonlinear distortions making the final output contain additional distortion components. Therefore potential solutions for such problems need to be devised. Before a solution can be reached, it is very important to quantify and evaluate such nonlinear distortions. This thesis partly deals with the evaluation of nonlinear distortions in RF circuits such as tunable/reconfigurable filters and the effect of interfering signals to the overall measured nonlinear distortion and suggests potential compensation methods that can be used in order to suppress such distortions. Several approaches in minimising effects of nonlinear distortions have been studied and can be extensively found in literature. Some of the methods of distortion suppression can be noted as follows [1.16 – 1.19]:

1) Feed forward
2) Feedback
3) Analogue pre-distortion
4) Digital pre-distortion (DPD)
5) Injection method

This thesis however focuses on using RF filters as a method for compensation of overall nonlinear distortion due to interfering signals [1.20]-[1.21]. The other compensation methods have been extensively explored in literature and each has its own drawbacks. Filters on the other band can be simple, easily integrated and cost effective. The important question to ask here is to what kind of filter would be a suitable option for such systems where interferences are a major issue. In such situations, it is better to use a band reject filter (BRF) due to the fact that such filters have low transmission loss in the passband. This makes it a desirable property for systems where the filter is cascaded with the rest of the structure [1.20]. The typical filter for such application would have high attenuation properties at the interfering frequency and low transmission loss at other frequencies.

RF and microwave filters can be designed using several technologies such as coaxial, waveguide, and microwave integrated circuit (MIC) to name a few. The following table summarises some of the properties of the few main

technologies such as coaxial, waveguide, MIC and monolithic microstrip integrated circuit (MMIC) [1.22-1.24].

Properties	Coaxial	Waveguide	MIC	MMIC
Insertion Loss	Low	Low	Comparatively High	Comparatively High
Size	Compact	Large	Very Compact	Very Compact
Power Handling	Relatively High	High	Low- Medium	Low
Fabrication Ease	Complex	Medium	Easy	Can be complex

Table 1-1: Comparison of various technologies.

The filters in this thesis are designed using microstrip technology which is a type of MIC. Conventional microstrip bandstop filters are designed using shunt open circuited stubs coupled to a through line [1.25]-[1.26].Recent advances of microstrip bandstop filter design includes the use of parallel-coupled line to develop a wideband filter [1.27], stepped impedance resonator bandstop filters [1.28], bandstop filter with cross coupling [1.29], ultra-wideband bandstop filter using defected ground structure (DGS) [1.30] and many such advanced designs. This research concentrates on developing novel bandstop filters which are miniaturized in size and has low transmission loss in the passband and high attenuation in the stopband. Such filters can be used in nonlinear distortion compensation applications where interfering signals are a major issue.

Fixed filters cannot always satisfy all the requirements of a multi-band system. In such systems where many standards or many bands are present it is imperative to use a filter which is flexible. Hence dual-band filters, tunable/reconfigurable filters are in great demand. In systems where the interfering signals appear at different frequencies can make good use of a tunable bandstop filter. The filter is electronically tuned and the centre frequency changed. The downside of such filters is the use of varactor diodes as tuning elements due to its inherent nonlinear property. These can lead to further distortions in the output spectra. Hence a complete evaluation of filters

designed is important to check for such imperfections. This thesis explores the design of novel tunable filters using defected microstrip structures (DMS). Such structures can help in miniaturization due to the slow wave effect. The application of such filters as discussed above is further explored in this thesis.

1.1 Overview of Past Research

In the 1950's microstrip was recognised as a planar transmission line while being further developed in the following years [1.31]. Thereafter, several planar MICs were built using microstrip transmission lines. Several components such as antennas [1.32], filters [1.33], power dividers [1.34], and amplifiers [1.35] have been developed using microstrip technology. Microstrip filters are an important part of the whole RF subsystem. A brief history into the microstrip filter design has been provided in [1.33]. Both bandpass filters and bandstop filters have been extensively designed in microstrip technology using advanced design techniques such as in [1.36]-[1.40]. In [1.36], an improved hairpin filter structure was designed using microstrip while in [1.37] a multi-stage coupled ring bandpass filter was designed. In [1.38], a very compact dual-mode resonator has been introduced which has effective dimensions of less than $\lambda_g/4$. In [1.39] and [1.40] , a dual mode microstrip bandstop filter using inverted open loop resonators were designed and spilt ring resonators were used in designing a miniaturized bandstop filter respectively. Later with the introduction of tunable/reconfigurable filters which required additional components for tuning such as varactor diodes [1.41], PIN diodes [1.42] and optical switch [1.43] it was imperative to study the nonlinear effects of these tuning/switching elements.

Varactor diodes having suitable properties for tuning RF circuits are extensively used for such purposes. However due to the nonlinear characteristic of varactor diodes, distortion measurement requires to be carried out. In literature, distortion measurements for varactor diodes are found in several places such as [1.44]-[1.47]. In these reviews, the varactor diodes are tested for distortion measurements using the Volterra series. Experimental verification using two tone signals are used in most cases. There is a lack of experimental verification of nonlinear distortion in varactor diodes using digitally modulated

signals. Recently low distortion varactor diodes have been developed using anti-parallel and anti-series varactor configuration [1.48].

In a similar fashion distortion evaluation has also been carried out for PIN diodes and optical switches. This switching element finds application in many RF reconfigurable filters and devices. In [1.49]-[1.52], PIN diodes have been tested for nonlinear distortion and a third order intercept point at 40dBm is measured approximately in [1.49]. The nonlinearity measurements in optical switch have very little data in literature as it is a fairly new concept. Distortion performance of an optically controlled microwave switch was proposed by Loughborough University in [1.53].

After the evaluation of nonlinear distortion in RF filters, it is important to give a brief history of problems faced due to interfering signals. The problems generally occur when one signal operating in a particular band leaks and interfere in another band very close to the original band. Due to the presence of nonlinear components, the leaked signal combines with the main signals and forms intermodulation distortion products which can distort the output signal considerably. In [1.54], the effect of interfering signal is shown with numerical analysis while [1.55] shows the effect of multi-tone interfering signal within a communication system which leads to additional nonlinear distortions and its effect can be seen in the output spectra.

The above problem of nonlinear distortion can be solved by various methods. In [1.21] several methods to suppress nonlinearity due to interfering signals are mentioned. Filters, especially bandstop filters seem to be a favourable option as in [1.20] and [1.56]. The design of bandstop filters using conventional approaches can be found in literature such as [1.57]-[1.58]. However DMS, a fairly new concept, having been initially proposed in [1.59]-[1.60], exploits the “band-gap” theory. This technique draws from the previous DGS structures but is proved to be much better in performance producing extremely miniaturized circuits with excellent characteristics. Tunable bandstop filters using DGS have also been proposed in [1.61]-[1.62] with excellent results. However there is a lack of research in tunable dual-band bandstop filters using DMS.

The literature review discusses briefly the research that has already been done and gaps where further research needs to be carried out. There has been

a lack of nonlinear distortion evaluation in RF circuits using advanced digitally modulated signals which has been addressed in this thesis. Compensation technique using novel BSFs were also explored and experimental verification provided. DMS filters were developed and fabricated with excellent results.

1.2 Objectives of Research

The research aims at finding a novel solution to suppress the effects of nonlinearities due to additional interfering signals in RF circuits comprising nonlinear elements such as PIN diode, varactor diode and optical switch. Examples of such circuits include reconfigurable filters with optical switch and PIN switch or a tunable filter with varactor diodes. It aims to create the solution to the existing problem of nonlinear distortions in RF circuits demonstrating the feasibility of the method which utilises a novel microstrip highly selective bandstop filter in improving these distortions due to unwanted signals in various RF circuits for multi standard wireless systems. The method aims at providing a good compensation technique at lower cost and relatively less complexity in design procedures. The following research objectives are undertaken:

1. Research in existing tuning/switching techniques applied to RF circuits. Research of nonlinear distortion in nonlinear RF devices and circuits.
2. Study the analysis of nonlinear distortion in PIN diode switches, varactor diodes and optical switches.
3. Experimental evaluation of nonlinear distortions in reconfigurable elements such as PIN diode switches and optical switches
4. Experimentally evaluate nonlinear distortion in reconfigurable filters using optical switch and PIN switch.
5. Study the effects of interfering signals in multi-band systems and provide mathematical explanation to the effect of interfering signals to the overall distortion.
6. Study methods of nonlinear distortion suppression that can be used.
7. Search for novel bandstop filter techniques that can be used in the compensation of nonlinear distortion.

8. Design of novel highly selective and compact bandstop microstrip filters for multi standard and multi band wireless applications.
9. To fabricate a novel tunable bandstop microstrip filter suitable for the proposed technique and SDR next generation wireless multi-standard systems
10. Investigate the nonlinear distortion compensation technique that can be applied to bandpass filters based on PIN diode switches, optical switches and transmitter system.
11. Experimental verification of the approach using a bandstop filter for nonlinear distortion compensation using nonlinear RF circuit such as a power amplifier , transmitter and reconfigurable filter as device under test (DUT).
12. The feasibility of the proposed approach simulated with a 5-MHz digitally modulated signal. Implement the compensation technique for nonlinear distortion improvement of RF devices and circuits such as reconfigurable filters and power amplifiers in transmitters.

1.3 Thesis Organization

This thesis written over a period of three years aims to provide brief description of the motivation of the thesis, work done and contributions made. It has been divided into several parts consisting of six chapters.

Chapter 1 provides a brief introduction to the ever changing wireless systems. It gives an overview of systems already in use and a brief introduction to 4G or LTE system. It explores the RF transceiver and its subcomponents which can contribute to nonlinear distortions. This chapter also introduces the readers to today's modern systems such as multi-band, multi-standard systems and the possibility of distortions due to interferences in these systems. Methods of compensation of such distortions are suggested and the introduction of bandstop filter as a potential method is given. The chapter details the aims and objectives of the thesis along with an overview of past research work carried out.

Chapter 2 deals with the background theory of topics covered in this thesis along with a review of general background theory for microstrip technology. The pros and cons are discussed. Microstrip coupled lines are introduced along with the discontinuities of microstrip lines. A brief summary of nonlinear distortion theory is given which details the causes of distortions, terminologies which help in defining distortions and the major types of distortions present in wireless transceivers. The chapter ends with a brief summary of the filter theory used. The basic bandstop filter theory is explained along with the introduction to DGS and DMS structures and its later use in the thesis.

Chapter 3 explains the nonlinear distortion concepts in further details with detailed mathematical analysis. Components such as PIN diodes, varactor diodes, optical switch etc which are used to switch or tune RF circuits are evaluated for nonlinear distortions. The later section describes the evaluation of nonlinear distortions in reconfigurable RF filters in further details.

Chapter 4 talks about microstrip bandstop filters that can be used to compensate for nonlinear distortions. The chapter begins with a detailed analysis of microstrip bandstop filter. Few filter structures using conventional design techniques are designed and fabricated. Theory of defected microstrip structure is introduced and several fixed single-band and dual-band novel DMS filters are designed and fabricated. The filter structures were further designed to be tunable for flexibility and ease of use.

Chapter 5 uses the designed bandstop filters in the compensation techniques. A brief summary and mathematical analysis of problems in wireless transceivers due to interfering signals are described. Compensation techniques available in literature are briefly summarised. The mathematical proof of theory using the bandstop filter is provided along with experimental verification using power amplifier as device under test. Finally a transmitter T_x containing the reconfigurable RF filter and power amplifier is tested using 5MHz QPSK signal with and without bandstop filter showing 15dB improvement in the case with filter as an inter-stage device.

Chapter 6 finally concludes the thesis with a brief summary of findings and results. Contributions made to knowledge are noted and suggestions for future work are also summarised.

1.4 References

[1.1] D.Tse and P.Viswanath, *Fundamentals of Wireless Communication*, Cambridge University Press, 2005, ISBN 0521845270.

[1.2] W. Webb, *The Future of Wireless Communication*, Artech House, 2001, ISBN1580532489.

[1.3] A. Goldsmith, *Wireless Communications*, Cambridge University Press, 2005, ISBN 0521837162.

[1.4] D. Bondar, and D. Budimir, "Digital baseband predistortion of wideband power amplifiers with improved memory effects," *Proc. IEEE Radio and Wireless Symposium*, Jan. 2009, pp. 284-287.

[1.5] E. Bostick, G. Bostick, *The basic description of MMDS Television Systems*, Electric Press, New York, 1995, ISBN 1888552026.

[1.6] P. M. Shankar, *Introduction to Wireless Systems*, John Wiley & Sons, Inc., 2002, ISBN 0471321672.

[1.7] W. E. Evans, K. G. Balb, "Application Consideration for Low-Power MMDS", *Private cable magazine (USA) and Cable communications (Canada)*, October 1991.

[1.8] F. Ellinger, *Radio Frequency Integrated Circuits and Technologies*, Berlin: Springer, 2007.

[1.9] Q. Gu, *RF System Design of Transceivers for Wireless Communications*. New-York: Springer, 2005.

[1.10] M. N. S. Swamy and K.-L. Du, *Wireless Communication Systems: From RF Subsystems to 4G Enabling Technologies*, New York: Cambridge University Press, 2010.

[1.11] A. Hussain, *Advance RF Engineering for Wireless Systems and Networks*, John Wiley, New Jersey, 2005, ISBN 0471674214.

[1.12] D. Bondar, and D. Budimir, "Digital baseband predistortion of wideband power amplifiers with improved memory effects," in *Proc. IEEE Radio and Wireless Symposium,* Jan. 2009, pp. 284-287.

[1.13] K. M. Gharaibeh, *Nonlinear Distortion in Wireless Systems: Modeling and Simulation with MATLAB,* Wiley, 2011.

[1.14] S. Wu and B. Razavi "A 900-MHz/1.8-GHz CMOS Receiver for Dual-band Applications" IEEE Journal of Solid State Vol-33, No-12, December 1998.

[1.15] M. Zargari et. al “A single-chip Dual-band Tri-Mode CMOS Transceiver for IEEE 802.11a/b/g Wireless LAN IEEE Journal of Solid State Vol-39, No-12, December 2004.

[1.16] S. P. Stapleton, “Adaptive feed forward linearization for RF power amplifiers,” in *Proc. 55th Automatic RF Techniques Group Conference Digest-Spring*, vol. 37, pp. 1-7, June 2000.

[1.17] Y. Y. Woo, J. Kim, J. Yi, S. Hong, I. Kim, J. Moon, and B. Kim, “Adaptive digital feedback predistortion technique for linearizing power amplifiers,” *IEEE Trans. Microw. Theory Tech.,* vol. 55, no. 5, pp. 932-940, May 2007.

[1.18] S. P. Stapleton and F. C. Costescu, “An adaptive predistorter for a power amplifier based on adjacent channel emission,” *IEEE Trans. Microw. Theory Tech*., vol. 41, no. 1, pp. 49–56, Feb. 1992.

[1.19] N. Mizusawa, and S. Kusunoki, “Third- and fifth-order baseband component injection for linearization of the power amplifier in a cellular phone,” *IEEE Trans. Microw. Theory Tech.,* vol. 53, no. 4, pp. 3327-3334, Apr. 2005.

[1.20]H.Uchida,H.Kamino,K.Totani,N.YonedaM.Miyazaki,Y.Konishi,S.Makino,J. Hirokawa and M. Ando, ”Dual-Band-Rejection Filter for Distortion Reduction in RF Transmitters”, Microwave Symposium Digest (MTT),vol.52,no.11,pp.2550-2556, 2004.

[1.21] E.C. Niehenke, “Linearization Techniques for Advanced Transmitter Architectures,” IEEE IMS2003, Workshop, WSB-3, 2003.

[1.22] R. J. Cameron, C. M. Kudsia, and R. R. Mansour, *Microwave filters for communication systems: fundamentals, design, and applications*. Hoboken, New Jersey: John Wiley & Sons, 2007.

[1.23] J. G. Hong and M. J. Lancaster, *Microstrip Filters for RF/Microwave Applications*, New York: John Wiley & Sons, 2001.

[1.24] I. C. Hunter, *Theory and design of microwave filters*. London: Institution of Electrical Engineers, 2001.

[1.25] G. Matthaei, L. Young, and E.M.T Jones, *Microwave impedance-matching networks, and coupling structures*, Artech House, Boston, MA, 1980

[1.26] I. C. Hunter, J.D. Rhodes, "Electronically Tunable Microwave Bandstop Filters," *Microwave Theory and Techniques, IEEE Transactions on*, vol.30, no.9, pp.1361-1367, Sep. 1982.

[1.27] M.K. Mandal, K. Divyabramham, and S. Sanyal, “Sharp-rejection wideband bandstop filters”, *IEEE Microw. Wirel. Compon. Lett.*, vol.18, no.10, pp. 662-664, 2008.

[1.28] V.K. Velidi, A.B. Guntupalli, and S. Sanyal, “Sharp-rejection ultrawide bandstop filters”, *IEEE Microw. Wirel. Compon. Lett.,* vol.19, no.8, pp. 503–505, 2009.

[1.29] H. Shaman, and J.S.Hong, “Wideband bandstop filter with cross coupling”, *IEEE Trans. Microw. Theory Tech*., vol. 55, no.8, pp. 1780–1785m, 2007.

[1.30] F. Chen; N. Zhang; P. Zhang; Q. Chu, "Design of ultra-wideband bandstop filter using defected ground structure," *Electronics Letters*, vol.49, no.16, pp.1010- 1011, Aug. 1 2013.

[1.31] H. Howe “Microwave Integrated Circuits--An Historical Perspective," *Microwave Theory and Techniques, IEEE Transactions on*, vol.32, no.9, pp.991- 996, Sep 1984.

[1.32] C. Peixeiro, "Microstrip patch antennas: An historical perspective of the development," *Microwave & Optoelectronics Conference (IMOC), 2011 SBMO/IEEE MTT-S International*, vol., no., pp.684-688, Oct. 29 2011-Nov. 1 2011.

[1.33] R. Levy, B. Cohn, "A History of Microwave Filter Research, Design, and Development," *Microwave Theory and Techniques, IEEE Transactions on*, vol.32, no.9, pp.1055-1067, Sep 1984.

[1.34] A.M. Moselhy, A.M. Nassar, M.A. El Gazzar, "Analysis and design of microstrip power divider," *Signals, Systems, and Electronics, 1995. ISSSE '95, Proceedings., 1995 URSI International Symposium on*, vol., no., pp.545-548, 25-27 Oct 1995.

[1.35] T.Horng; S. Wu, "Radiation from a microstrip amplifier," *Microwave Theory and Techniques, IEEE Transactions on*, vol.50, no.8, pp.2005-2010, Aug 2002.

[1.36] A. Lotfi-Neyestanak, A. Lalbakhsh, "Improved microstrip hairpin-line bandpass filters for spurious response suppression," *Electronics Letters*, vol.48, no.14, pp.858-859, July 5 2012.

[1.37] A. Griol, J. Marti, L. Sempere, "Microstrip multistage coupled ring bandpass filters using spur-line filters for harmonic suppression," *Electronics Letters*, vol.37, no.9, pp.572-573, 26 Apr 2001.

[1.38] J.S. Hong, H. Shaman and Y.H. Chun, “Dual-mode microstrip open-loop resonators and filters”, *IEEE Transactions on Microwave Theory and Techniques*, vol. 55, no. 8, pp. 1764-1770, Aug. 2007.

[1.39] G.M. Eryilmaz, G.B. Elif, G.C. Adnan and K.D. Ceyhun, "Dual-mode microstrip bandstop filters," *Microwave Conference, 2008. APMC 2008. Asia-Pacific*, vol., no., pp.1-4, 16-20 Dec. 2008.

[1.40] J. Lee, Y. Oh and N. Myung, "A novel compact microstrip bandstop filter based on complementary split-ring resonators," *Microwave Conference, 2006. APMC 2006. Asia-Pacific*, vol., no., pp.1435-1438, 12-15 Dec. 2006.

[1.41] B. Kim, S. Yun, “Varactor-tuned combline bandpass filter using step-impedance microstrip lines”, *IEEE Transactions on Microwave Theory and Techniques*, vol. 52, no. 4, pp.1279-1283, Apr. 2004.

[1.42] M.F. Karim, X. Yong, Z.N.; Chen and L.C. Ong, "Miniaturized reconfigurable filter using PIN diode for UWB applications," *Microwave Symposium Digest, 2008 IEEE MTT-S International* , vol., no., pp.1031-1034, 15-20 June 2008.

[1.43] L. Athukorala, K. Rabbi, C. Panagamuwa, J.C. Vardaxoglou, M. Philippakis and D. Budimir, "Optically reconfigurable microstrip UWB bandpass filters," *Antennas and Propagation Conference (LAPC), 2010 Loughborough* , vol., no., pp.617- 620, 8-9 Nov. 2010.

[1.44] J.H. Mulligan and A. Paludi, "Varactor Tuning Diodes as a Source of Intermodulation in RF Amplifiers," *Electromagnetic Compatibility, IEEE Transactions on*, vol.EMC-25, no.4, pp.412-421, Nov. 1983.

[1.45] M.F.A. Khalid, A.S. Holland, J.R. Scott and K. Ghorbani, "Analysis of third-order intermodulation distortion in BST varactors," *Microwave Conference Proceedings (APMC), 2010 Asia-Pacific*, vol., no., pp.650-653, 7-10 Dec. 2010.

[1.46] L. Dussopt and G.M. Rebeiz, "Intermodulation distortion and power handling in RF MEMS switches, varactors, and tunable filters," *Microwave Theory and Techniques, IEEE Transactions on*, vol.51, no.4, pp.1247-1256, Apr 2003.

[1.47] B.E. Carey-Smith and P.A. Warr, "Distortion Mechanisms in Varactor Diode-Tuned Microwave Filters," *Microwave Theory and Techniques, IEEE Transactions on*, vol.54, no.9, pp.3492-3500, Sept. 2006.

[1.48] K. Buisman, L.C.N. de Vreede, L.E.Larson, M. Spirito, A. Akhnoukh, T.L.M. Scholtes and L.K. Nanver, "Distortion-free varactor diode topologies for RF adaptivity," *Microwave Symposium Digest, 2005 IEEE MTT-S International* , 12-17 June 2005.

[1.49] R.H. Caverley and G. Hiller, "Distortion properties of MESFET and PIN diode microwave switches," *Microwave Symposium Digest, 1992., IEEE MTT-S International* , vol., no., pp.533-536 vol.2, 1-5 June 1992.

[1.50] R.H. Caverly and G. Hiller, "Distortion in microwave and RF switches by reverse biased PIN diodes," *Microwave Symposium Digest, 1989., IEEE MTT-S International* , vol., no., pp.1073,1076 vol.3, 13-15 June 1989.

[1.51] R.H. Caverly, "Distortion modeling of PIN diode switches and attenuators," *Microwave Symposium Digest, 2004 IEEE MTT-S International* , vol.2, no., pp.957-962 Vol.2, 6-11 June 2004.

[1.52] R.H. Caverly and G. Phaneuf, "Nonlinear and transient microwave and RF modeling of the PIN diode," *Circuits and Systems, 1989, IEEE International Symposium on*, vol., no., pp.2209-2214 vol.3, 8-11 May 1989.

[1.53] E.K. Kowalczuk, R.D. Seager, C.J. Panagamuwa, K. Bass and J.C. Vardaxoglou, "Optimising the performance of an optically controlled microwave switch," *Antennas and Propagation Conference (LAPC), 2012 Loughborough* , vol., no., pp.1-5, 12-13 Nov. 2012.

[1.54] R. W.Ottinger, “The Effect of Hard Limiting in the Presence of Large Out-of-Band Interfering Signals," *Aerospace and Electronic Systems, IEEE Transactions on*, vol.AES-3, no.5, pp.830-834, Sept. 1967.

[1.55] L.B. Milstein, S. Davidovici, D.L. Schilling, "The Effect of Multiple-Tone Interfering Signals on a Direct Sequence Spread Spectrum Communication System," *Communications, IEEE Transactions on*, vol.30, no.3, pp.436-446, Mar 1982.

[1.56] T. Ito, M. Kanemaru, S. Furuya, D. Huy , K. Okada and A. Matsuzawa, "A 0.8–1.5GHz multi-standard WCDMA receiver with an inter-stage tunable notch filter," *Microwave Conference (EuMC), 2010 European* , pp.1118-1121, 28-30 Sept. 2010.

[1.57] K.S.Chin, J.H. Yeh, and S.H. Chao, “Compact dual-band bandstop filters using stepped-impedance resonators", *IEEE Microw. Wireless Compon.Lett.,* vol.17, no. 12, pp. 849–851, 2007.

[1.58] V.K.Velidi and S.Sanyal, “Compact planar dual-wideband bandstop filters with cross coupling and open-ended stepped impedance resonators”, *ETRI Journal*, vol.32, no.1, 2010.

[1.59]J. Lim, Skim, Yulee, D. An and S. Nam, "Design of lowpass filters using defected ground structure and compensated microstrip line," *Electronics Letters*, vol.38, no.22, pp.1357-1358, 24 Oct 2002.

[1.60] J.A. Tirado-Mendez, H. Jardon-Aguilar, "Comparison of defected ground structure (DGS) and defected microstrip structure (DGS) behaviour at high frequencies," *Electrical and Electronics Engineering, (ICEEE). 1st International Conference on*, vol., no., pp.7-10, 8-10 Sept. 2004.

[1.61] D.Woo, T.Lee, J.Lee, C.Pyo and W.Choi, "Novel U-slot and V-slot DGSs for bandstop filter with improved Q factor," Microwave Theory and Techniques, IEEE Transactions on, vol.54, no.6, pp.2840-2847, June 2006.

[1.62] S.Huang and Y.Lee, "A Compact E-Shaped Patterned Ground Structure and Its Applications to Tunable Bandstop Resonator," Microwave Theory and Techniques, IEEE Transactions on, vol.57, no.3, pp.657-666, March 2009.

Chapter 2 Background

This chapter gives a concise summary of the background theory of the various topics covered in this thesis. The main consideration of the thesis was to evaluate and compensate for nonlinear distortions in RF circuits for a multi-standard wireless system using DMS bandstop filters. In most systems the occurrence of interfering signals is a common issue. The problem arises when the interfering signals combine with the other main signals and are passed through nonlinear elements giving rise to intermodulation distortion components which affects the final output to a great deal. Nonlinear components in a wireless transceiver could be a power amplifier, a low noise amplifier, a mixer or a reconfigurable/ tunable RF filter. In this thesis RF filters having nonlinear tuning/switching elements such as varactor diode, PIN diode and optical switch are extensively studied for distortions. A novel bandstop filter using defected microstrip structure is developed in order to get rid of the problem of interfering signals and hence reducing the overall distortions.

Hence it is important to delve into the background theory of microstrip technology which was used to design these RF circuits, the theory of nonlinearity and finally a glimpse into the bandstop filter theory. These three major elements form the core of the thesis and therefore briefly described here. The discussion starts with the overview of microstrip lines and is discussed in detail in the next section.

2.1 Microstrip Lines

Transmission lines being the medium of propagation between two places for em waves or other form of energy does so with minimum signal loss and interference and are commonly used in many applications [2.1]. In literature, there is a variety of choice in transmission line which includes microstrip, stripline and finline to name a few. Among these entire collections, microstrip transmission line has proved to be very popular in the design of filters and other applications.

These can provide a good frequency range up to 110GHz, beyond which the quasi-TEM approximation of the microstrip line is not valid which results in the waves travelling at different speeds increasing the dispersion effect considerably at higher frequencies. The losses in the microstrip line also increases with higher frequencies which renders it unsuitable [2.2]. The unloaded quality factor of such lines are around 250 at 30GHz, while the characteristic impedance ranges from 20-125 Ω and the ease of fabrication using printed circuit board (PCB) technology are some of the desirable qualities of this planar transmission line [2.2]-[2.3].

The structure of the microstrip line contains a dielectric substrate which is present between a thin strip of metal conductor at the top and a ground plane at the bottom. Figure 2-1 shows the side view of the microstrip line along with the field distribution. The thin metallic conductor has a width of W and a thickness of t which is negligible. The dielectric layer has a height of h and a dielectric constant of ε_r and relative permeability of μ_r. The air dielectric constant is given as ε_0 and the permeability as μ_0.

Inhomogeneous nature of microstrip line is due to the presence of two dielectric media (substrate and air), the electromagnetic field in the microstrip line, meaning it has its presence in both air and the dielectric as shown from the field distribution in Figure 2-1 (b). The electric field E is concentrated in the dielectric medium itself while the magnetic field H extends in both medium. Due to this inhomogeneous nature a pure transverse electric and magnetic (TEM) wave cannot be supported. This is due to the varying speeds of propagation of the waves in two different mediums namely air and dielectric. When the horizontal components of the field are greater than the longitudinal components, the quasi-TEM approximation is used while solving the characteristics of the line [2.2]-[2.5].

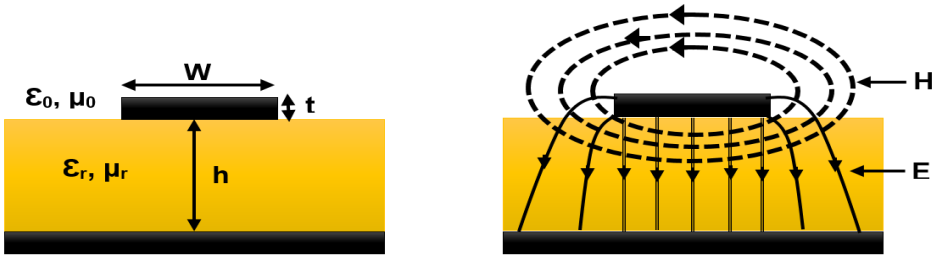

(a) (b)

Figure 2-1: Side view of microstrip transmission line showing (a) geometry (b) electromagnetic field distribution.

The open structure of the microstrip line can be more subjected to losses when compared to other structures. Such losses can include conductor loss, radiation loss, dielectric loss, and surface wave propagation. Loss due to the conductor at higher frequencies is aggravated by the skin effect [2.4]. The formation of eddy currents leads to the disappearance of the signal current from the centre of the conductor being concentrated at the sides. This results in the reduction of the cross-sectional area at high frequencies resulting in loss due to the finite conductance of the metal strip. The dielectric loss is due to the transportation of charge between the conductors through the dielectric which can have severe consequences at higher frequencies. The radiation loss is due to the discontinuities present in the microstrip line [2.5].

In order to calculate some of the line characteristics such as the effective relative dielectric constant ε_{eff}, the characteristic impedance Z_0, phase constant, β, and phase velocity, V_p, the quasi-TEM approximation is used. This helps in simplifying the equations and involves the determination of the capacitance per unit length in two cases, one with the dielectric and the other without the dielectric C_{wd} and $C_{w/o}$ respectively. The following equations are expressed in terms of the capacitance as from (2.1) - (2.4).

$$\varepsilon_{eff} = \frac{C_{wd}}{C_{w/o}} \tag{2.1}$$

$$Z_0 = \frac{1}{c\sqrt{C_{wd} * C_{w/o}}} \tag{2.2}$$

$$v_p = c\sqrt{\frac{C_{w/0}}{C_{wd}}} \tag{2.3}$$

$$\beta = \frac{\omega}{c}\left(\frac{C_{wd}}{C_{w/o}}\right) \tag{2.4}$$

Where, *c* is the speed of light in free space and ω is the angular frequency. Recent computation techniques use Maxwell's equation to be solved using advanced numerical methods enabling more accurate values for the transmission line characteristics. Software packages such as Agilent ADS use a full wave electromagnetic analysis to solve the same characteristics more accurately [2.6].

Another important concept is that of a microstrip coupled line. This has a wide range of application including filter design, couplers etc. Due to the presence of two transmission lines close to each other, coupling occur which results in the interaction of the electromagnetic field as shown in Figure 2-2. There are two modes of propagation supported by the coupled lines which are the even and the odd mode as shown.

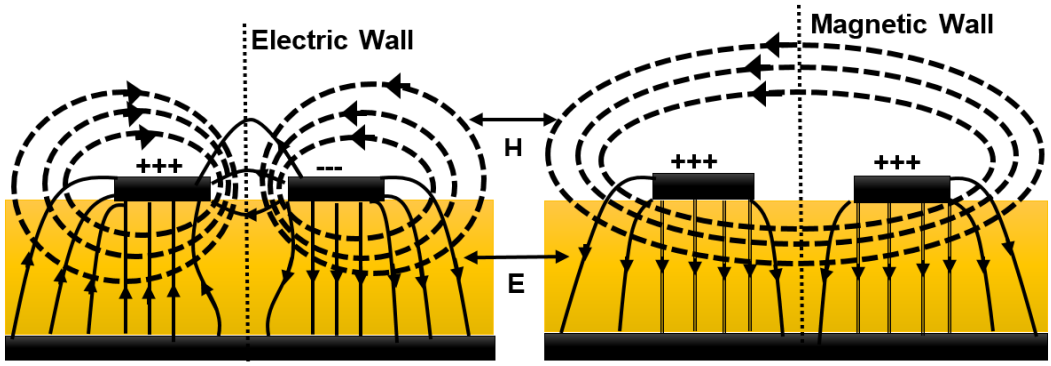

(a) (b)

Figure 2-2: Coupled line EM field distribution for (a) odd and (b) even mode.

The odd mode is created when the two transmission lines have opposite voltage which gives rise to an electric wall. The even mode is caused due to equivalent potential for the coupled transmission lines. This in turn gives rise to a symmetric magnetic wall. The distribution of the EM field is irregular in nature and this property gives rise to different phase velocities, effective dielectric constant and other characteristics of the line .In order to analyze such cases, characteristics due to both even and odd mode needs to be considered. When designing coupled resonators, it becomes imperative to set the coupling strength. Even though the coupling is a contribution of both fields, the structure can be designed in such a way so as to create a destructive coupling or a constructive coupling depending on the need [2.7]-[2.8].

Microstrip discontinuity is an important property which not only helps in designing various types of filters but also other circuits. For example in DMS, a defect or discontinuity is created on the microstrip transmission line itself in order to modify certain properties of the line. Any sudden alteration of the microstrip line such as bends, gaps, junctions etc results in discontinuity. A few important discontinuities are briefly discussed. This can be further modelled accurately in electromagnetic simulation software. Figure 2-3 shows the equivalent lumped element circuits for various discontinuities in microstrip line.

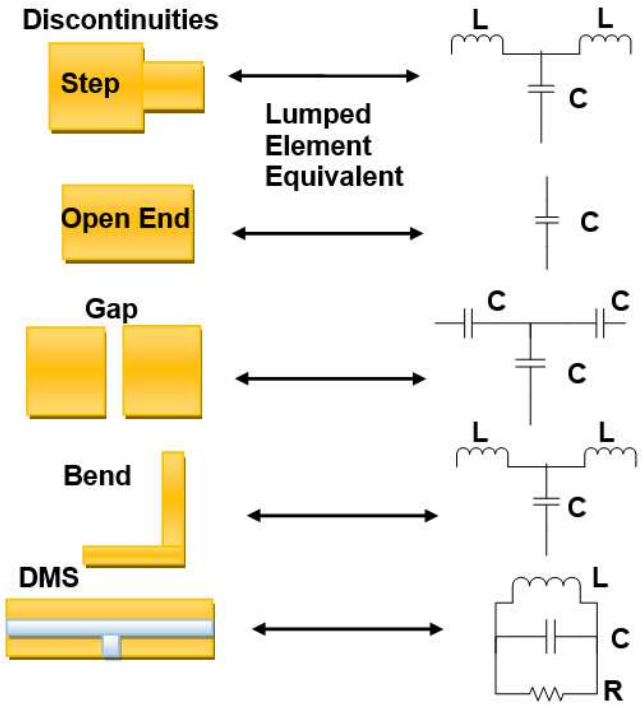

Figure 2-3: Microstrip discontinuities and their equivalent lumped element circuit.

The width of the microstrip line controls the impedance. Hence steps are a result of different characteristic impedance indicated by thin or thicker lines. The wider section behaves like a shunt capacitor and the thinner section acts as a series inductor. The lumped equivalent circuit is represented by the LC ladder circuit. Hence a lowpass filter is easily designed from this type of discontinuities [2.9].

At the end of microstrip line fringing fields results in the elongation of the electric field. Such discontinuity effect can be represented with an increase in

length of transmission line or by an equivalent capacitance .This can be used as microstrip bandpass filter elements.

Gaps are another fundamental discontinuity and are widely used in filter design. Gaps can increase the series capacitance of the structure. An equivalent circuit for gap consists of series and shunt capacitors to model the microstrip line. The capacitive gaps are widely used to couple two microstrip lines [2.3].

Bends appears at the junctions of the line. A T-network which is made of two series inductor and a shunt capacitor can be used to represent such discontinuity. These are another popular discontinuities appearing in various RF circuits. Another important phenomenon described in respect to discontinuity is the defected microstrip structure. A T-shaped structure is etched on the microstrip line creating a discontinuity and multiple current paths. Such etching creates a band gap which can be very useful in designing bandstop filters as discussed in chapter 4. The equivalent circuit is a simple bandstop resonator consisting of an inductor, capacitor and resistor in parallel.

2.2 Nonlinear Distortion Theory

This section gives a brief introduction to nonlinear distortion theory. The wireless transceiver consists of many nonlinear components; hence it becomes important to learn about the nonlinear distortion contribution of each element. The transmitter alone is designed using various components such as a mixer, power amplifier, reconfigurable filter etc. The mixer is used for up/down-conversion of frequency in a wireless transceiver and is inherently nonlinear. Another important contribution of nonlinearity comes from the local oscillator which fails to be exactly ninety degree out of phase leading to phase imbalance. This introduces distortions in the final output. Power amplifier, on the other hand operates near the saturation zone which is the nonlinear zone for better efficiency reason. This leads to the introduction of harmonics and intermodulation distortion products. In order to analyse the nonlinear distortion, Taylor’s series is used to model the nonlinear transfer function as follows:

$$V_o(t) = \left(\frac{\eth V_o}{\eth V_i}\right) * V_{i*}(t) + \left(\frac{1}{2!}\right) * \left(\frac{\eth^2 V_0}{\eth V_i^2}\right) * V_i^2(t) + \left(\frac{1}{3!}\right) * \left(\frac{\eth^3 V_0}{\eth V_i^3}\right) * V_i^3(t) + \cdots + \left(\frac{1}{n!}\right) * \left(\frac{\eth^n V_0}{\eth V_i^n}\right) * V_i^n(t) \quad (2.5)$$

Where, V_0 = Output Voltage and V_{in} =Input Voltage. When two closely spaced signals are taken as V_{in}, then the 2nd term of the series results into a D.C. component, a 2nd harmonic also some frequency terms at $f_1 \pm f_2$. A similar operation happens due to the 3rd term. This results in the output to not only have the main signal but also several other unnecessary side signals at various frequencies. This is the nonlinearity that is seen very frequently in wireless transmitters.

The disruption to the output spectrum caused due to the presence of the 3rd order intermodulation product has the maximum effect. In a digital signal this can cause spread spectrum, where the adjacent channel signal leaks into the main channel signal. Signal accuracy is therefore compromised along with bandwidth. Two such important measures of nonlinearity are the 1dB compression point and 3rd order intercept point.

The concept of the 1dB compression point can be defined by the drop in gain by 1dB due to a particular output power. The point where this occurs is termed as the 1dB compression point. This can be an important measure of nonlinearity of a system. It is a good indicator of the nonlinearity and gain compression of a power amplifier. The following Figure 2-4 illustrates the compression point.

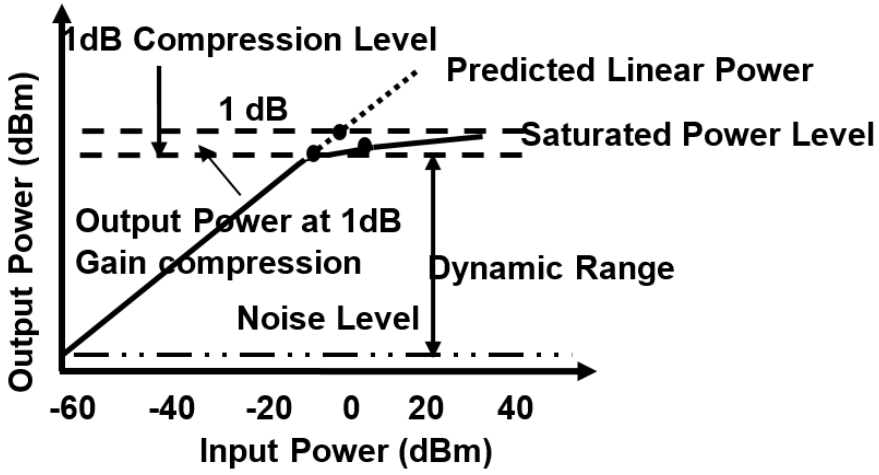

Figure 2-4: Illustration of the 1dB compression point.

. Similarly the 3rd order intercept point is defined here. The 3rd order intercept point lies, where gain rises by 3dB for the output power. A simple way of explaining this would be to consider two tone input signal with equal power level. It is evident that with every change in input power, the 3rd order intermodulation product power level will also change. It is found that the 3rd order IMD product increases by nearly 3dB for every 1dB rise in signal power. Such signals appear in the pass band causing major interference for large input values [2.10]. The meeting point of the 3rd order IMD product and the extrapolated output signal is known as the 3rd order intercept point as shown in Figure 2-5 below.

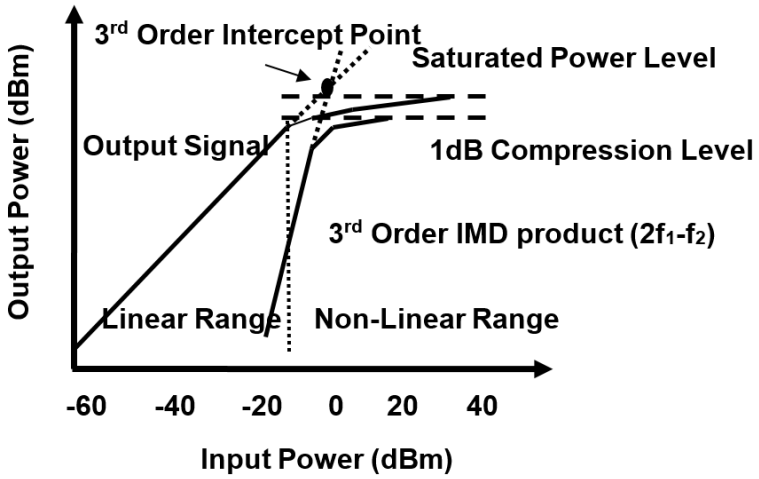

Figure 2-5: Illustration of the 3rd order intercept point.

From the above figure, it is clear that the 3rd order intercept point is an imaginary concept and does not occur in real life. This is due to the fact that the output signal gets saturated before that. Equation (2.6) below, gives the 3rd order intermodulation signal power.

$$P = 3 * S - 2 * I \tag{2.6}$$

Where, *P* is the 3rd order intermodulation power (dBm), *S*= input signal power (dBm) and *I*= 3rd order intercept point (dBm).This is later used in chapter 5 for the mathematical analysis of the compensation technique of the nonlinear distortions.

Distortions are fundamentally categorised into three sub-parts, one being the harmonic distortions, the second being the intermodulation distortions and the

third being the cross-modulation distortions. The harmonic distortions are generally formed outside the main passband. These lie at multiples of the fundamental frequency. In order to evaluate the harmonic distortions, the ratio of the amplitude of the harmonic distortion V_{HDx} and the main signal V_M are evaluated as in equation (2.7), where x denotes the order of the harmonics.

$$HD_x = \frac{V_{HDx}}{V_M} \tag{2.7}$$

The intermodulation distortions contribute to the majority of the nonlinear distortion. The reason being that, this type of distortion can also appear inside the passband of the system. This type of distortion is produced when there are more than one signal component, forming distortion products at combinations of frequency terms. It is measured by the amplitude ratio of the intermodulation distortion to the fundamental frequency. The cross modulation distortion is also very common type of distortion which is formed by the transference of the amplitude modulation to another signal. The analysis of cross modulation distortion is carried out by using a single tone signal and another amplitude modulated signal [2.11] – [2.14]. A detailed discussion will be carried out in chapter 3 where nonlinear distortion evaluation is mathematically explained.

2.3 Filter Theory

A filter performs by selecting a band of frequencies to pass through while attenuating the other set. Different filtering techniques are already in place such as a lowpass filter where only the lower range of frequency is allowed to pass through while attenuating the rest. A highpass acts in the inverse way as a lowpass. It only allows the higher range of frequencies to pass through while attenuating the lower range. A bandpass filter selects a certain band of frequencies to pass through while attenuating the rest. The bandstop filter is an inverse of the bandpass filter where a selected range of frequency is attenuated and the rest is allowed to pass. The allpass filter allows all frequencies to pass through without exception. A maximum gain of 1 can be reached using a passive filter. Hence for applications requiring a higher gain, active filter needs to be chosen. Example of passive filter includes the LC ladder circuit. An example of an active filter can be a sallen key lowpass filter using operational

amplifiers (op-amps) [2.2]. Several other filters are proposed where multiple operations are achieved by using a single device. For example in a reconfigurable filter with a switch, the filter can be made to operate in either bandstop or bandpass depending on the switching [2.15]. Tunability in filters is also introduced where the centre frequency, attenuation, bandwidth etc. can be tuned to the required specifications [2.16]-[2.17].

In order to describe the conventional microstrip filter design, a useful technique is the utilization of the inverter coupled theory. Lumped element filter design becomes difficult for higher frequencies and hence distributed filter design is more popular. One drawback of this concept is that sometimes it becomes difficult to fabricate certain elements. For example shunt elements becomes impractical in microstrip as drilling holes for vias are required. Hence to do away with such problems, a convenient approach using inverter coupled filter prototypes are used containing either series elements or shunt elements.

Hence a structure containing both can be easily converted to an equivalent inverter coupled prototype for the ease of design. Such conversions happen with the help of immittance inverters which can convert shunt elements to series elements and vice versa. The following Figure 2- 6, shows the equivalent circuit for a bandstop filter which uses the slope reactance/susceptance technique. Here the low pass prototype is converted to an equivalent bandstop filter through admittance and impedance inverters [2.2].

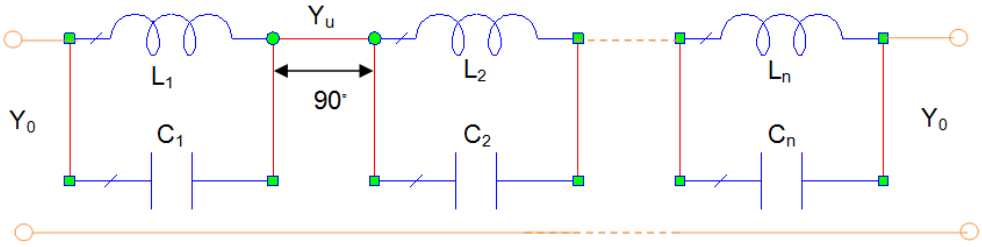

Figure 2-6: Bandstop filter using admittance inverters

Such filters can be frequency mapped using the following equations (2.8)-(2.10) [2.2].

$$\Omega = \frac{\Omega_c FBW}{\frac{\omega}{\omega_0} - \frac{\omega_0}{\omega}} \tag{2.8}$$

$$\left(\frac{Y_u}{Y_0}\right)^2 = \frac{1}{g_0 g_{n+1}} \tag{2.9}$$

$$b_i = \omega_0 C_i = \frac{1}{\omega_0 L_i} = Y_0 \left(\frac{Y_u}{Y_0}\right)^2 \frac{g_0}{g_i \Omega_c FBW} \tag{2.10}$$

Where the normalized frequency of the lowpass prototype is represented by Ω, FBW is the fractional bandwidth; ω_0 is the centre frequency of the BSF, Y_u and Y_0 are the characteristic admittance of the inverter and terminal admittance respectively, b_i represents the slope susceptance and i range from 1 to n, g is the lowpass prototype element value. Hence the conventional bandstop filters can be designed using this concept.

The coupled bandstop filters on the other hand requires the use of coupling coefficient and EM simulation in order to get the correct spacing in between the resonators. The coupling coefficient can be expressed as K as in equation (2.11).

$$K = \frac{\omega_2^2 - \omega_1^2}{\omega_2^2 + \omega_1^2} \tag{2.11}$$

Hence the spacing of the filter is adjusted in order to get the correct value of the calculated coupling. This way the external quality factor of the filter can also be calculated [2.2].

Recent demands in higher filtering capabilities with miniaturized size have led to the development of several new approaches. One such recent concept uses etching in the ground plane to achieve excellent results with circuit miniaturization. This technique is widely known as the defected ground structure [2.18]-[2.20]. One drawback of this kind of structures is the difficulty in modelling as there are number of parameters which can have effect on the structure such as the etched design lattice, the number of such lattice etc. On the basis of DGS, DMS was introduced in order to inculcate some of the benefits of DGS. DMS modelling can be done by breaking the structure into parts and modelling individual components. A gap is modelled by a pi network of capacitance. Similarly a bandgap represents a parallel combination of inductor and capacitor [2.20]-[2.21]. Chapter 4 details some of the filters that have been designed using this concept.

2.4 References

[2.1] H. Howe, “Microwave Integrated Circuits--An Historical Perspective," *Microwave Theory and Techniques, IEEE Transactions on*, vol.32, no.9, pp.991-996, Sep 1984.

[2.2] J. Hong and J. Lancaster, *Microstrip Filters for RF/Microwave Applications*, New York, John Wiley & Sons, 2001.

[2.3] D. M. Pozar, *Microwave engineering*, 3rd edition, New York: John Wiley & Sons, 2004.

[2.4] R.A. Pucel, D.J. Masse and C. P. Hartwig, “Losses in Microstrip”, *IEEE Transactions on Microwave Theory and Techniques*, vol. 16, no. 6, pp. 342 - 350, Jun. 1968.

[2.5] K.C. Gupta, R. Garg, I.J. Bahl and P. Bhartia *Microstrip Lines and Slotlines*, 2nd edition. Boston: Artech House, 1996.

[2.6] T. Edwards, *Foundations for microstrip circuit design*. 2nd edition, Chichester, U.K.: John Wiley & Sons, 1991.

[2.7] S. B. Cohn, “Dissipation Loss in Multiple-Coupled-Resonator Filters”, *Proceedings of the IRE*, vol. 47, no. 8, pp. 1342 - 1348, Aug. 1959.

[2.8] R. Garg and I. J. Bahl, "Characteristics of Coupled Microstrip lines," *IEEE Trans. on Microwave Theory and Tech.,* vol.27, no.7, pp. 700-705, July 1979.

[2.9] A.K. Verma, H. Singh, Nasimuddin, "Closed-form model of shunt capacitance of microstrip step discontinuity," *Microwave Conference Proceedings, 2005. APMC 2005. Asia-Pacific Conference Proceedings*, vol.1, no., pp.3 pp., 4-7 Dec. 2005.

[2.10] R. G. Meyer, M. J. Shensa, and R. Eschenbach, "Cross modulation and Intermodulation in amplifiers at high frequencies," *IEEE Journal of Solid-State Circuits*, vol. 7, no. 1, pp. 16-23, Feb. 1972.

[2.11] J. Vuolevi and T. Rahkonen, *Distortion in RF Power Amplifiers*, Artech House Inc., 2003, ISBN 1580535399.

[2.12] W. Sansen, “Distortion in elementary transistor circuits,” *IEEE Transactions on Circuits and Systems-II: Analog and Digital Signal Processing*, vol. 46, no. 3, pp.315-325, Mar. 1999.

[2.13] S. C. Cripps, *RF Power Amplifiers for Wireless Communications*, Artech House Inc., 1999, ISBN 0890069891.

[2.14] S. Maas, *Nonlinear Microwave and RF Circuits*, Artech House Publishers, 2003, ISBN 1580534848.

[2.15] M.F. Karim, G. Yong-Xin, Z.N. Chen and L.C. Ong, "Miniaturized reconfigurable and switchable filter from UWB to 2.4GHz WLAN using PIN diodes," *Microwave Symposium Digest, 2009. MTT '09. IEEE MTT-S International*, vol., no., pp.509-512, 7-12 June 2009.

[2.16] R. Douglas Jachowski and C. Rauscher, "Frequency-agile bandstop filter with tunable attenuation," *Microwave Symposium Digest, 2009. MTT '09. IEEE MTT-S International*, vol., no., pp.649-652, 7-12 June 2009.

[2.17] I. C. Hunter and J.D. Rhodes, "Electronically Tunable Microwave Bandstop Filters," *Microwave Theory and Techniques, IEEE Transactions on* , vol.30, no.9, pp.1361,1367, Sep. 1982.

[2.18] Dal Ahn; Jun-Seok Park; Chul-Soo Kim; Juno Kim; Yongxi Qian; T. Itoh , "A design of the low-pass filter using the novel microstrip defected ground structure," *Microwave Theory and Techniques, IEEE Transactions on* , vol.49, no.1, pp.86,93, Jan 2001.

[2.19] Jae-Kwan Lee; Young-Sik Kim, "Ultra-Wideband Bandpass Filter With Improved Upper Stopband Performance Using Defected Ground Structure," *Microwave and Wireless Components Letters, IEEE* , vol.20, no.6, pp.316,318, June 2010.

[2.20] D.Woo, T.Lee, J.Lee, C.Pyo and W.Choi, "Novel U-slot and V-slot DGSs for bandstop filter with improved Q factor," Microwave Theory and Techniques, IEEE Transactions on, vol.54, no.6, pp.2840-2847, June 2006.

[2.21] Jong-Sik Lim; Chul-Soo Kim; Young-Taek Lee; Dal Ahn; Sangwook Nam, "Design of lowpass filters using defected ground structure and compensated microstrip line," *Electronics Letters* , vol.38, no.22, pp.1357,1358, 24 Oct 2002.

[2.22] J.A. Tirado-Mendez, H. Jardon-Aguilar, "Comparison of defected ground structure (DGS) and defected microstrip structure (DGS) behaviour at high frequencies," *Electrical and Electronics Engineering, 2004. (ICEEE). 1st International Conference on*, vol., no., pp.7, 10, 8-10 Sept. 2004.

Chapter 3 Nonlinear Distortion in Passive RF Reconfigurable Circuits

This chapter deals with the discussions on nonlinear elements in transceivers. Such elements can include a power amplifier, a low noise amplifier, mixers, and reconfigurable or tunable filters. Elements such as varactor diode, PIN diode, optical switch, MEMS are discussed here due to their inherent nonlinear property and their use in reconfigurability and tunability of filters and other devices. Such elements are an important part of RF circuits today. Hence, applications of such elements in RF circuits namely filters are also discussed. Due to their inherent nonlinear property, it is imperative to analyse the effect of nonlinear distortion in the final outputs. Interfering signals when mixed with main signals are passed through such components; an increase in nonlinear distortion is noticed. Hence it is imperative to carry out a complete evaluation of the above components as nonlinear elements to understand the contribution of nonlinear distortion due to such components on its own. This can enable an easier analysis in later chapters where such components in a Tx chain are subjected to interfering signals.

3.1 Non linearity and Intermodulation Distortion

A system can be defined to be an object which gives a response y(t) when a signal x(t) passes through it. Examples are a transceiver, mixer, filter, power amplifier etc. A system can be expressed as follows:

$$y(t) = A[x(t)] \tag{3.1}$$

Where, y(t) is the response of the system, x(t) is the input signal, A is the operation performed by the system and t is the independent time variable. A linear system is defined as one which follows the principle of superposition, such that the output is a linear combination of two or more outputs of the

system when two or more input signals is passed through them. Mathematically such a system can be defined as:

$$A[k_1x_1(t) + k_2x_2(t)]= k_1A[x_1(t)] + k_2A[x_2(t)] \quad (3.2)$$

Where, k_1 and k_2 are constants. Hence a system which does not follow the relationship in (3.2) is defined as nonlinear systems [3.1]-[3.3]. In reality all systems are nonlinear but act linear within a specified set of conditions. In order to describe the measure of nonlinearity in RF transceivers it is important to understand a few terms related to nonlinear distortions. The following subsections explain the terms related to nonlinear distortion.

3.1.1 Analysis of Nonlinearity

There are several approaches to analyse an electronic device. The four main methods are listed as follows [3.2]:

1. Load Pulling
2. Scattering Parameter Analysis
3. Time domain (Transient) Analysis
4. Frequency domain Analysis

Load pulling Analysis is mostly applied to large signal circuits where the contours of the load impedances are plotted on a Smith Chart. Such a system requires the use of various impedance loads thus making it practically difficult. On the other hand, the analysis has little use of the multi-tone input signals which can significantly decrease the possibility of a wider measurement system.

Scattering parameter analysis (S-parameter) is mainly used to determine the impendence matching for the source and load of a circuit. The applications of this analysis are limited in the nonlinear context as the two port S- parameters itself are linear parameters. These are mostly used for large signal circuits as well.

Time domain analysis is used for both low and high frequency and digital circuits. The time domain method of moments is used in solving Maxwell's equations. It uses the time domain differential equations to characterise the circuits. Such analysis is not very compatible with multiple frequency input signal. It can however be used in large circuits with strong nonlinearities.

Frequency domain analysis is applicable to both types of nonlinearity which are categorised as weakly nonlinear and strongly nonlinear. The power series and the Volterra series are commonly used in the weakly nonlinear circuit analysis while the harmonic balance is mostly used for the strongly nonlinear circuits. This analysis method is very important as it considers the excitation of circuits due to multi-tone inputs. Due to its simplicity the power series has become an important tool and will be discussed here to theoretically describe the nonlinear effects [3.2].

3.1.2 Power Series Analysis and Two Tone Test

The power series is a convenient method of nonlinear analysis especially in a power amplifier [3.4]-[3.5]. Such series is a polynomial approximation of a nonlinear transfer function and is given by the following expression:

$$V_0\,(t) = a_1 * V_i(t) + \ a_2 * V_i^2(t) + a_3 * V_i^3(t) + \cdots + a_n * V_i^n(t) \tag{3.3}$$

The expression can be written in a more concise form as:

$$V_o(t) = \sum_{n=1}^{\infty} a_n V_i^n\,(t) \tag{3.4}$$

Where, V_0 = Output Voltage and V_i=Input Voltage and a_n= coefficient at the nth term. A power series as described by (3.4) assumes a memoryless effect which means that there is no effect on the final output due to previous input excitations. But in reality, circuits having energy storage elements such as inductors and capacitors affect the output signal not only due to the current input excitations but also previous excitations. This is also known as the memory effect. This changes the standard equation in (3.4) and a new variable needs to be added in order to cater for the memory effect. This is done by using a time constant in the equation (3.4) which can now be written as follows [3.6]:

$$V_o(t) = \sum_{n=1}^{\infty} a_n V_i^n\,(t - t_n) \tag{3.5}$$

This expression can be expanded further as:

$$V_0\,(t) = a_1 * V_i(t - t_1) + \ a_2 * V_i^2(t - t_2) + a_3 * V_i^3(t - t_3) + \cdots + a_n * V_i^n(t - t_n) \tag{3.6}$$

Hence when amplitude modulated and phase modulated signal is passed through such a system represented by the above equation (3.6), it results in

several terms representing various distortions. Therefore if the input voltage is written as (3.7),

$$V_i(t) = V(t)\cos\left(\omega t + \varphi(t)\right) \tag{3.7}$$

Then, the output voltage can be written as in equation (3.8)

$$\begin{aligned} V_0(t) = {} & [a_1 * V(t-t_1) * \cos\left(\omega(t-t_1) + \varphi(t-t_1)\right)] + [a_2 * V^2(t-t_2) * \\ & \cos^2\left(\omega(t-t_2) + \varphi(t-t_2)\right)] + [a_3 * V^3(t-t_3) * \cos^3\left(\omega(t-t_3) + \right. \\ & \left. \varphi(t-t_3)\right)] + \cdots + [a_n * V^n(t-t_n) * \cos^{\mathrm{n}}\left(\omega(t-t_n) + \varphi(t-t_n)\right)] \end{aligned} \tag{3.8}$$

Applying trigonometric identities, the above equation can be further reduced to the equation in (3.9) below. The first three terms are evaluated as the third order intermodulation term is the most important in the analysis here.

$$\begin{aligned} V_0(t) = {} & \left[\frac{a_2}{2} * V^2(t-t_2)\right] \\ & + \left[\begin{matrix} a_1 * V(t-t_1) * \cos\left(\omega(t-t_1) + \varphi(t-t_1)\right. \\ + \frac{3*a_3}{4} * V^3(t-t_3) * \cos\left(\omega(t-t_3) + \varphi(t-t_3)\right) \end{matrix}\right] \\ & + \left[\frac{a_2}{2} * V^2(t-t_2) * \cos\left(2\omega t + 2\varphi t - 2(\omega t_2 + \varphi t_2)\right)\right] \\ & + \left[\frac{3*a_3}{4} * V^3(t-t_3) * \cos\left(3\omega t + 3\varphi t - 3(\omega t_3 + \varphi t_3)\right)\right] \end{aligned} \tag{3.9}$$

In the above equation, the first term indicates a D.C. signal which shifts the operating point by some amount. The 2nd and 3rd terms are indicative of the linear amplification by some gain and in band distortions respectively. The 4th and 5th terms indicate the harmonic distortions that are present due to the nonlinear effect of the system.

The above case was for a single modulated signal. Now two signals at ω_1 and ω_2 are passed through a system which can be characterised by the equation (3.4). Then the resultant output will contain not only harmonic distortions but also intermodulation distortions. Here, the memoryless case is considered in order to keep the equations simple. The two tone test is a simple way to determine the different types of distortions for a given device under test. In this thesis, two tone test set up has been extensively used. In order to get a better understanding, it is further analysed mathematically. Let the input signal for the two tone test be described by the following equation.

$$V_i(t) = V_a * \cos(\omega_1 t) + V_b * \cos\left(\omega_2 t\right) \tag{3.10}$$

Now, considering only a 3rd order expression, the output voltage can be written as:

$$V_o(t) = \frac{a_2 V_a^2}{2} + \frac{a_2 V_b^2}{2}$$
$$+ \left(a_1 V_a + \frac{3a_3 V_a^3}{4} + \frac{3a_3 V_a V_b^2}{2}\right) * \cos(\omega_1 t) + \left(a_1 V_b + \frac{3a_3 V_b^3}{4} + \frac{3a_3 V_b V_a^2}{2}\right) * \cos(\omega_2 t)$$
$$+ \frac{a_2 V_a^2}{2} * \cos(2\omega_1 t) + \frac{a_2 V_b^2}{2} * \cos(2\omega_2 t) + \frac{a_3 V_a^3}{4} * \cos(3\omega_1 t) + \frac{a_3 V_b^3}{4} * \cos(3\omega_2 t)$$
$$+ a_2 V_a V_b * \cos(\omega_1 - \omega_2)\, t + a_2 V_a V_b * \cos(\omega_1 + \omega_2)\, t + \frac{a_3 V_a^2 V_b}{4} [\cos(2\omega_1 -$$
$$\omega_2)\, t + \cos(2\omega_1 + \omega_2)\, t] + \frac{a_3 V_b^2 V_a}{4} \begin{bmatrix} \cos(2\omega_2 - \omega_1)\, t \\ + \cos(2\omega_2 + \omega_1)\, t \end{bmatrix} \quad (3.11)$$

The components of the above equations includes the D.C. signal (the constant terms), harmonics of the fundamental frequency ($\omega_1, \omega_2, 2\omega_1, 2\omega_2, 3\omega_1, 3\omega_2$) and the intermodulation distortions arising due to the mixing of the two frequencies ($\omega_1 and\ \omega_2$). Hence the second order intermodulation terms are denoted by ($\omega_1 - \omega_2\ and\ \omega_1 + \omega_2$). The third order intermodulation terms are denoted by ($2\omega_1 - \omega_2\ , 2\omega_1 + \omega_2, \omega_1 - 2\omega_2\ and\ \omega_1 + 2\omega_2$).The following figure is an illustration to show the intermodulation distortions.

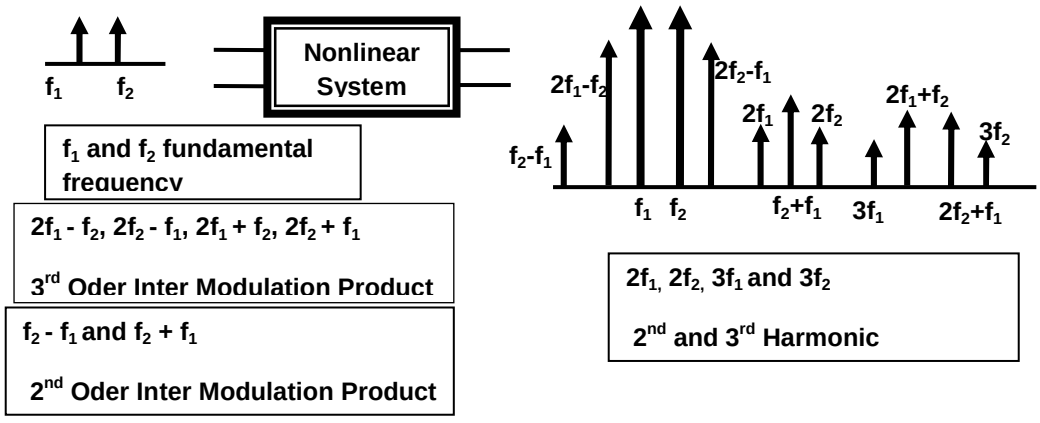

Figure 3-1 : Illustration of nonlinear effect showing various distortion products.

Most of the harmonics and D.C. components can be easily filtered out as they are mostly out-of band distortions. On the other hand, the odd order intermodulation products formed due to the mixing of two or more frequencies fall in the in-band region causing significant distortions in the output level as it becomes difficult to filter out such components. The power level of the 3rd order intermodulation distortion is found to be the highest and most significant and

hence greater emphasis is given to remove the 3rd order intermodulation distortions from the final output[3.5]-[3.6].

3.2 Tunable/Reconfigurable elements in RF Circuits

Due to the recent demand in adaptive circuits for multi-band wireless communication, there has been a surge in the use of tunable elements in filters and other RF circuits. The thesis concentrates on the nonlinear distortion evaluation of such reconfigurable/tunable elements used in filters. When compared to a fixed set of filters, a tunable filter can be beneficial, cost effective and can save a lot of space. Reconfigurability in filters can include the switching from bandpass to a bandstop response, tuning the centre frequency and also bandwidth. Various techniques which are used for switching and tuning include varactor diodes, PIN diodes, RF MEMS, ferroelectrics, liquid crystals and optical switches. Each element has both advantages and disadvantages depending on their application and usage. The three important semiconductor elements used in reconfigurability and tunability of RF circuits are discussed in this report:

i) PIN Diodes
ii) Varactor Diodes
iii) Optical Switch

These reactive elements can be used as a switch (switching between bandpass to bandstop response or switching between two frequencies) or can also act as a tuning element where various tuning range of the centre frequency can be achieved. In order to understand the working of the semiconductor devices in RF filters, it's important to study the devices individually.

3.2.1 PIN Diodes

A pure intrinsic semiconductor layer in the middle along with p and n doped region on the side makes a P-I-N diode. PIN diode is a current controlled resistance for high frequency signals [3.7]. The working of the PIN diode in the

forward biased condition depends on the holes and electrons which are injected from the P and N region to the I region. Since the charges do not recombine immediately this is stored in it [3.8]. Non linearity arises due to the time varying forward resistance, which is varied because of the modulation of this stored charge by the microwave signal [3.9]. In order to mathematically define the stored charge in the PIN diode, we consider *Qs* as the stored charge [3.7].

$$Q_S = I_F \tau \tag{3.12}$$

Where, I_F is denoted as the forward bias current and τ is the minority charge carrier lifetime. The total series resistance can be expressed as an inverse proportion of the total charge Q_S. Hence any variation in the stored charge will also result in the variation of the resistance. This makes the PIN diode nonlinear and leads to distortions in the output spectrum [3.7]. Nonlinear distortion analysis shown in [3.7], [3.9], and [3.10] proved that the distortion due a PIN diode is much lesser for small RF signals as compared to varactor diode.

BAP65-02, a silicon PIN diode has been used in order to analyse the nonlinear effects [3.11]. These diodes are further used in filters as switches in order to switch it from bandpass to bandstop response [3.12].The equivalent circuits for the PIN diode for both forward bias and reverse bias are given in Figure 3-2. The ON state can be modelled by a simple series resistance R_S and a parasitic inductance L_S. The OFF state or the reverse biased condition can be denoted by a capacitance C and shunt loss element R_L. The inductance L_P represents parasitic inductance. In the ON state, the forward resistance is low, while in the off state the resistance tends be much higher. This is how the PIN diode acts a switch in RF circuits [3.13].

(a) (b)

Figure 3-2: Equivalent circuits for (a) forward biased (b) reversed biased for PIN diode.

In order to test for the nonlinear distortion in a PIN diode, a two tone simulation test set-up was carried out with frequencies at 0.975GHz and 1.025GHz. The following Figure 3-3 shows the schematic used in order to analyse the nonlinear effect of the PIN diode.

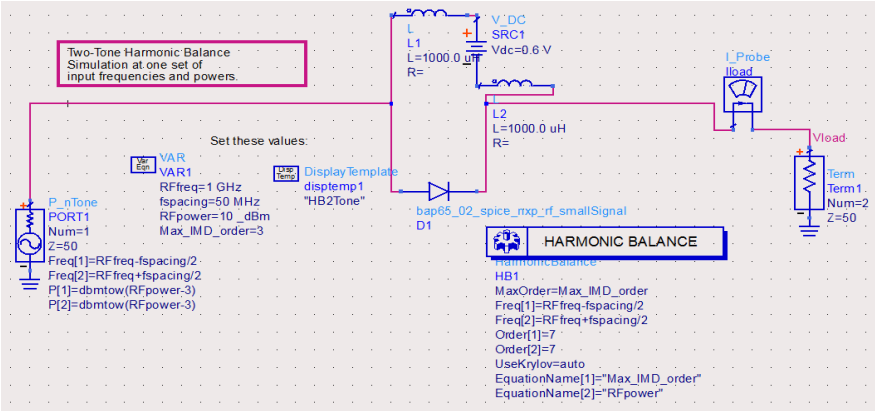

Figure 3-3: Schematic of the PIN diode configuration.

In order to measure nonlinear distortions a harmonic balance simulator has been used where the inductor acts as a RF choke. Hence the third order intermodulation products which arise due to the nonlinearity of the system can be clearly seen. The bias voltage has been varied ranging from 0.5 V to 1 V and decrease in the nonlinearity with higher bias voltage was observed. It is also seen that for 0.6 V the nonlinear effect is more pronounced. The system input power was also varied and results noted. For low reverse bias voltages, phase distortions can occur in PIN diodes. Figure 3-4 shows response of the third order intermodulation product (IMD3) for a PIN diode at a bias voltage (V_{bias}) of 0.6 V and input power (P_{in}) of 10dBm.

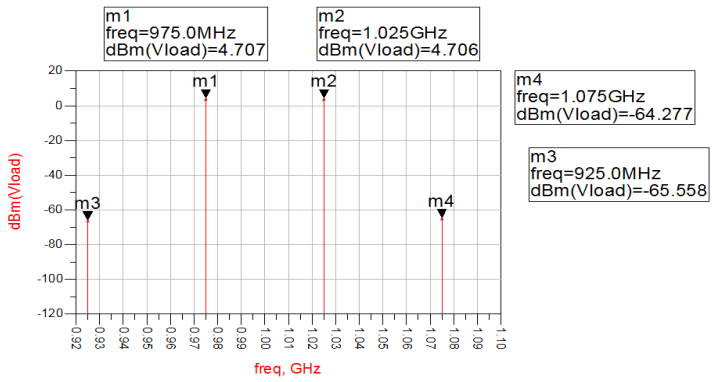

Figure 3-4: Response showing the IMD3 for a PIN diode with V_{bias} =0.6V.

As can be seen from the above figure, the third order intermodulation product appears at $2f_1$-f_2 (925MHz) and $2f_2$-f_1 (1.975GHz) at marker m3 and m4, and has a power level of -64dBm. The main tone output signals occur at f_1 and f_2 at 975MHz and 1.025GHz. The distortion level measured is relatively low but it is still not a desirable property in a filter, due to the filter's utilization in removing distortions and unwanted signal.

The PIN diode shows distortions in both ON and OFF state. In the OFF state, the distortion is generated due to the capacitance modulation [3.14]. Figure 3-5 shows the effects of change in output power (P_{out}) with respect to change in input power (P_{in}) at the bias voltage of 0.6 V. It also shows the change of the higher 3rd order intermodulation product (IMD3) at frequency 1.975GHz with respect to the input power (P_{in}) which ranges from -10 to 20dBm.

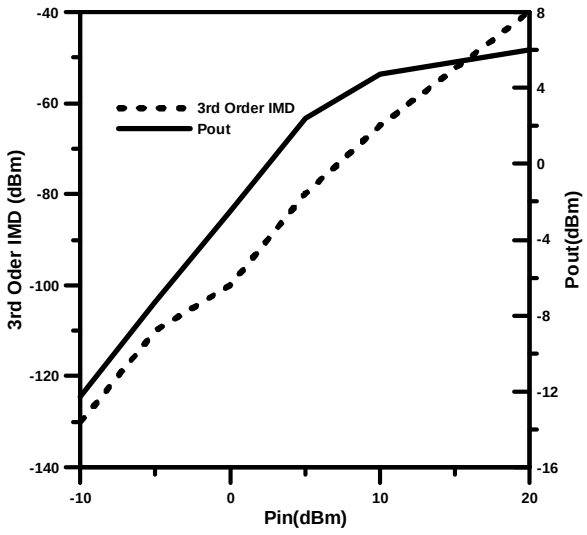

Figure 3-5: Variation in P_{out} and IMD3 with reference to different P_{in} when V_{bias} = 0.6V or ON stage.

As can be seen from Figure 3-5, the P_{out} curve is not linear. A saturation point is seen around -5dBm for the input power P_{in}. For higher input power levels, the third order intermodulation is much higher reaching to as high as -40dBm which can cause problem in many RF applications.

3.2.2 Varactor Diodes

As compared to the PIN diode, a varactor diode's main mode of operation is as a variable capacitor, which can change the centre frequency of a filter. Since it works in reverse bias condition, there is no current flow, but the capacitance is varied by the bias voltage. The changing thickness of the depletion layer that is formed in the diode gives rise to the capacitance [3.15]. In order to describe this mathematically we use the following equation (3.13).

$$C_j = \frac{C_{j0}}{\left(1+\frac{v_R}{V_j}\right)^{m_j}} \tag{3.13}$$

Where, C_{j0} is defined as the junction capacitance at zero bias, v_R is the voltage for the reverse bias, m_j is the doping coefficient and V_j is the junction potential. The nonlinearity of the varactor diode arises because of the modulation of the capacitance by the RF signal [3.16]. The capacitance is also a nonlinear function of the bias voltage as can be seen from the equation (3.13). For lower bias voltages, when the RF signal is comparable to the D.C. biasing, the distortions seen are more severe [3.15], [3.16] and [3.17]. An equivalent circuit model for the varactor is shown in Figure 3-6.

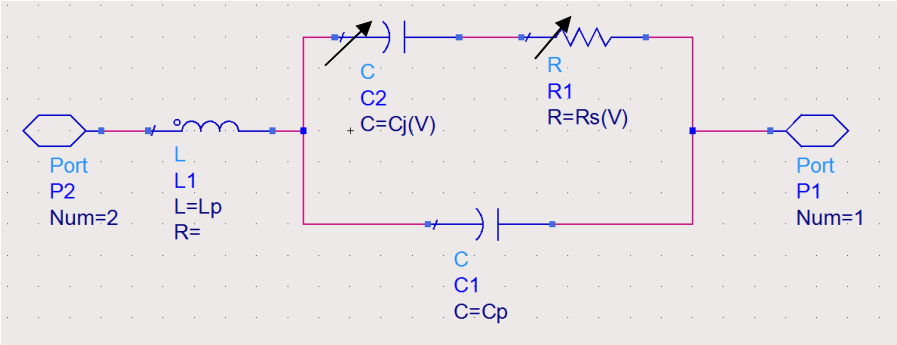

Figure 3-6: Equivalent circuit model for varactor diode.

The variable junction capacitance C_j and the junction resistance R_s are both functions of the junction voltage. The parasitic capacitance C_p and inductance L_p are also modelled in the equivalent circuit. An ADS harmonic balance simulation is carried out on a varactor model to analyse nonlinearity, as it contributes towards further distortions in the output signal. A two tone test was for the commercial varactor diode model NXP BB135 with different sets of input

power and reverse bias voltages. The setup for two tone testing is shown in Figure 3-7.

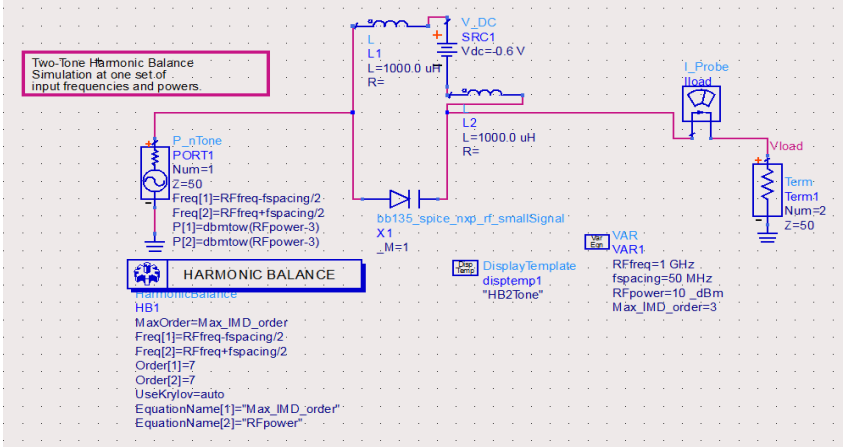

Figure 3-7: Schematic of the varactor model for two tone testing.

Similar to the PIN diode setup, the same harmonic simulator is used, in order to find the intermodulation products due to a varactor diode. It was found that by decreasing the bias voltage value the inter modulation products had a higher power level. Hence for a smaller bias voltage the intermodulation products were more severe; this is because of the modulation of the smaller bias voltages by the RF signal [3.18]-[3.20].

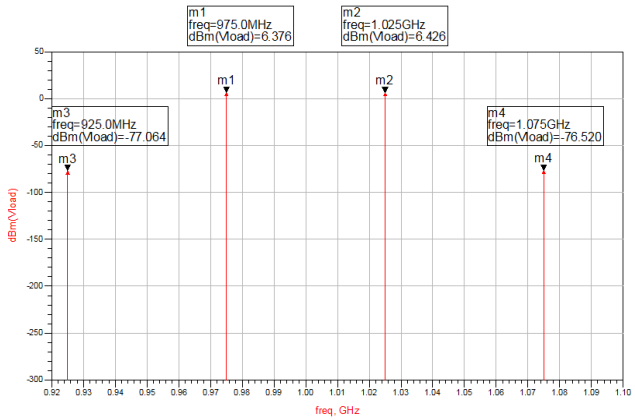

Figure 3-8: Third order intermodulation distortion produced for the varactor diode when a reverse bias voltage of 30V is used.

Figure 3-8 illustrates the nonlinear nature of the varactor. Marker m3 and m4 indicates the power level and the frequency of the 3rd order IMD product. The

fundamental tones were set at 0.975 and 1.025GHz. The third order IMD is obtained at 0.925 and 1.075GHz respectively with a power level of -76.5dBm. The reverse bias voltage is kept around 30 V and the input power level is kept considerably high at 10dBm. Lower the power of the input signal, lower the IMD products obtained. Ideally the intermodulation products should have been negligible but a different observation is made here. Recent research has utilized "distortion-free" varactor diodes [3.19] - [3.20], where the varactor diode is used in an anti-series and anti-parallel configuration and the IMD products are considerably reduced. Table 3-1 shows the variation of output power and IMD3 with varying bias voltage while the input power is kept constant at 10dBm:

V_{bias} (in V)	P_{out} (in dBm)	IMD3 (in dBm)
-15	8.745	-58
-20	8.125	-64
-25	7.454	-70
-30	6.762	-76

Table 3-1: Variation of P_{out} and IMD3 with reference to different V_{bias} when, P_{in} = 10dBm.

It was found from these figures that for V_{bias} = -15V, the IMD3 had the highest value. It is seen in [3.18] that with a higher reverse bias voltage the intermodulation distortions are lower. A complete set of values are provided in Figure 3-9 to show the effect of varying input power P_{in} for a constant V_{bias} = -15 V. It is measured that for a higher input power, the power level for the third order intermodulation product is around -41dBm. The following Figure 3-9 shows the variation of P_{out} and IMD with P_{in}.

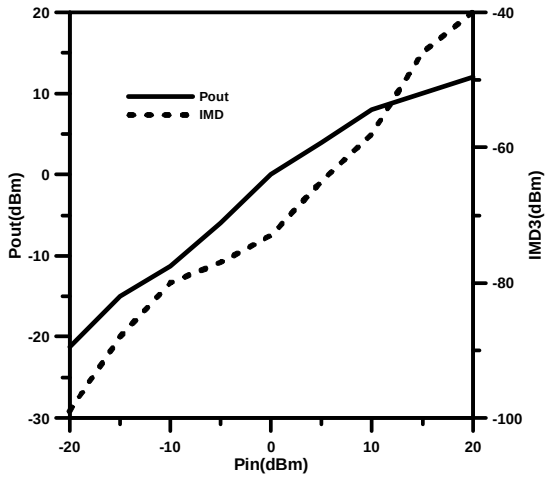

Figure 3-9: Variation in P_{out} and IMD3 with reference to different P_{in}, for V_{bias} = -15V.

The above figure shows the variation of P_{out} and IMD3 to the P_{in}. The plot for the output power sees a slight saturation around 7-10dBm. The IMD increases with the power level reaching -40dBm for a P_{in} = 20dBm.

3.2.3 Optical Switch

In recent years, photoconductive silicon switches (PSS) are used as a switch in RF circuits. These switches are optically controlled and can be used in tuning circuits because of the change in their conductivity when subjected to optical illumination. The light should have a particular wavelength and flux density in order to change the conductivity of the silicon switch [3.19]-[3.20].The switches used here to model distortions have been diced from silicon wafers having a very high resistivity (>6000Ωcm) . In the original form, the silicon dices acts as insulators but on illumination, the switches starts conducting. Phosphorus is often used to dope the n-type switches to increase the static conductivity [3.21]-[3.25].

The equivalent circuit for an optical switch can be modelled as given in Figure 3-10. Experimental data in [3.23]-[3.25] suggests that in the ON state, the values of R_G and R_S decrease while C_G and C_S increase. Additionally in [3.24], an overall insertion-loss of around 0.68dB was found in the ON state (under an illumination of 200mW optical power) of a single silicon switch while

in the OFF state, there was an increase in the total series resistance while capacitance C_G and C_S decreased. The capacitance C_G and C_P represents the gap on which the silicon dice is mounted. On the other hand, R_G and C_S are there to model the photoconductive effect of silicon. The other elements which include resistors and inductors model the losses in the circuit.

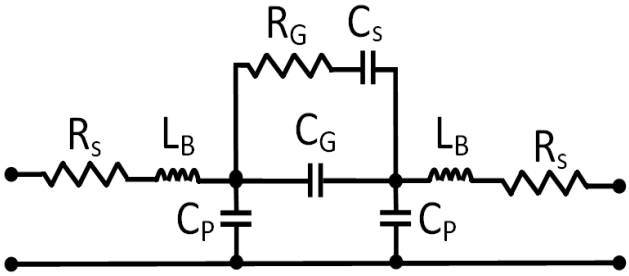

Figure 3-10: Equivalent circuit of a silicon switch.

The silicon switch was illuminated using a laser light with intensity greater than the band gap of the PCSS to ensure sufficient intrinsic absorption [3.26]-[3.27]. The inherent nonlinear property of the silicon switch is further explained in [3.27]-[3.29]. Nonlinearity is an effect due to the formation of electron-hole pairs termed as “lock-on” which are optically generated. In later section, the experimental evaluation of nonlinearity for an optical switch is provided.

3.2.4 Comparison between Tuning/Switching Elements

Varactor diodes as a tuning element can have many disadvantages such as high insertion loss, higher power consumption and the level of distortion is significantly higher [3.12]. In comparison, the PIN diode has more linear characteristics and also lower losses which limit the degradation in the bandwidth and filter operation. A PIN diode also offers high power handling capability with better switching speed while provides quality factor Q>50 below 10GHz at a lesser cost, easier packaging and a lower bias voltage [3.12]-[3.15].

Optically controlled silicon switches offer high power handling capability, immunity to electromagnetic interference, excellent isolation between the microwave and switch control circuits and, low distortion [3.22]. Optically controlled antennas [3.23], resonators [3.24] and couplers [3.25] have already

been demonstrated. They are cheap and can be easily integrated in circuits without compromising the size [3.23]. Tunable/Reconfigurable elements are very useful in RF filter design since it can be used over a wide range of frequency, easy to fabricate and cost effective.

3.3 Evaluation of Nonlinear Distortion in Reconfigurable Elements

In this section, the reconfigurable elements are further subjected to experiments to evaluate the nonlinear distortion effects. A surface mount commercial PIN diode is tested and the harmonic distortions for a range of input signals are presented. The PIN diode used was BAP65-02, same as the one used in the simulations. An experimental set up was first done in order to measure the distortions for the surface mount silicon PIN diode.

Figure 3-11: Photograph of the surface mounted PIN diode.

Figure 3-11 shows the fabricated PIN diode switch. The circuit was constructed on a Rogers Duroid 5880 substrate with relative dielectric constant of 2.2 and height of 1.575 mm. Two resistors of 3.3 kΩ form the bias circuitry and it provides sufficient RF isolation. Adequate forward biased voltage was provided for testing of the PIN diode in the ON state. This was further tested for intermodulation distortions using a two tone setup, 3G signals (QPSK,16 QAM and 64 QAM) and 4G signals (16QAM OFDM, 64QAM OFDM) . Testing was carried out with digitally modulated signals because in a real transceiver system the inputs are mostly digitally modulated signals. The results were further

analysed and noted. The experimental set up which was used is shown in Figure 3-12.

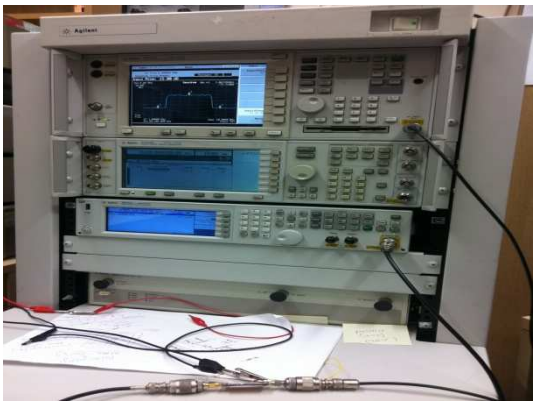

Figure 3-12: Photograph of the experimental setup used for testing IMD in the commercial PIN diode.

The Agilent MXG vector signal generator N5182A was used to supply the input signals and Agilent VSA series transmitter tester E4406A was used to capture the output spectrum generated. Two sets of two tone testing were carried out. The two frequencies chosen for the fundamental tone had a centre frequency of 3GHz with a gap of 0.5MHz and 1MHz in between the two tones. In the first case, one fundamental tone was at 2.99975GHz and the other one was at 3.0025GHz. Therefore the lower and upper third order intermodulation product was at 2.99425GHz and 3.00525GHz respectively. In the second set of experiment where the spacing between two tones was 1MHz, one fundamental tone was at 2.9995GHz and the other one at 3.0005GHz. Therefore the lower and upper third order intermodulation product was found at 2.9985GHz and 3.0015GHz respectively. The input power P_{in} is varied from -20dBm to 15dBm to see the variation of the output power P_{out} and IMD3. The Figure 3-13 and 3-14 shows the distortions generated due to a PIN diode when two tone signals are passed through it.

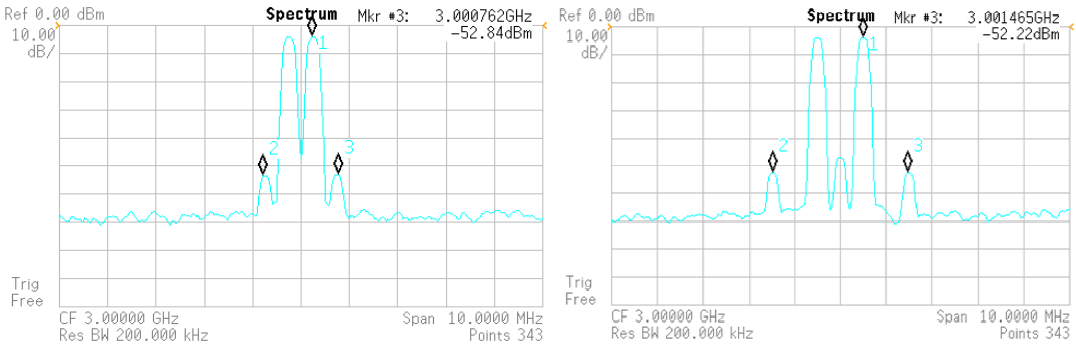

(a) (b)

Figure 3-13: Spectrum showing the 3rd order intermodulation distortion for a PIN diode for P_{in} =15dBm (a) with 0.5MHz (b) with 1MHz spacing.

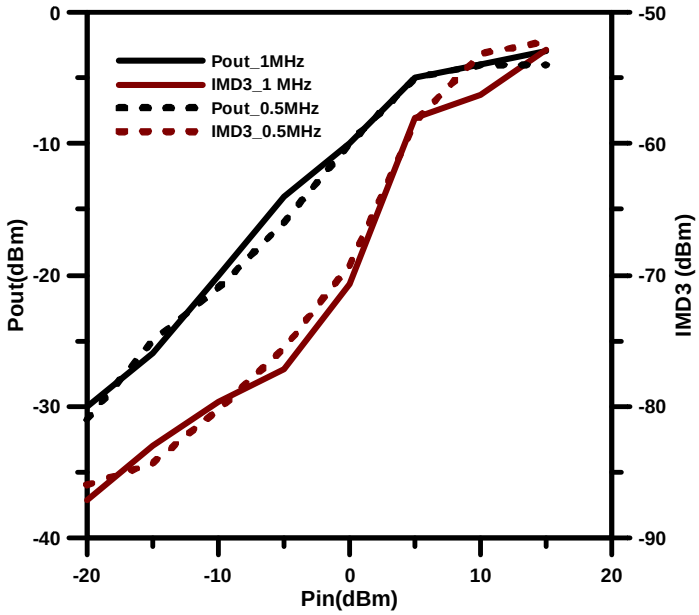

Figure 3-14: Variation of P_{out} and IMD3 with respect to various input power P_{in} for the PIN diode.

From Figure 3-14, it can be seen that third order distortion seen for a spacing of 1MHz is relatively lower as compared to 0.5MHz. This is because distortions are more pronounced for closely spaced signals. Cross-modulation of the two signals can also contribute to the increased distortion for closely spaced signals.

The PIN diode was subjected to various other digitally modulated signals. These comprised of 5MHz 3G signals (QPSK, 16QAM, 64 QAM) and 4G signals (16QAMOFDM and 64QAMOFDM). Again a similar set up was used in order to test the distortions in PIN diode. The 5MHz output spectrum has been

captured and shown. Data for each P_{out} and IMD was noted and plotted against the P_{in} which ranged from -20dBm to 15dBm. Figure 3-15 shows the variation of P_{out} and IMD for the PIN diode under test for 3G signals.

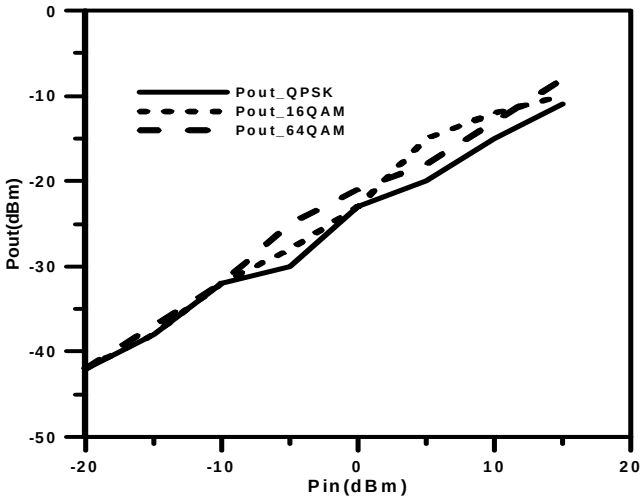

(a)

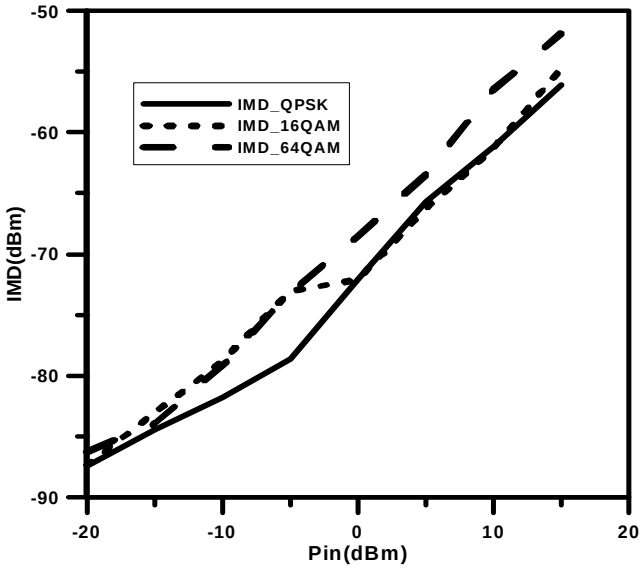

(b)

Figure 3-15: Variation of (a) P_{out} and (b) IMD with respect to various P_{in} for 3G signals.

As expected, the distortions were much higher for higher input power. It was also noted that distortions were higher for a more complex digitally modulated signal. Distortions obtained for 64QAM signal was much higher than QPSK signal as input. For example, when the input power is 15dBm, the values of distortion for QPSK, 16QAM, 64QAM are around -58dBm, -55dBm and -51dBm.

In a digitally modulated signal, the significance of a third order intermodulation distortion is very less. Distortions are mostly measured in the adjacent channel band. The main channel creeps into the adjacent band causing distortions in the output spectrum as shown in Figure 3-16. The 5MHz output spectrum measured was for a 64QAM input signal when passed through a PIN diode for P_{in} =15dBm. A centre frequency of 3GHz was taken. The channel bandwidth was 5MHz.

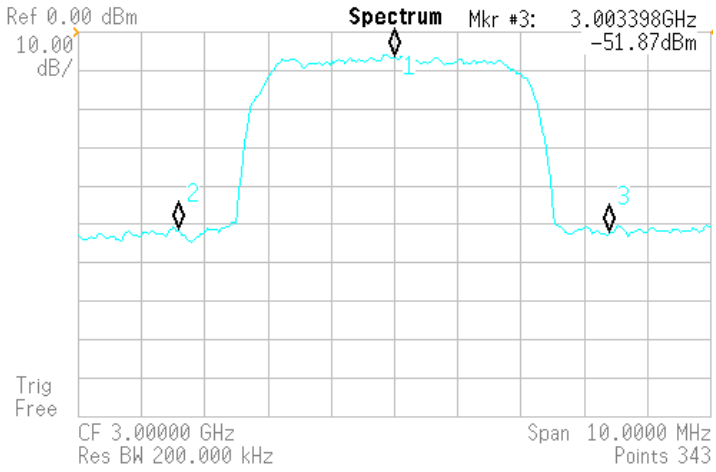

Figure 3-16: Measured 5MHz output spectrum for a 64QAM input signal for an input power of 15dBm in a PIN diode.

As can be seen in the above Figure 3-16, the distortions in the adjacent channel are higher. This level of distortion will be unacceptable for applications where a much lower distortion is required. Most of the standard modulation schemes require relative distortion to be around 35dB [3.30]. For systems requiring good image quality, the relative distortion should be greater than 70dB [3.31]. The average power of the adjacent channel is around -51dBm. Figure 3-17 shows the variation of Pout and IMD with P_{in} for 4G signals with the PIN diode as device under test. The IMD for 64QAMOFDM increased as compared to 16QAMOFDM after a certain input signal of 0-5dBm. For higher input levels, the distortions for the PIN diode were more pronounced.

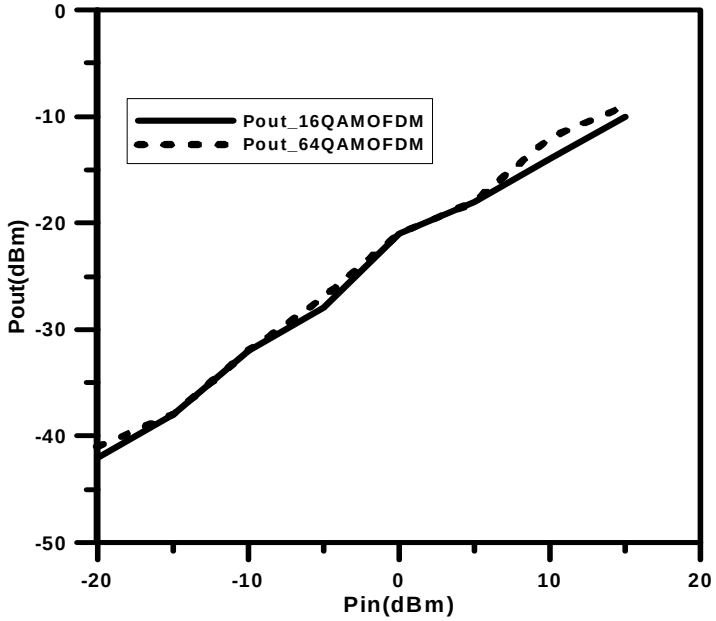

(a)

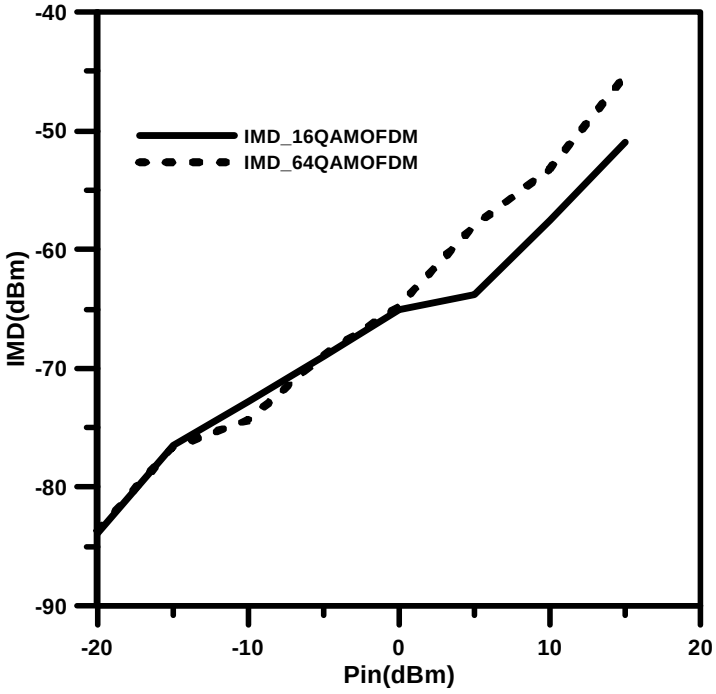

(b)

Figure 3-17: Variation of (a) P_{out} and (b) IMD with respect to various P_{in} for 4G signals.

Figure 3-18 shows the measured spectrum for a 64QAMOFDM as input signal. Again, a centre frequency of 3GHz was taken along with 5MHz channel bandwidth.

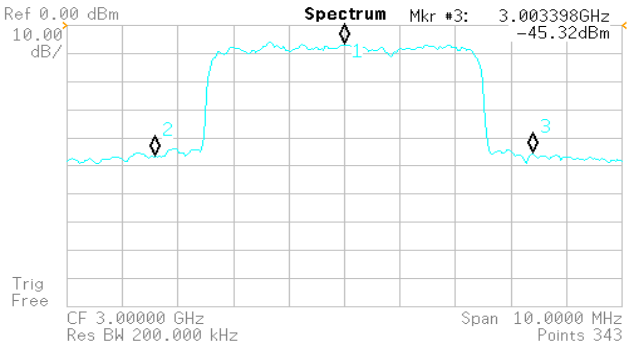

Figure 3-18: Measured 5MHz output spectrum for a 64QAMOFDM input signal for an input power of 15dBm in a PIN diode.

The average power level measured in the adjacent channel was around -45dBm which is quite high for RF applications requiring very high linearity. The relative distortion which is calculated by subtracting the average power of the adjacent channel from the main channel is given as 37dB.

From the results obtained, it was clearly shown that the PIN diodes are significantly nonlinear. Hence in applications which require PIN diodes as switches such as a filter, it will contribute to the overall nonlinear distortion. In later sections, filters using these diodes as switches will be analysed for nonlinear distortion.

Optical switches as described in previous section are also inherently nonlinear. Hence it becomes imperative to evaluate distortions in these elements. A similar experimental set up was used for the measurement as in the case of PIN diodes. The only difference was that instead of external bias voltages, the optical switch was illuminated by using 980 nm near infrared laser diodes (200mW power). The photograph of a fabricated optical switch on Rogers RT Duroid 5880 substrate with relative dielectric constant of 2.2 and height of 1.575 mm is shown in Figure 3-19. The dice was 1mm by 2mm by 0.3 mm in dimension which was placed over a 0.5 mm gap

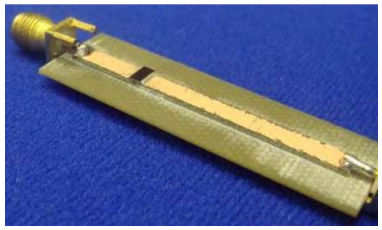

Figure 3-19: Photograph of the fabricated optical switch.

The optical switch was tested for nonlinearity in the ON state. Various digitally modulated input signals such as QPSK, 16QAM, 16QAMOFDM, 64QAMOFDM were used in order to evaluate nonlinear distortion produced in the final output spectrum. The following Figure 3-20 shows the comparison of intermodulation distortion in 3G signals.

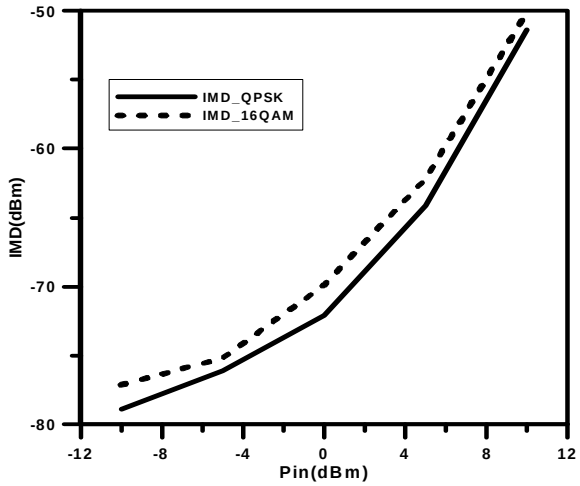

Figure 3-20: Comparison of intermodulation distortion for QPSK and 16QAM input signal for varying input power at 2GHz for an optical switch.

The distortion for 16QAM was much higher when compared with the distortions produced for QPSK input signal at the same input power. As expected, distortions increased with increasing input power and a distortion of -51dBm and -52dBm for 16QAM and QPSK signals respectively were measured. Figure 3-21 shows the output spectrum for 16 QAM signal measured at 2GHz.

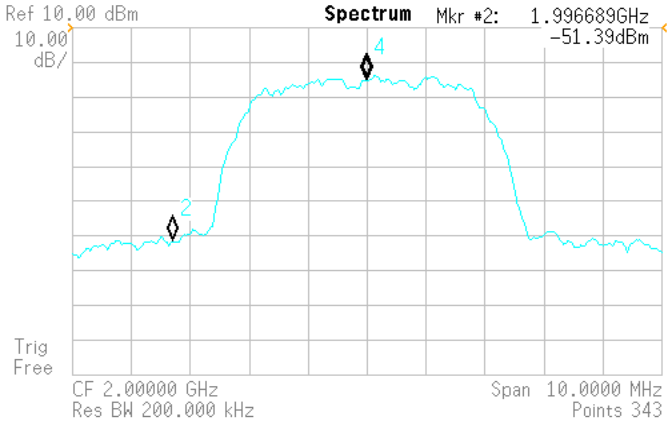

Figure 3-21: Measured 5MHz output spectra for the 16QAM input signal.

From Figure 3-21, it is evident that the distortion measured is quite severe and the relative distortion of 46.39dB was measured. The main channel creeps into the adjacent channel causing spectral growth and degradation of the primary output signal. The measurement was carried out at a frequency of 2GHz for an input power of 10dBm. Similar experimental verification was carried out for 4G signals (16QAMOFDM and 64QAMOFDM). The distortion comparison is shown in Figure 3-22 below:

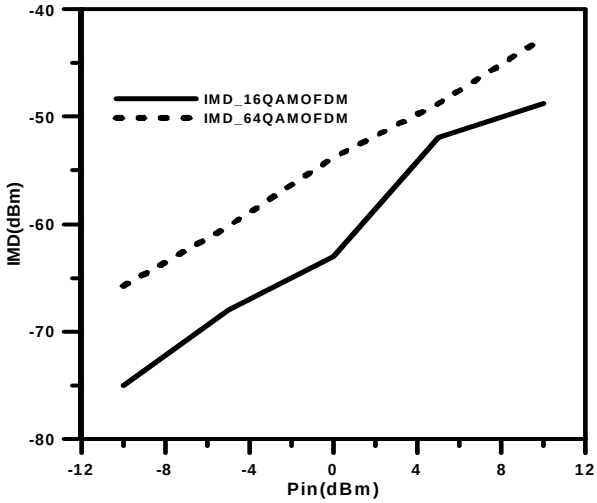

Figure 3-22: Comparison of intermodulation distortion for 16QAMOFDM and 64QAMOFDM input signal for varying input power at 2GHz for an optical switch.

From the above figure, it can be seen that the distortions for a more complex modulated signal such as 64QAMOFDM are more prominent with values reaching -42dBm, while 16QAMOFDM shows a value of -48dBm for the same input power. Figure 3-23 shows the output spectra of the 64QAMOFDM for an input power of 10dBm at 2GHz frequency.

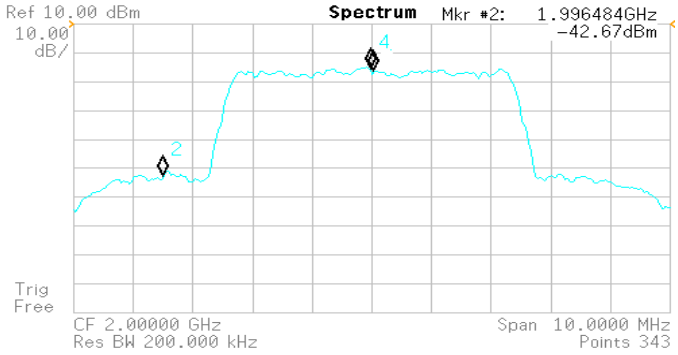

Figure 3-23: Measured 5MHz output spectra for the 64QAMOFDM input signal.

From Figure 3-23, the relative distortion measured is around 38dB which is quite high for many RF applications. Hence from the evaluations above, an optical switch can have high distortions depending on the type of the input signal and its power.

3.4 Distortion Evaluation of RF Reconfigurable Filters

In the previous section a detailed evaluation of the individual reconfigurable elements were presented. In recent years, these elements have been widely used in the development of reconfigurable and tunable RF components. This section deals with the distortion evaluation of reconfigurable filters which are widely used in various applications. Such filters are beneficial in many ways saving costs, space and are easy to use. The experimental set up used in order to evaluate these filters is shown in Figure 3-24.

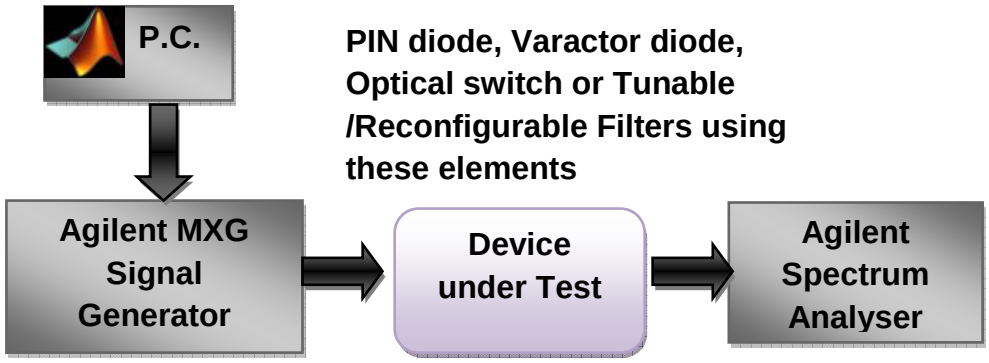

Figure 3-24: Experimental set-up for distortion evaluation in reconfigurable filters.

The personal computer (P.C.) helps in generating the suitable code using MATLAB for the 3G and 4G signals. These are transferred to the Agilent MXG Signal Generator which is then used as input signals. Some signals are in-built while others need to be created. The output spectrum is then captured with the help of Agilent Spectrum Analyser and relative distortion or adjacent channel power ratio is evaluated. The MXG helps in varying the power level of the input

signal. Hence a comprehensive set of results are obtained to evaluate distortions.

3.4.1 Filters using PIN diode as Reconfigurable Element

Filters using PIN diode as reconfigurable elements are widely found in literature. In [3.32] and [3.33], reconfigurable filters have been designed using PIN diodes. Such filters help in switching from one response to another. For example in [3.32], four PIN diodes are used in order to switch from a bandpass to a bandstop response. Here a reconfigurable ultra wide band (UWB) filter was chosen as DUT [3.34]. The filter is briefly described and then distortion results are presented.

The structure of the filter is shown below in Figure 3-25. The filter works as a bandpass filter in the ON state and as a bandstop filter in the OFF state. The PIN diode (BAP65-02) is placed on a 0.3 mm gap. The filter operates within 3.1-5GHz with the mid-band frequency at 4GHz.

Figure3-25: Photograph of the UWB reconfigurable filter (DUT).

The above filter is then evaluated for distortions using various input signals with varying power level. A two tone set up was used where the signals were placed 0.5MHz and 1MHz apart with centre frequency at 3.5GHz which falls in the passband of the filter. For the first case where 0.5MHz was used to space the two fundamental tones, it was found that the two fundamental frequencies were at 3.49975GHz and 3.50025GHz. Hence the third order intermodulation distortions will arise at 3.49925GHz and 3.50075GHz. For the second case, the fundamental tones were at 3.4995GHz and 3.5005GHz while the third order

IMD occurs at 3.4985GHz and 3.5015GHz. Figure 3-26 shows the spectrum captured in Agilent spectrum analyser. The IMD3 is prominently visible. The input power of 15dBm was chosen to show the maximum effect of distortions.

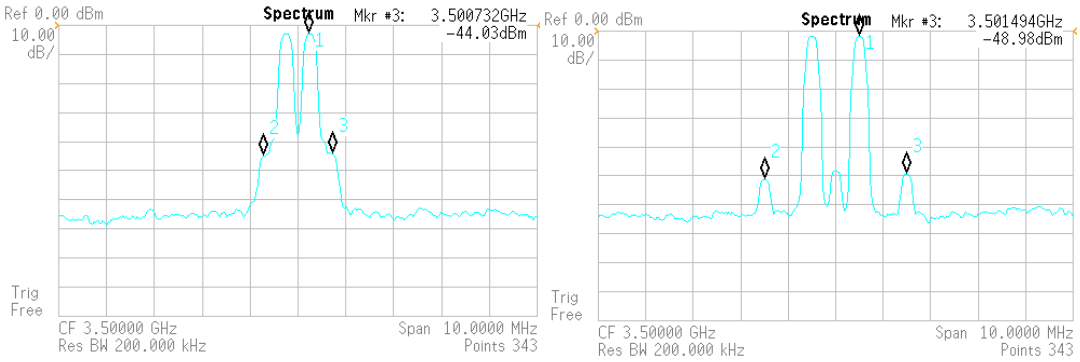

(a) (b)

Figure 3-26: Spectrum showing the 3rd order intermodulation distortion for a filter with PIN diode for P_{in} =15dBm (a) with 0.5MHz (b) with 1MHz spacing.

It is clear from the above figure that the distortions for 0.5MHz spaced fundamental signals are more than the distortions for 1MHz spaced signals. A similar result was found when the PIN diode was evaluated for distortions in the previous section. Figure 3-27 shows the comparison of the third order IMD for both cases along with the output power P_{out} when the input power P_{in} is varied.

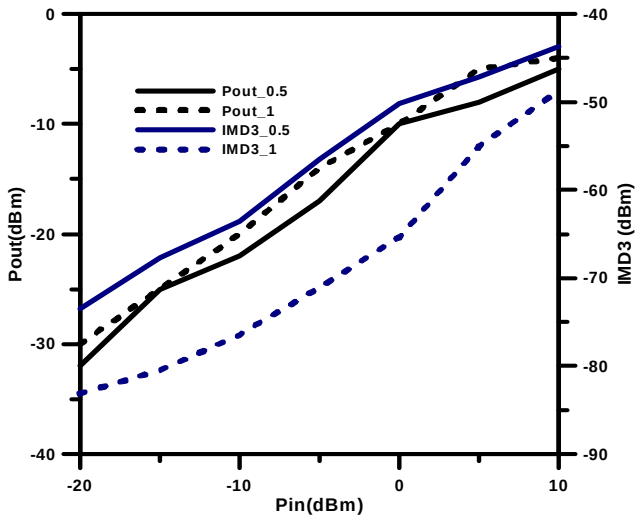

Figure 3-27: Variation of P_{out} and IMD3 with respect to various input power P_{in} for the reconfigurable filter using PIN diode.

From Figure 3-27, it can be seen that the distortions for 0.5MHz increases with increase in input power levels, while the distortions for 1MHz spacing remains considerably less for the same input power. Digitally modulated signals are also used in order to evaluate distortions in these types of RF filters. Both 3G and 4G signals which include QPSK, 16QAM, 64QAM, 16QAMOFDM and 64QAMOFDM are used to compare the distortions for varying power from -20 to 15dBm.

For the P_{out} represented in the graphs, it should be noted that this does not actually represent the actual output power. For digitally modulated signal, the measured spectrum is the power spectral density plots, where the Pout is just the power at a central point in the main channel. In order to calculate the real power of the main channel P_{out}, P(f) needs to be integrated from two defined points f_{m1} and f_{m2} as shown in Figure 3-28.

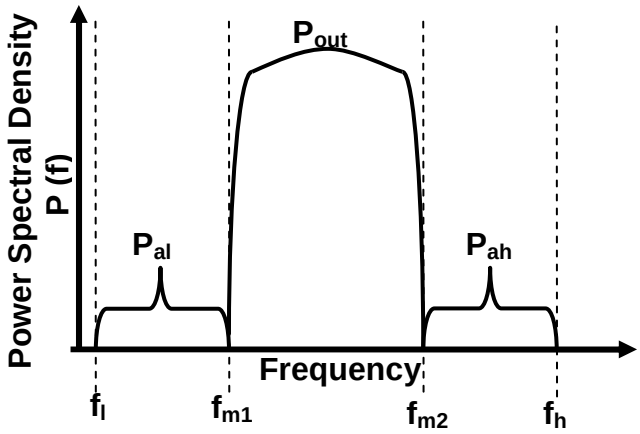

Figure 3-28: Graphical representation of P_{out} in digitally modulated signal.

Hence from the figure above, the P_{out} can be shown as the following equation.

$$P_{out} = \int_{f_{m1}}^{f_{m2}} P(f)df \quad (3.14)$$

$$P_{al} = \int_{f_l}^{f_{m1}} P(f)df \quad (3.15)$$

$$P_{ah} = \int_{f_{m2}}^{f_h} P(f)df \quad (3.16)$$

Where, P_{out} is the output of the main channel, P_{al} is the output of the lower adjacent channel and P_{ah} is the output of the higher adjacent channel, f_{m1} and

f_{m2} are the main channel frequency while f_l and f_h are lower and higher limit of the adjacent channel frequency as illustrated in Figure 3-28.

Figure 3-29 shows the variation of Pout and IMD for 3G signals using the reconfigurable filter as device under test against varying input power.

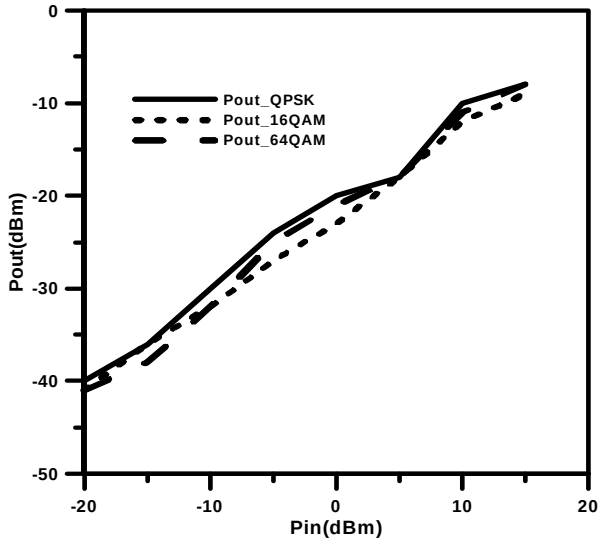

(a)

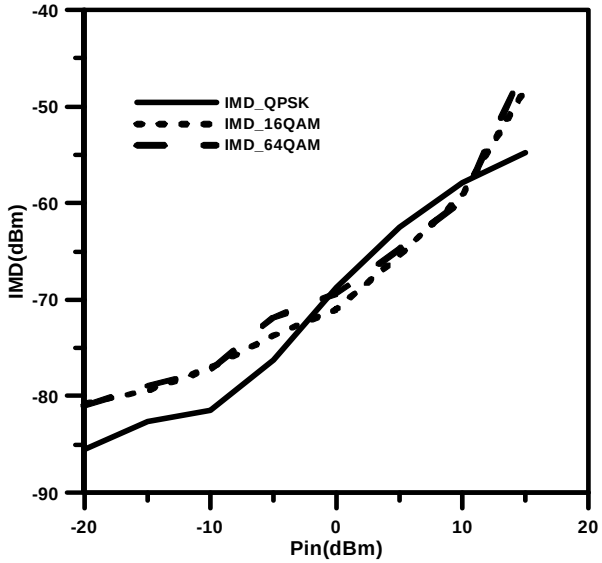

(b)

Figure 3-29: Variation of (a) P_{out} and (b) IMD with respect to various P_{in} for 3G signals using the reconfigurable filter as DUT.

From Figure 3-29 (b) it is clear that the distortions for 64QAM are much higher than 16QAM and QPSK for the same input power. The distortions are measured as -55dBm, -50dBm and -45dBm for an input power of 15dBm for

QPSK, 16QAM, 64QAM input signals. Figure 3-30 shows the spectrum captured with centre frequency at 3.5GHz and channel bandwidth 5MHz.

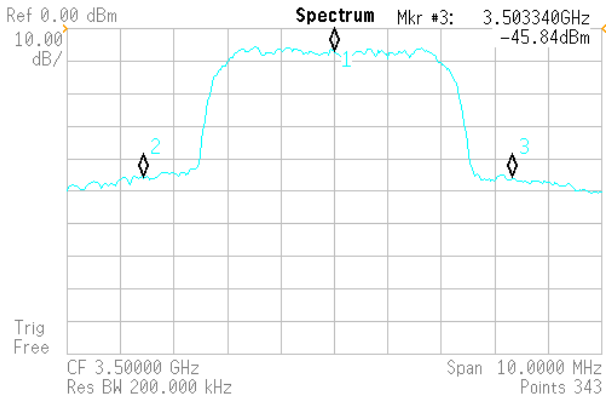

Figure 3-30: Measured 5MHz output spectra for the 64QAM input signal.

Relative distortion measured from the above figure is around 37dB for an input power of 15dBm. The main channel creeps into the adjacent channel causing distortions. The reconfigurable filter was also tested with various 4G signals. Figure 3-31 shows the variation of Pout and IMD with respect to the varying input power from -20 to 15dBm.

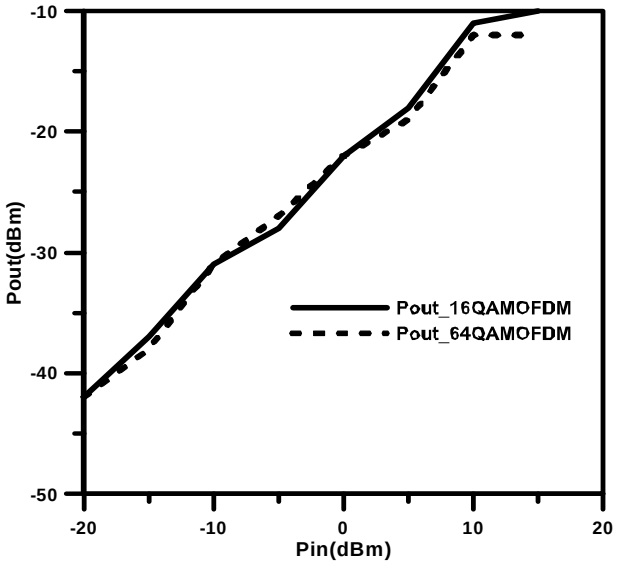

(a)

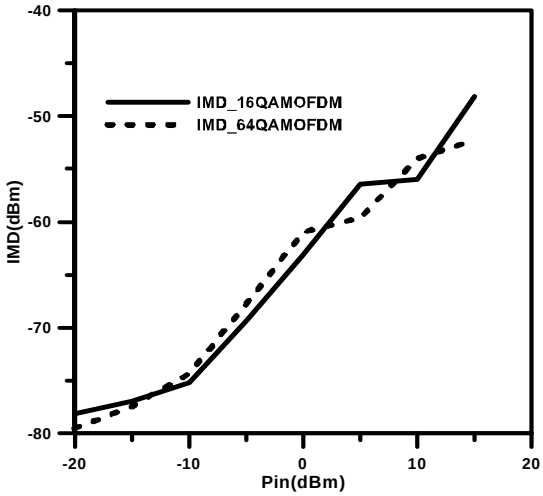

(b)

Figure 3-31: Variation of (a) P_{out} and (b) IMD with respect to various P_{in} for 4G signals using the reconfigurable filter as DUT.

The distortion measured for 16QAMOFDM is -46dBm while for 64QAMOFDM the distortion was -52dBm for the same input power of 15dBm. The distortions increase with increase in input power from -20 to 15dBm. Figure 3-32 shows the spectral representation of the output measured at 3.5GHz. An input power of 15dBm was used.

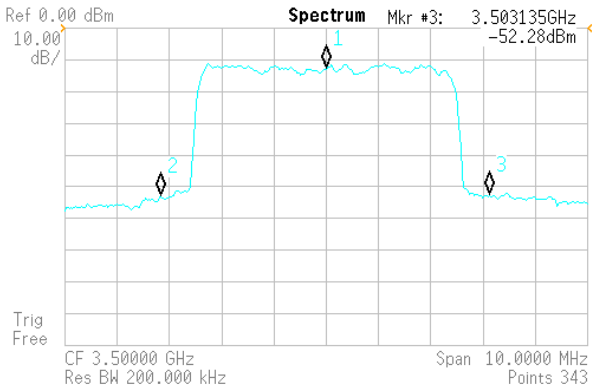

Figure 3-32: Measured 5MHz output spectra for the 64QAMOFDM input signal.

The relative distortion measured was 41.28dBm approximately. Measured results shows that the filter can be nonlinear when subjected to high power applications.

The second filter which also uses a PIN diode for switching is shown in Figure 3-33. A pair of identical switches is placed across the gaps for switching between the ON and OFF states. When the switches are ON, the gaps are bridged and the structure behaves as a second order bandpass filter. A second order switchable filter at 1.5GHz centre frequency was evaluated for distortions [3.35].

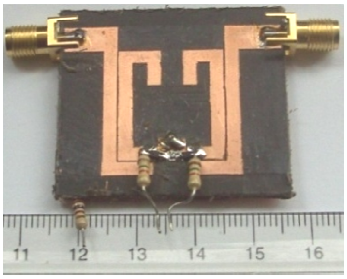

Figure 3-33: Photograph of the switchable filter with inserted PIN switches and biasing resistors.

Distortion of the switchable filter was evaluated in the ON-state using 5MHz digitally modulated signals such as QPSK,16QAM ,16QAMOFDM and 64QAMOFDM using the test setup shown in Figure 3-24 above. In this filter the effect of different bias voltage on the intermodulation distortion has been evaluated. The measured spectra are illustrated in Figure 3-34. The measured results produce more distortions for a lower bias voltage as compared to a higher value. Additionally, the distortions are more evident at higher values of input power. The distortions are measured using marker 2.

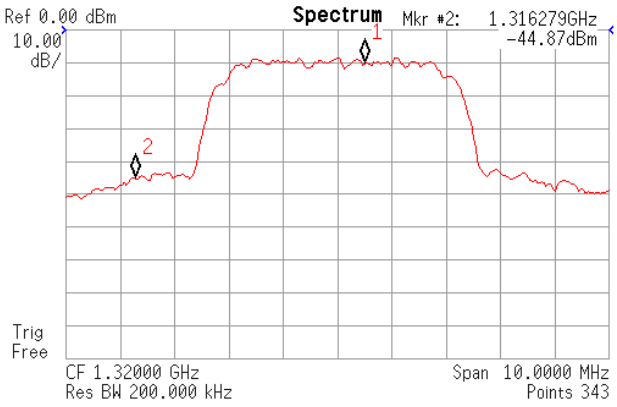

(a)

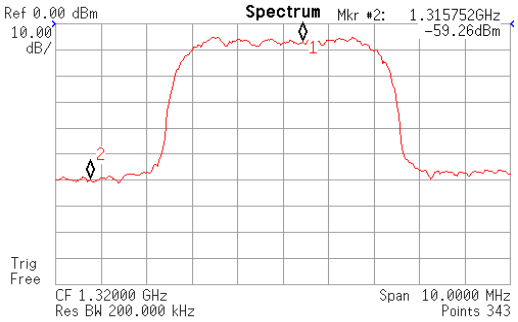

(b)

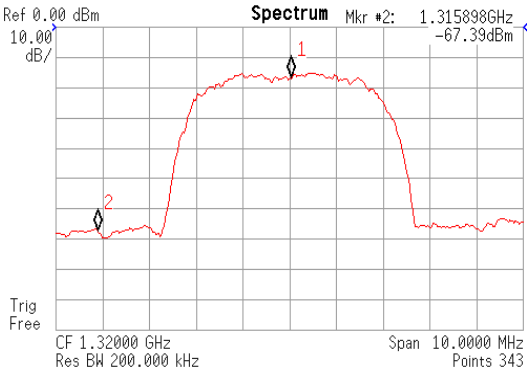

(c)

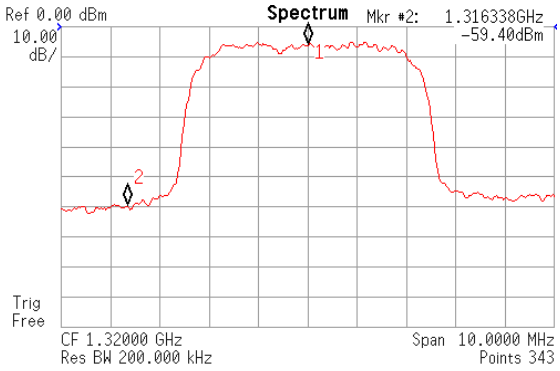

(d)

Figure 3-34: Measured 5MHz 16 QAM spectra of the filter for (a) 5V and (b) 9V forward biasing. Measured 5MHz QPSK spectra of the filter for (c) 5V and (d) 9V forward biasing.

Distortion power against input signal power for various bias voltages are illustrated in Figure 3-35 for both 16 QAM and QPSK signals. The results confirm the fact that the distortions are more for a higher input power level and low bias voltage. There is a slight difference between QPSK and 16 QAM results but both show similar findings.

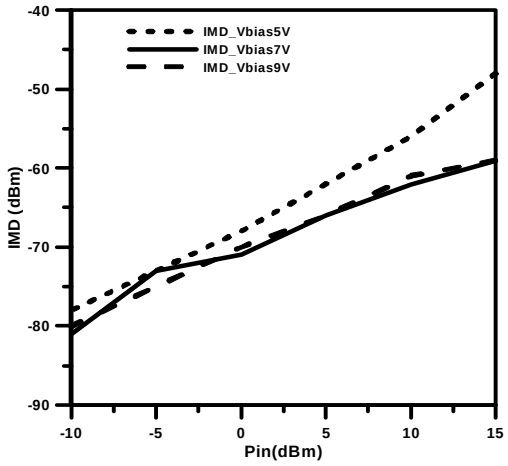

(a)

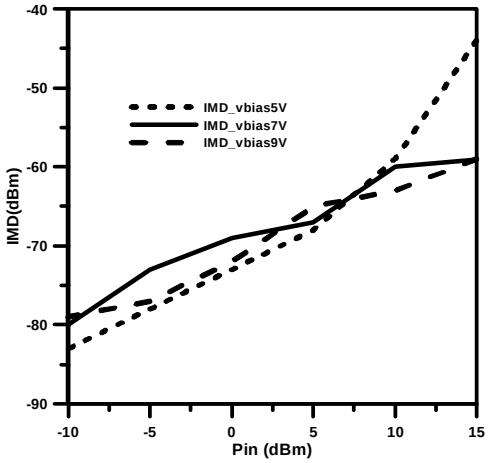

(b)

Figure 3-35: (a) Comparison of the distortions for a range of input power values with three different bias voltages for QPSK input signal (b) Comparison of the distortions for a range of input power values with three different bias voltages for 16 QAM input signal.

The filter was further tested with LTE signals in order to see the effect of nonlinear distortion.The relative distortions measured for both signals are nearly equal at the same input power of 10dBm being equal to 42dB and 41dB. The switchable filter is linear but for high power application can tend to show nonlinear distortions. The following Figure 3-36 shows the measured spectra for the 4G signals measured at 1.5GHz which is the centre frequency of the filter in the ON state.

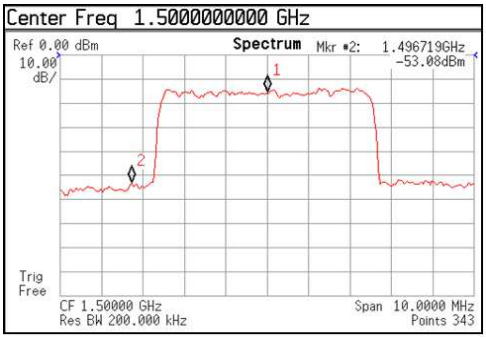

(a)

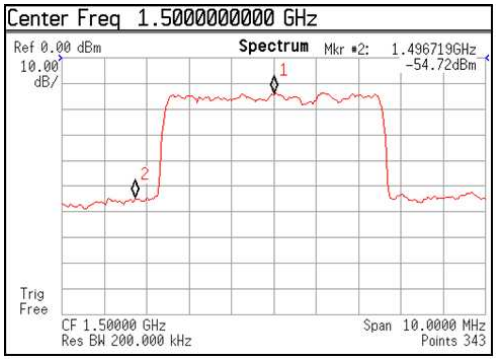

(b)

Figure 3-36: Measured 5MHz (a) 16QAMOFDM (b) 64QAMOFDM spectra at the output of the optical switch filter at 1.5GHz for P_{in}=10dBm in the ON state.

For both spectrums captured, the distoritons are nearly equal with slight variation of 1dB. The following Figure 3-37 shows the variation of P_{out} and IMD with varying input power P_{in}.

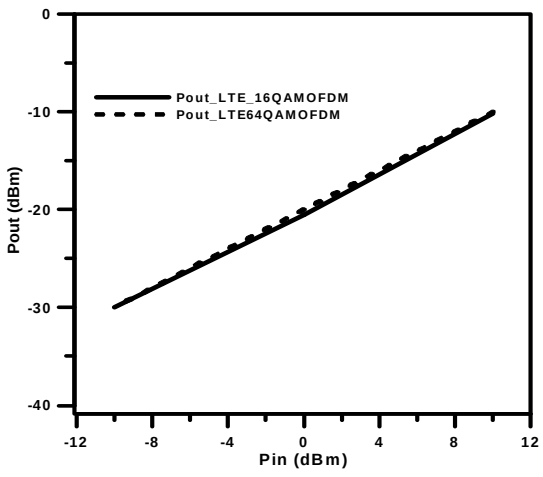

(a)

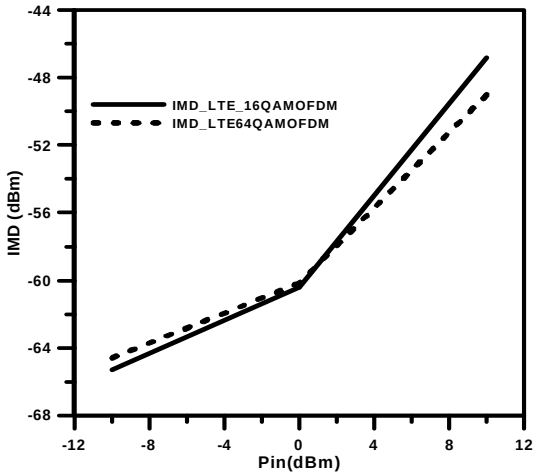

(b)

Figure 3-37: Comparing the (a) output power spectrum and (b) distortion power spectrum against the input power for 4G digitally modulated signals.

The above figure shows the output spectrum using 4G 16QAM and 64QAM OFDM respectively as input signals. The output clearly has certain amount of distortions. The IMD has been plotted against the input power and it is clearly seen that the distortions increases for higher power levels. The plot for the output power spectrum is linear indicating that the filter is also linear in nature. Nonlinear distortion evaluation of a dual-mode PIN switched microstrip bandpass filter was presented. As expected, the linearity of the filter suffers more at higher input powers.

3.4.2 Filters using Optical Switch as Reconfigurable Element

This section deals with the evaluation of distortion of RF filters using optical switch as the switching element. For this purpose a reconfigurable UWB bandpass filter, is taken and distortions evaluated. The filter layout is shown in Figure 3-38 which has a 3dB passband from 3.1GHz – 5.0GHz with a mid-band frequency of 4GHz [3-34] & [3-36].

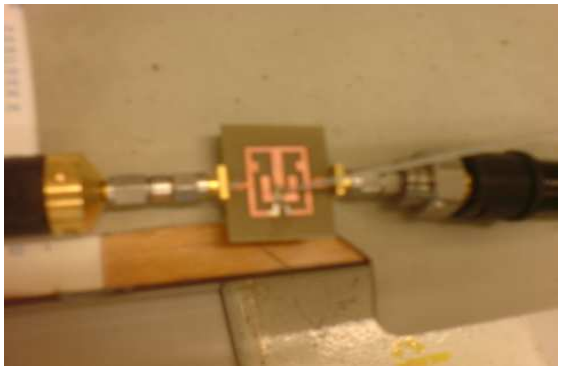

Figure 3-38: Proposed fabricated filter with optical switch.

For linearity validation purposes, the linearity characteristics of the proposed filter were assessed using various digitally modulated signals such as quadrature phase shift keying (QPSK), 16 quadrature amplitude modulation (QAM), 64QAM, 16QAMOFDM and 64QAMOFDM. Input power (P_{in}) ranging from -10dBm to 10dBm produced excellent linearity performance at 2.6GHz carrier frequency. The following Figure 3-39 shows the output power and the IMD vs. the input power for the proposed filter. The 3G signals were generated through the MXG and passed through the device under test. The optical switch was illuminated by a laser light of 200 mW power. The spectrum was measured for each input power level in the ON state of the optical switch.

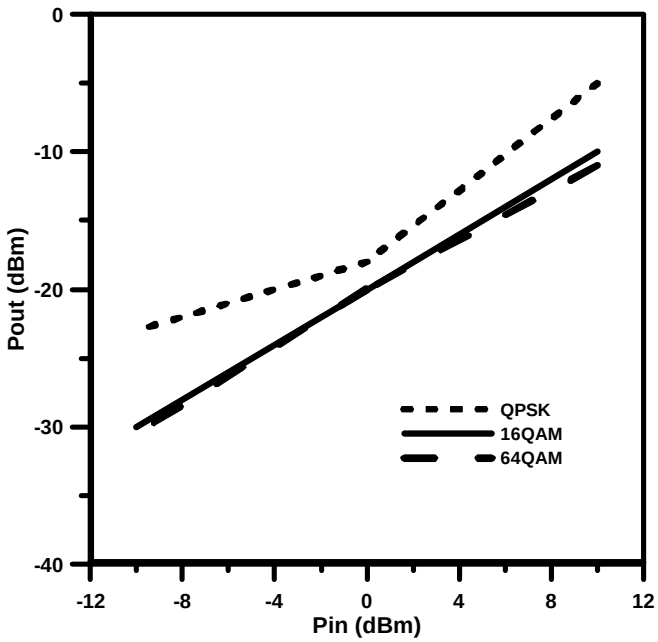

(a)

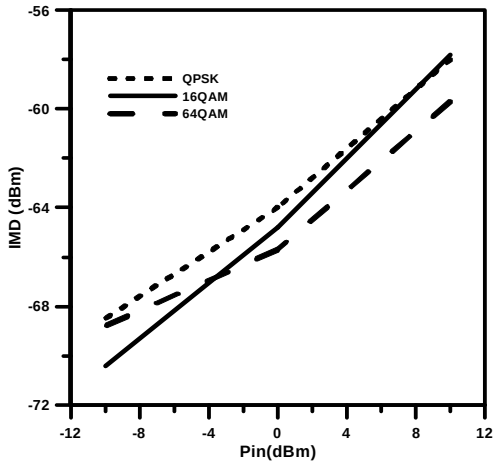

(b)

Figure 3-39: Measured response for (a) output power P_{out} (b) IMD vs. P_{in} for different digitally modulated signals (3G) for 2.6GHz carrier in the ON state of the optical switch.

The distortions occur near the junction of the main channel and the adjacent channel as shown in Figure 3-40. Using the spectrum, the relative distortion for each can be calculated. The figure shows the output spectrum at 2.6GHz for an input power of 10dBm.

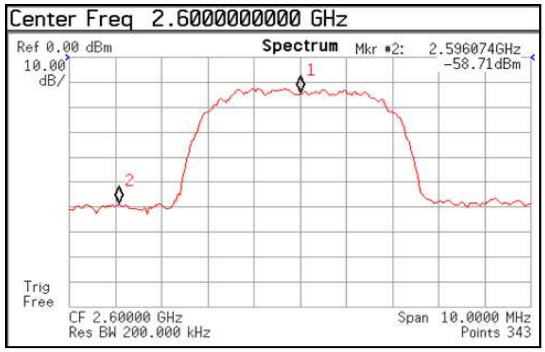

(a)

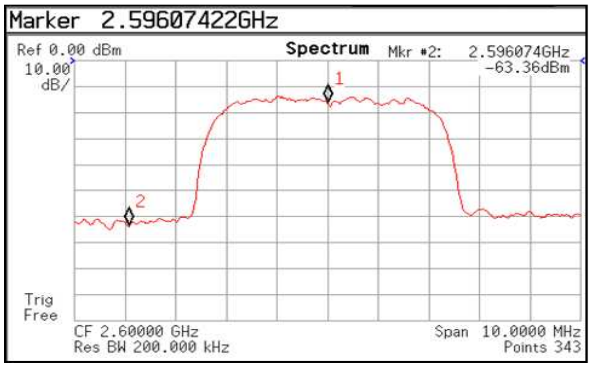

(b)

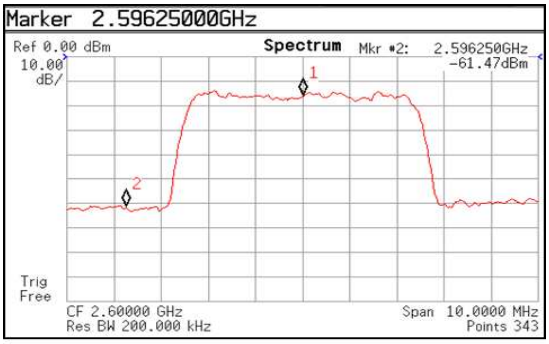

(c)

Figure 3-40: Measured 5-MHz (a) QPSK (b) 16 QAM and (c) 64 QAM spectra at the output of the proposed filter at 2.6GHz carrier for 10dBm input power in the ON state of the optical switch.

The relative distortions measured for QPSK, 16QAM and 64QAM are 46dB, 51dB and 48dB respectively. Even though the distortions generally increase with increase in modulation complexity, it was seen that the QPSK input signal had more distortions as compared to the other two signals. This was possibly due to interference or noise and measurement error.

The following Figure 3-41, shows the distortion levels measured for the filter with optical switch in the ON state using 16QAM and 64QAM OFDM digitally modulated signals.

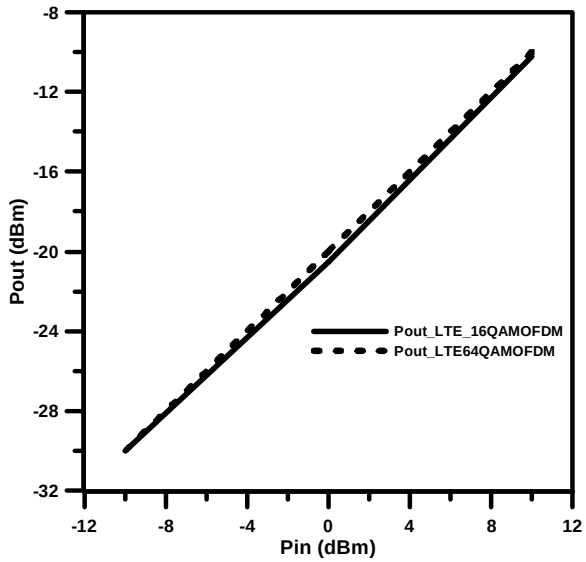

(a)

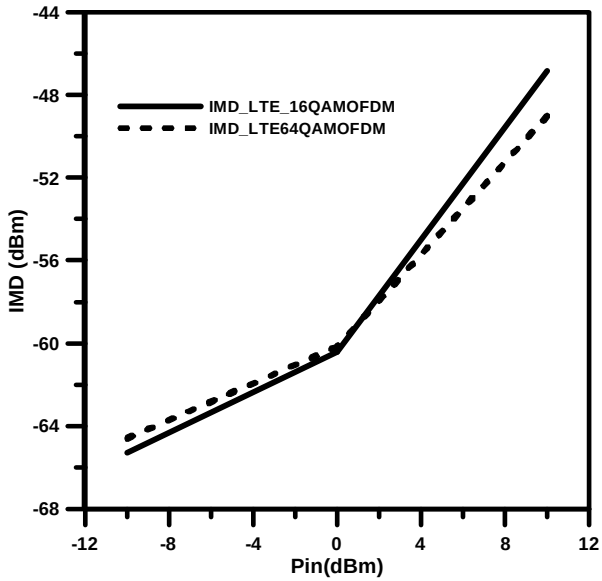

(b)

Figure 3-41: Variation of (a) Pout (b) IMD vs. P_{in} for different 4G digitally modulated signals for 2.6GHz frequency in the ON state.

From the figure above, the output power spectrum has a linear curve when plotted against the input power indicating that the filter has a linear response. The distortions are not significant, though a higher distortion is noticed with higher values of input power. The following Figure 3-42 shows the measured response for different digital LTE signals with 5MHz bandwidth. The distortions in the output spectrum gradually increase with higher input power.

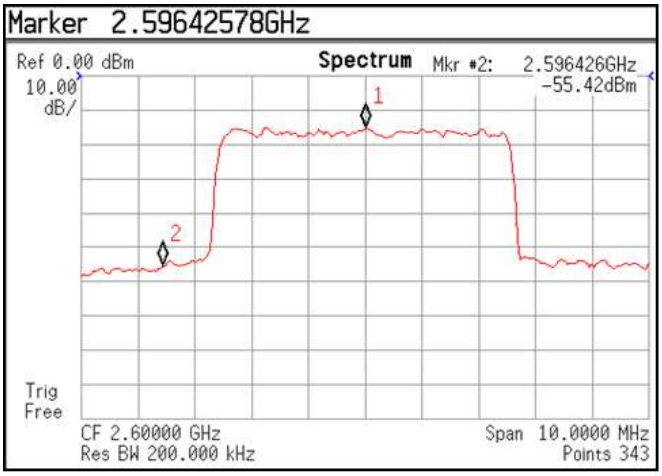

(a)

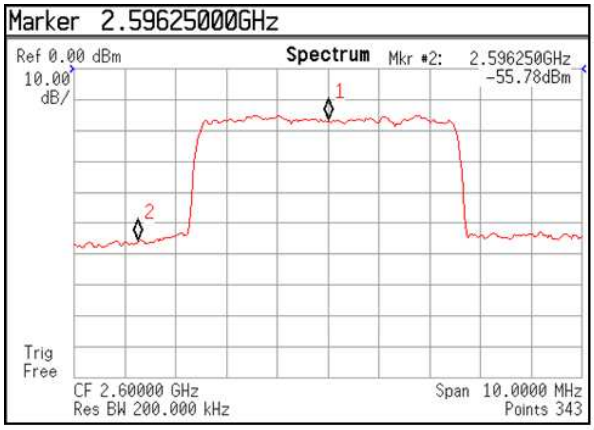

(b)

Figure 3-42: Measured 5-MHz spectra at the output of the optical switch filter at 2.6GHz for (a) 16QAMOFDM and (b) 64QAMOFDM for 10dBm input power for different 4G input signals for the ON state.

Figure 3-42 shows that the increase of nonlinear distortions with input power. The upper adjacent channel power ratio (ACPR) is also measured and tabulated in Table 3-2 & 3-3 for both 16QAM and 64QAM OFDM input signals respectively. Marker 1 represents the average power level of the main channel (P_{out}) while Marker 2 represents the average power level of the lower adjacent channel (IMD). The output spectra for the higher input power level of 10dbm are presented. This is a measure of the relative distortion in the lower channel or the difference between the main channel average power level and the lower adjacent channel average power level. Due to the effects of nonlinearity, the signal in the adjacent channel sometimes interferes with the main channel signal. This leads to spectral regrowth. Hence relative distortion gives a good measure for digitally modulated signals. Higher the relative distortion more is the linearity of the DUT.

PIN (dBm)	**POUT (dBm)**	**IMD (dBm)**	**ACPR (dB)**
-10	-30	-70.6	40.6
0	-20.5	-60.4	39.9
10	-10.2	-46.8	36.6

Table 3-2: Measured data for distortion evaluation using 16QAMOFDM.

PIN (dBm)	POUT (dBm)	IMD (dBm)	ACPR (dB)
-10	-30	-71.2	41.2
0	-20	-60.17	40.17
10	-10	-49.02	39.02

Table 3-3: Measured data for distortion evaluation using 64QAMOFDM.

Table 3-2 & 3-3 shows the tabulated measured value of the output spectrum for 16QAM OFDM and 64QAM OFDM input signal respectively. By comparing the relative distortion or ACPR we can see that with higher power levels, distortion increases. Overall the filter is highly linear and can be used in most applications.

3.5 Conclusion

This chapter introduced the main concepts of nonlinear distortions including numerical analysis of third order intermodulation distortion, power series analysis and using two tone tests for distortion measurements. The various elements used in RF reconfigurable/tunable circuits such as PIN diodes, varactor diodes and optical switches were introduced. A comprehensive set of simulations to establish the amount of distortion were presented for all three components.

Further experimental verification was made for PIN diodes and optical switches using various input signals with power varying from -20dBm to 15dBm. The results were thoroughly discussed and a set of comparison was given among various other tunable/switchable elements such as RF MEMS, liquid crystal etc. Few reconfigurable filters using PIN switch and optical switch were further evaluated for distortions. A variation of input power, bias voltage, 3G and 4G signals have been used to measure and evaluate distortions to get a complete picture. Measuring the nonlinear distortion of these components helps in quantifying the amount of nonlinear distortion contribution made by such elements in a transceiver system when interfering signals form additional distortion products in the final output.

3.6 References

[3.1] Q.Gu, RF System Design of Transceivers for Wireless Communications, Springer, 2005, ISBN: 978-0-387-24161-6.

[3.2] S. Maas, *Nonlinear Microwave and RF Circuits*, Artech House Publishers, 2003, ISBN 1580534848.

[3.3] D. Pozar, *Microwave Engineering*, 3rd edition, John Wiley & Sons, 2004, ISBN0471170968.

[3.4] J. C. Pedro, and N. B. De Carvalho, "On the use of multi-tone techniques for assessing RF components' intermodulation distortion," *IEEE Transactions on Microwave Theory and Techniques*, vol. 47, no. 12, pp. 2393-2402, Dec. 1999.

[3.5] J. Vuolevi, T. Rahkonen, *Distortion in RF Power Amplifiers*, Artech House Inc., 2003, ISBN 1580535399.

[3.6] G. Collins, and D. W. Runton, "Nonlinear analysis of power amplifiers," *Microwave Journal*, vol. 50, no. 9, p. 164, Sept. 2007.

[3.7] B. Carey-Smith, and P. Warr, “Distortion Mechanisms in Varactor Diode-Tuned Microwave Filters”, *IEEE Transactions on Microwave Theory and Techniques*, Vol-54, No-9, Sept 2006, pp. 3492-3500.

[3.8] B. Doherty, “PIN Diode Fundamentals”, Microsemi Watertown, MicroNote Series 701, available from < http://www.microsemi.com/micnotes/701.pdf> accessed on 14th January, 2011.

[3.9] R.Caverly and G. Hiller, “Distortion Properties of MESFET and PIN Diode Microwave Switches” *IEEE MTT-S Digest*, 1992, pp. 533-536.

[3.10] R.Caverly and G. Hiller, “Distortion in p-i-n Diode Control Circuits” *IEEE Transactions on Microwave Theory and Techniques*, Vol.MTT-35,No-5,May 1987, pp.492-501.

[3.11] BAP65-02 Product Data Sheet, NXP Semiconductors, January 2008.

[3.12] K.Rabbi, L. Athukorala, C.J. Panagamuwa, J.C. Vardaxoglou, D.Budimir, “High-Linearity Reconfigurable Microstrip UWB Bandpass Filters” *IEEE Microwave and Wireless Components Letters*, Oct 2010.

[3.13] M. Watertown, “The PIN diode circuit designers’ handbook,” Microsemi Corporation, Santa-Ana, CA, Jul. 1992.

[3.14] V. Cojocaru and F. Sischka, "Non-linear modelling of microwave PIN diode switches for harmonic and intermodulation distortion simulation," *Microwave Symposium Digest, 2003 IEEE MTT-S International* , vol.2, no., pp.655,658 vol.2, 8-13 June 2003.

[3.15] B. Carey-Smith, and P. Warr, "Distortion Mechanisms in Varactor Diode-Tuned Microwave Filters", *IEEE Transactions on Microwave Theory and Techniques*, Vol-54, No-9, Sept 2006, pp. 3492-3500.

[3.16] V. Sekar and K. Entesari, " Nonlinear Nodal Analysis of Varactor-tuned Microwave Filters" ,*Proceedings of the 40th European Microwave Conference* , Paris, Sept 2010, pp. 1241-1244

[3.17]Skyworks Solutions "Varactor Diodes", available from <http://www.skyworksinc.com/uploads/documents/200824a.pdf> accessed on 20th September, 2012.

[3.18] V. Sekar and K. Entesari, " Nonlinear Nodal Analysis of Varactor-tuned Microwave Filters" ,*Proceedings of the 40th European Microwave Conference* , Paris, Sept 2010, pp. 1241-1244.

[3.19] K.Buisman, L.C.N. de Vreede, L.K. Nanver, ""Distortion-Free" Varactor Diode Topologies for RF Adaptivity" *IEEE, 2005*, pp.157-160.

[3.20] K.Buisman, C.Huang, A.Akhnoukh, L.K.Nanver,"Varactor Topologies for RF Adaptivity with Improved Power Handling and Linearity", *IEEE, 2007*, pp-319-322.

[3.21] C. H. Lee, P. S. Mak, and A. P. DeFonzo, "Optical control of millimetre wave propagation in dielectric waveguides," IEEE J. Quantum Electron., vol. 16, no. 3, pp. 277–288, 1980

[3.22] D. Draskovic and D. Budimir, *"Optically controlled negative refractive index transmission lines"*, *European Conference on Antennas and Propagation*, pp. 1672-1674, 2009.

[3.23] C.J. Panagamuwa, A. Chauraya and J.Y.C Vardaxoglu, "*Frequency and beam reconfigurable antenna using photoconducting switches*", *IEEE Transactions of Antennas and Propagation*, vol. 54, No. 2, pp. 449 -454, 2006.

[3.24] G. Zouganelis and D. Budimir, "Silicon gap-loaded microstrip slit-tetragonal resonator under IR-radiation", *Microwave and Optical Technology Letters*, vol. 49, pp. 699-702, 2007.

[3.25] D. Draskovic and D. Budimir, *"*Optically reconfigurable dual-band compact branch-line couplers*"*, *European Conference on Antennas and Propagation*, pp. 1-3, 2007.

[3.26] G.M.Loubriel, F.J. Zutavern, A.G. Baca, H.P. Hjalmarson, T.A. Plut, W.D. Helgeson, M.W. O'Malley, M.H. Ruebush and D.J. Brown, "Photoconductive semiconductor switches," *Plasma Science, IEEE Transactions on* , vol.25, no.2, pp.124,130, Apr 1997.

[3.27] A. Karabegovic, M. Robert O'Connell and W.C. Nunnally, "Photoconductive Semiconductor Switch for Microwave Applications," *IEEE International Power Modulators and High Voltage Conference, Proceedings of the 2008*, vol., no., pp.9, 12, 27-31 May 2008.

[3.28] T. Bouchemat, F. Hobar, A. Koster, S. Laval, M. Bouchemat, and D. Pascal. "Theoretical study of a nonlinear fast silicon photoconductive switch." *The European Physical Journal Applied Physics* 6, no. 02, 1999, pp: 165-169.

[3.29] G.M.Loubriel, et al., "Longevity of optically activated, high gain GaAs photoconductive semiconductor switches", IEEE Transactions on Plasma Science, vol. 26, no. 5, October 1998, pp1393–1402.

[3.30]Federal Communication Commission, "Revision of part 15 of the Commission's rules regarding ultra-wideband transmission systems", <http://transition.fcc.gov/Bureaus/Engineering_Technology/Orders/2002/fcc02048.pdf > Accessed on 19th Aug 2014.

[3.31] National Telecommunication and Information Administration, "Spectrum Sharing Innovation Test-bed Pilot Program Phase 1 Test Plan", February 2009, <http://www.ntia.doc.gov/files/ntia/publications/phase_i_test_plan_final_02122009.pdf> Accessed on 20th Aug 2014.

[3.32] M.F. Karim, Y.X Guo, Z.N. Chan and L.C. Ong, "Miniaturized reconfigurable and switchable filter from UWB to 2.4 Hz LAN using PIN diodes", IEEE MTT-S, pp. 509-512, 2009.

[3.33]Y.H. Chun, H. Shamman, J.S. Hong, "Switchable embedded notch structure for UWB bandpass filter", IEEE Microwave and Wireless Component Letters, vol. 18, no. 9, pp. 590 –592, 2008.

[3.34] K. Rabbi, L. Athukorala, C.J. Panagamuwa, J.C. Vardaxoglou, D. Budimir, "High-linearity reconfigurable microstrip UWB bandpass filters,"

Microwave Integrated Circuits Conference (EuMIC), 2011 European , vol., no., pp.172,175, 10-11 Oct. 2011.

[3.36] K. Chakrabarty, L. Athukorala and D. Budimir, "High linearity switchable dual-mode microstrip bandpass filters," *Microwave Conference Proceedings (APMC), 2011 Asia-Pacific* , vol., no., pp.1019,1022, 5-8 Dec. 2011.

Chapter 4 Compact Microstrip Bandstop Filters

Bandstop filters can be used in many applications where a selected band of frequency needs to be suppressed. In many wireless applications, a strong interfering signal can appear which will play havoc with the main signal spectrum. In such cases, filtering is essential and bandpass filters fails to be as effective in filtering out such interfering signals especially when they lie in the passband. These leads to the usage and design of bandstop filters capable of filtering out selected signals at particular frequency.

As a consequence of interfering signals in wireless systems, additional nonlinear distortions are noticed. In any real system, cross modulation, interference due to noise or other channels etc are a common phenomenon. These can lead to further degradation of the output spectrum as it will combine with the main channel signal and when passed through circuits with nonlinear transfer function will result in additional distortions. Hence a simple bandstop filter can be used to attenuate the interfering signal by choosing a suitable centre frequency of the bandstop filter. This prevents the use of complex algorithms and helps in saving costs. The application of such a bandstop filter will be discussed in detail in the next chapter.

The above problem leads to another important question of specification for the BSF. The primary requirement for such a filter would be a relatively narrowband response with enough attenuation to kill the interfering signal completely. Stepper transition bands will signify a better filter as only one particular interfering signals needs to be eliminated from a group of wanted signals [4.1]. Another point to be noted while designing such a filter is to make sure that the size of the filter does not increase too much, as it will increase the overall cost and complexity of the system. Figure 4-1 shows the response of the bandstop filter required for such a purpose. Designing such a bandstop filter in microwave frequency is a challenge as a trade-off has to be made in order to design a bandstop filter which can be realized in reality while it achieves the necessary goals. This chapter deals with the design of novel miniaturized

bandstop filters using defected microstrip structures which can be used in applications mentioned above.

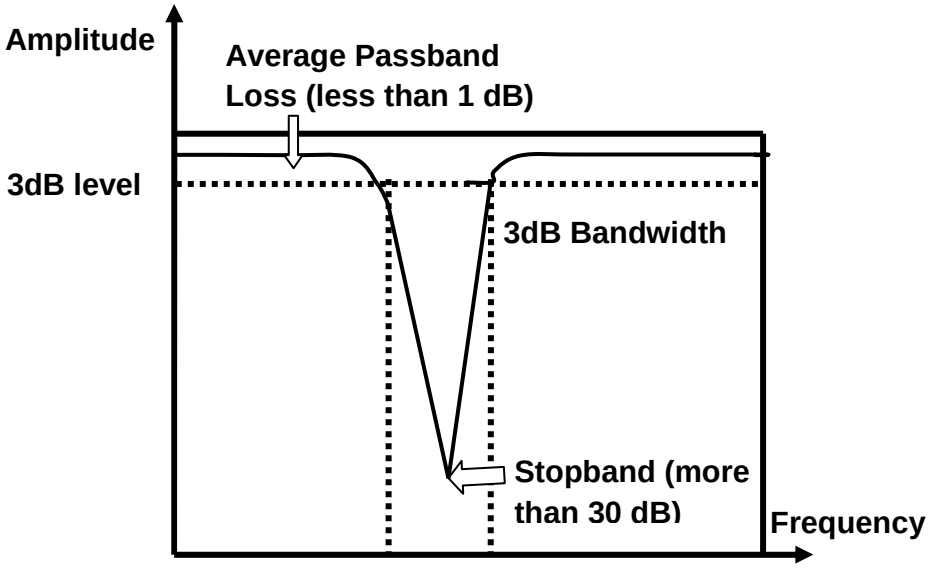

Figure 4-1: Typical bandstop filter response.

A typical response of a bandstop filter is shown where the attenuation can be specified according to the system requirement. There is a slight loss in the passband. Care should be taken to have minimum loss in this particular case, as the main signal falls in the passband of the BSF and shouldn't suffer from too much passband loss. Stepper the stopband, better is the selectivity of the filter which will be beneficial in cases where only one interfering signal needs to be eliminated out of all the other good signals.

4.1 Microstrip Bandstop Filter Design

In recent years advancements in the theory of novel microstrip bandstop filter include the analysis of new technology using photonic band gap (PGB) theory. A simple bandstop filter using traditional planar microstrip technology consists of $90°$ short circuited stub coupled through a gap to the main transmission line. The stubs act as inductors while the gap acts as capacitance when compared to the lumped element equivalent [4.2]-[4.3]. Previous bandstop filter theory included the use of folded line topology in order to make a

compact filter [4.4]. Design of BSF includes the use of open circuited stubs which leads to radiation and launching of surface waves. In order to overcome these problems new compact type of filter was proposed in [4.5]. A new class of BSF was proposed in 1964 and then in 1977 with the introduction of spurline filters which are not only very compact but also has very little radiation effects [4.6]. Microstrip BSF using dielectric resonator was also proposed in [4.7]. In more recent years, direct coupled BSF are proposed as in [4.8] and [4.9]. Another interesting concept proposed in [4.10] is BSF design using cancellation technique of the broadband phase. Recent exploration of another range of microstrip bandstop filters which are absorptive in nature as opposed to reflective structures are proposed in [4.11]. In literature, several such structures have been developed as recent as 2009 as seen in [4.12]-[4.15]. The proposed filters have quasi infinite attenuation and do not change with tuning the filter over a wide range of frequencies [4.12].

A design of conventional microstrip bandstop filter and its response is shown in Figure 4-2. The design is made in Agilent Advanced Design System (ADS). It contains open circuited stub connected directly to the microstrip line.

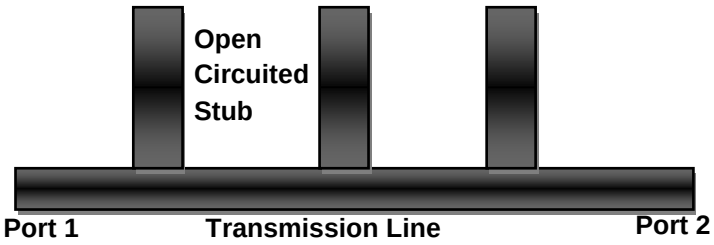

(a)

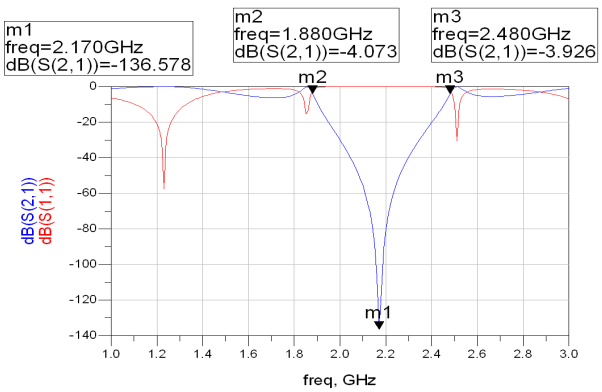

(b)

Figure 4-2: (a) Layout and (b) S-parameters of the microstrip bandstop filter.

The above structure has been designed in ADS using transmission lines and quarter wavelength resonators. The transmission zeroes for the above circuit is created at 2.18GHz. The S-parameter response of the BSF shows an attenuation of nearly 140dB. As can be seen from the above response, the filter has a very good attenuation but while calculating the 3dB bandwidth of the BSF from the markers m2 and m3 it was found to be 0.6GHz. While trying to optimize the circuit further it was noticed that there is an inverse relationship to the amount of attenuation that can be achieved and the bandwidth of the filter. Hence a balance was created, but this structure can be further improvised to get a narrower bandwidth but at the expense of attenuation in the stopband. The downside of the structure is the increased size of the filter.

Another example of a coupled microstrip bandstop filter is shown in Figure 4-3. The design which is discussed here is that of a compact microstrip bandstop filter and has a miniaturized structure with a narrower bandwidth, but the attenuation of the filter, is reduced to around 16dB. The following Figure 4-3 shows the layout of the structure developed in EM Sonnet.

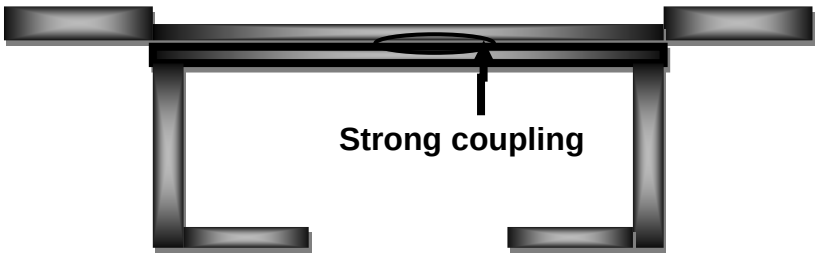

Figure 4-3: Layout of the proposed structure of the bandstop filter.

As can be seen, there is a strong coupling between the two transmission lines as shown in the figure above. A hairpin structure has been implemented with the u-shaped resonator folded in order to reduce space. The resonator is strongly coupled to the main transmission line through a gap. The gap is capacitive in nature. The variation of the coupling determines the response of the filter. With a weaker coupling the stopband response is degraded. Figure 4-4 shows the measured response of the fabricated filter.

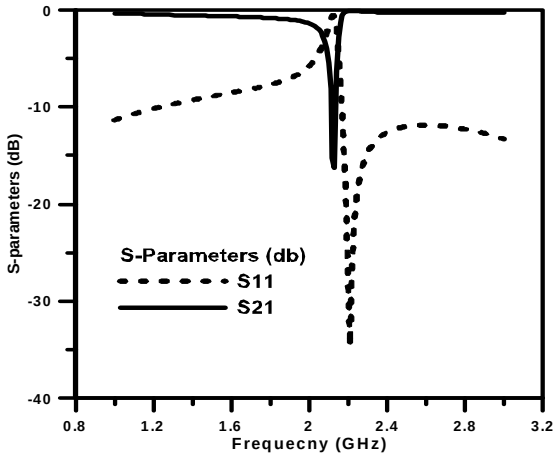

Figure 4-4: Measured S-parameters of the designed bandstop filter.

As can be clearly seen from Figure 4-4, the 3dB bandwidth is now 0.07GHz. The attenuation of the filter however is around 16dB. This BSF can be used in cases where weak signal with low amplitude needs to be filtered out. A deeper attenuation would have been better suited when the interfering signal in question has a much stronger presence. But a trade-off had to be made as a narrower bandwidth is an essential property for getting rid of isolated interfering signals. Therefore this filter can be used in situations where there are weak interfering signals. The filter passband shows less than 3dB loss. Overall the filter is quite compact with good filter response.

A major problem that may arise with the above fixed filter is the appearance of interfering signals at some other frequency other than the stopband of the filter. Then the designed filter renders itself useless in such cases. Hence certain amount of flexibility is required in order to make these filters applicable to a wider field. The introduction of dual and triple- band bandstop filters are made for this reason. In this case there will be two or three bands available for the suppression of more than one interfering signal. This is a slightly better case than single fixed band BSFs. A much flexible and cost saving approach would be the use of tunabale/reconfigurable filter. Using tuning elements such as varactor diode, PIN switch etc, where the centre frequency of the filter can be electronically tuned enabling the use of such filters in a wider range of application. In certain events the filter needs to be completely switched off in the system when no interfering signals are present. One solution to this problem is to design the filter with a switching element such as a PIN diode or an optical

switch in a way that it acts as a bandstop filter when the switch is ON and as an allpass filter when the switch is OFF. In this way the unnecessary filter can be bypassed in the system when not in use.

The dual-band bandstop filter has two distinct bands at separate frequencies which can help systems where two interfering signals at either side of the main passband are present. For example, a RF transmitter Tx1 operates at 2.5GHz. There are two more RF transmitters Tx2 and Tx3 whose operating frequencies are at 2.45GHz and 2.55GHz. Hence both Tx2 and Tx3 act as interference for Tx1. Here a dual-band bandstop filter with zeros at 2.45 and 2.55GHz would be ideal. The filter still allows the Tx1 to operate without problem, while attenuating other unnecessary signals. Another important parameter here is the bandwidth of the channel. Hence care needs to taken while designing the dual-band filter. A dual-band filter is designed and fabricated. Figure 4-5 shows the dual-band bandstop filter designed.

Figure 4-5: Layout of Dual-band Bandstop Filter.

The above figure is a compact dual-band microstrip bandstop filter with strong couplings at either side of the main transmission line with half wavelength resonators. The structure is folded in order to increase coupling as well as to miniaturize the circuit further. Both u-shaped resonators produce a single-band at different frequencies creating a simple dual-band bandstop filter. Both filters in Figure 4-3 and Figure 4-5 are fabricated using the substrate RT/Duroid 5880 of Rogers with dielectric constant of ε_r =2.2 and thickness of h=1.54 mm. The following Figure 4-6 shows the simulated S-parameter response of the dual-band filter:

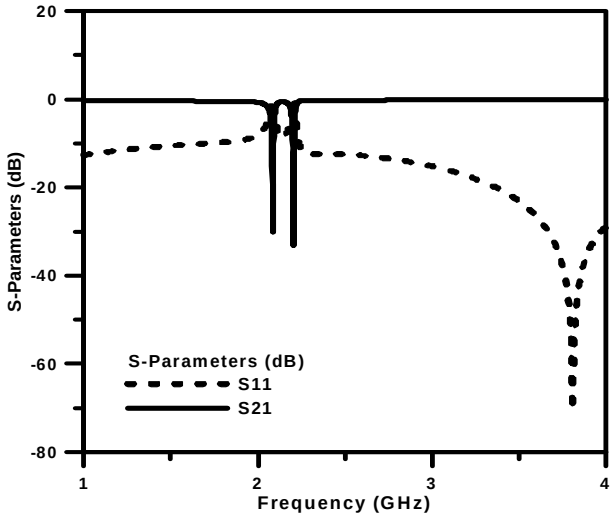

Figure 4-6: S-parameters of the dual-band bandstop filter.

As seen from Figure 4-6, the two bands are at 2.087 and 2.206GHz. The bandwidth of the first band is 0.03GHz and the bandwidth of the second band is 0.022GHz. The attenuation of both bands is nearly 30dB. This filter has a good potential for further use in the mentioned application and can be further converted into a tunable dual-band filter. The filter was fabricated and the experimental result of the bandstop filter is shown in Figure 4-7.

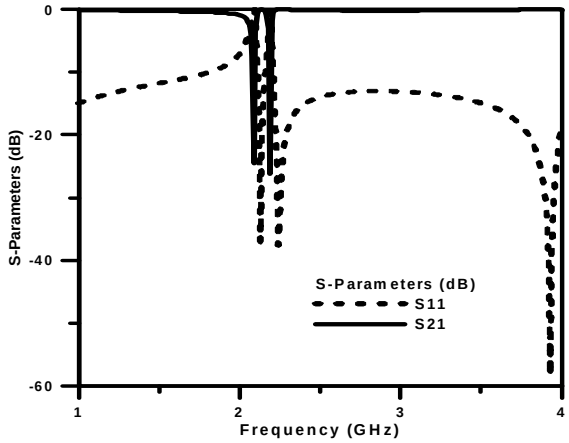

Figure 4-7: Measured S-parameter response of the dual-band filter.

From the above figure, it can be clearly seen that simulated and the experimental results vary slightly. The attenuation is lower in the fabricated structure and a slight shift of frequency is also noticed. The discrepancies are due to fabrication errors and tolerances. The passband of the filter shows a loss of less than 1dB. Figure 4-8 shows the tunability of the structure.

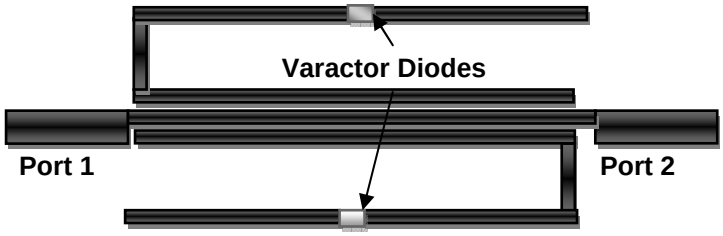

(a)

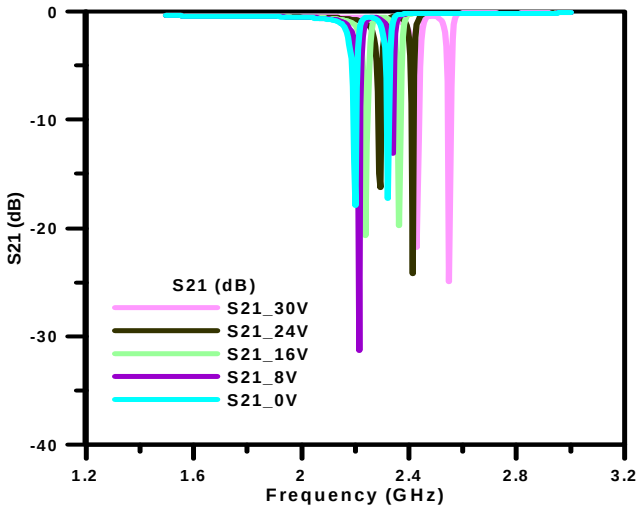

(b)

Figure 4-8: (a) Modified tunable BSF (b) Simulated S21 showing tunability of the dual-band BSF.

The above filter is further modified into a tunable structure. The varactor model as shown in chapter 3 is used in order to tune the centre frequency of the filter. Figure 4-8 shows the response of the tunable microstrip dual-band filter. It is clear from the figure that tunability is achieved but at the expense of the attenuation of the stopband. The attenuation is more than 10dB in all the different cases. The structure in Figure 4-7 is modified and two gaps of 0.3 mm are kept for the varactors. One pair of varactor is used in order to tune both bands of the filter. For the lower band, the tuning range is from 2.2GHz to 2.45GHz, which is 11 % tuning range. For the upper band a tuning range of 9% is achieved (2.35GHz to 2.58GHz).

The above were a few examples of microstrip bandstop filter. However after considering several such structures, it was found that the attenuation has a typically low value for narrowband bandstop filters along with bulky filter size. This led to the exploration of an alternative range of filters which are bandstop in nature but extremely miniaturized with excellent stopband properties. The

next section discusses this new range of filters using defected microstrip structures.

4.2 Defected Microstrip Structure (DMS)

With the introduction of PBG crystals or electromagnetic band gap (EBG) materials where the homogeneous background of one permittivity has a periodic embedding of a material of different permittivity, there has been a massive application of these in microwave fields right from filter structures, antennas etc [4.16]-[4.17] . Due to this characteristic of the materials, a stop band is created where no electromagnetic wave at any frequency within the stopband can propagate [4.18]-[4.19]. This important property can be manipulated into creating bandstop filters. A plethora of microwave structures are found in literature utilizing the above mentioned property such as antenna [4.20]-[4.21], filters [4.22]-[4.23], waveguides [4.24] etc.

Recent years has seen the emergence of DGS which is derived from the EBG concept. It has very attractive characteristics such as slow wave effect and size reduction [4.25]-[4.29]. Several structures of DGS has been proposed which works by etching patterns on the ground plane therefore modifying the effective inductance and capacitance thus exhibiting stopband characteristics and slow wave effects [4.28]. But due to certain disadvantages of the DGS such as leakage through ground plane and radiation through the slotted pattern, the DGS can cause considerable distortions in measurements [4.30].

The DMS on the other hand has similar characteristics such as DGS but without the drawbacks that DGS suffers. This has enabled DMS to be used in many applications such as power amplifiers, lowpass filters, bandpass filters and antennas [4.29]-[4.33]. The DMS works by etching different patterns or slots on the transmission line itself. Hence ground plane leakage problem is eliminated. An important characteristic of DMS is the modification of the line impedance and hence a higher impedance transmission line can still be realized using DMS as compared to conventional filters [4.33].

In order to explain the working of a DGS and DMS, the layout of a transmission line with a rectangular defect in the ground plane and the layout of

a transmission line with a T-shaped defect on the line itself respectively are shown. When the ground plane is defected, the current distribution changes along with the change in the propagation properties. A similar case is seen in the case of the DMS, where the current distribution is affected because of the etched slot on the line. Figure 4-9 shows the layout of the two structures. The shape of the defects and the periodicity of the defect can be varied in order to create different effects and hence different components [4.34]-[4.35].

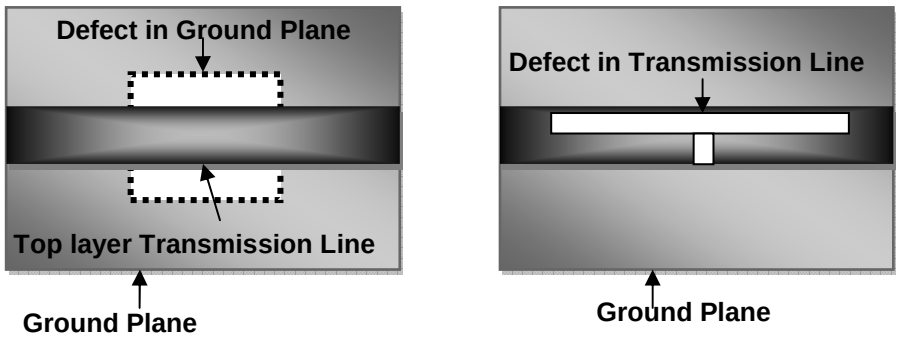

(a) (b)

Figure 4-9: Layout of (a) DGS and (b) DMS.

4.3 Fixed DMS Bandstop Filter Design

Bandstop filters are very important in recent years due to the emergence of multi-standard systems. A basic application of such a bandstop filter can be in multi-standard transceivers where one band can act as interfering signal to the other band. Such applications also require the use of tunable bandstop filter which can adapt to the change in frequencies as will be further discussed in chapter 5. Miniaturization is therefore an important necessity for such applications where size restriction is of paramount importance.

In this section the design techniques of a few bandstop filter using novel defected microstrip structures are discussed and fabricated. These filters range from single-band to dual-band structures. When compared with traditional filters, the designed ones are far better in terms of size, filter characteristics and cost. These filters also give excellent bandstop responses with stopband attenuation reaching 50dB in some cases. A fixed filter with centre frequency of

2.75GHz was simulated and fabricated with excellent match in both results. Figure 4-10 shows the geometry of the proposed defected microstrip bandstop filter structure.

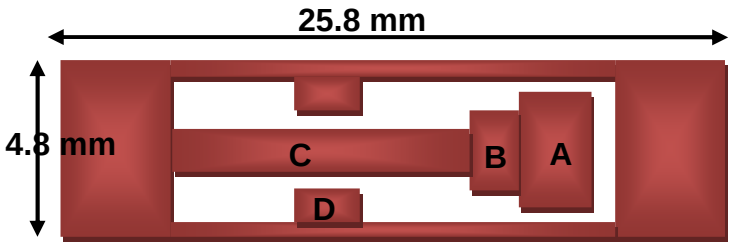

Figure 4-10: Geometry of the proposed filter using defected microstrip structure.

A conventional T shaped slot as in [4.33] has been modified in order to get a more compact structure. Such compactness can be achieved by introducing stepped impedance resonators (SIR). The structure A has a dimension of 5.1 mm by 3.6 mm. The structure B has a dimension of 1.2 mm by 2.4 mm. C has a dimension of 8.7 mm by 1.2 mm. D has a dimension of 1.8 mm by 1.2 mm. The etched pattern disturbs the current distribution in the structure when compared with the conventional type. This is due to the control of the way the electromagnetic wave propagates in the structure. This results in the modification of the line properties and increase in the effective inductance and capacitance. Any conventional microstrip line has certain amount of inductance due to flux linkage while in DMS creating defects changes the inductance as the flux linkage changes. The delay is represented by the inductance and capacitance. Hence with larger values, the group delay is higher resulting in a slower propagation of the wave or the slow wave effect. Due to this modified properties of the line, the slow wave effect can be seen, due to which there is a considerable size reduction. The added defects on the microstrip line increases the slow wave factor. The current distribution near the stopband frequency of the filter is depicted in Figure 4-11.

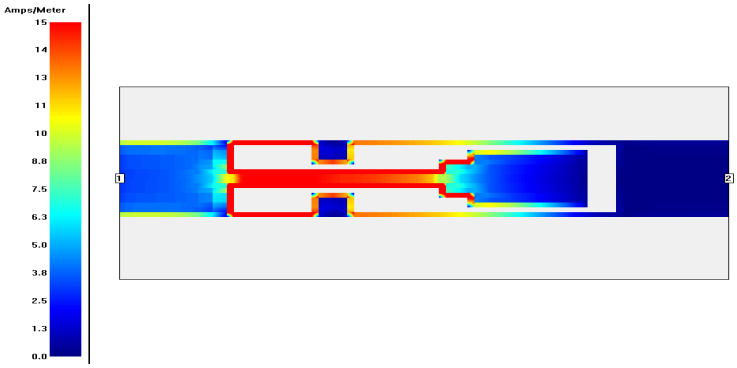

Figure 4-11: Current distribution of the proposed filter at 2.75GHz.

The current is mostly distributed in the etched slots at 2.75GHz frequency increasing the effective inductance of the structure as can be seen from the above figure. The red indicates a higher current concentration when compared with the blue. The current is mostly concentrated in the T-shaped junction. The simulated result of the filter is shown in Figure 4-12. EM analysis over a frequency range of 0.1GHz -10GHz is carried out.

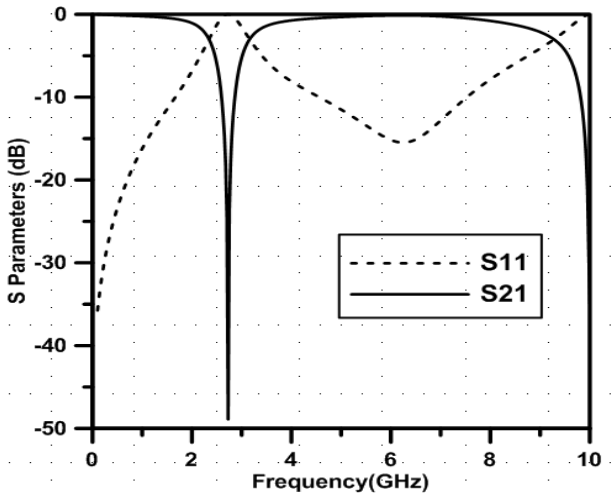

Figure 4-12: Simulated S-parameters of the proposed filter.

Figure 4-12 shows S-parameter response of the filter. The first band appears at 2.75GHz and has a stopband attenuation of -48.9dB. The passband of the filter is good exhibiting less than -0.5dB loss. The second harmonic stopband of the filter occurs above 10GHz, which appears due to the peridiocity of the microwave line. It appears at a frequency of 3.8 times the fundamental

frequency . This shows that a good upper passband response is obtained from the designed filter and can be used in various applications.

In this proposed geometry additional small patches have been added in order to increase the stopband attenuation. These small patches helps in increasing the effective capacitance and has an effect of increasing the stopband attenuation of the filter. The structure has been simulated with patches having varying dimensions in order to achieve the best possible attenuation. Lowering the width and length of patch minimizes the attenuation. This was done by keeping one variable constant and changing the other variable. Figure 4-13 shows the variation of the attenuation with different patch sizes.

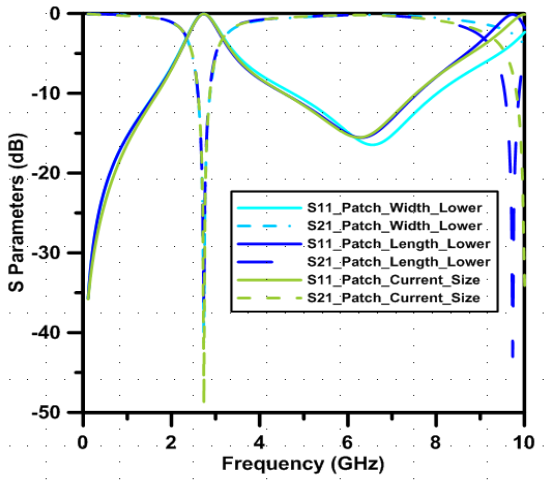

Figure 4-13: Simulated S-parameters of the proposed filter with varying patch (D) dimensions.

The stepped impedance concept has been utilized in the T shaped geometry. The different sections namely A and B have been utilized in order to make the circuit much smaller. By choosing appropriate ratio of the impedances of these blocks a reduced circuit size can be achieved. For this particular stepped impedance structure, the resonant condition of the structure can be adjusted by fine tuning the impedance ratio of the two length segments. This gives better flexibility in designing a filter as now the size of the filter can be greatly reduced along with control of the spurious bands which now appears above $3f_0$. Figure 4-14 shows the effect of section A and B in the overall response of the circuit. A second stopband is also noticed at frequencies further away above 10GHz. Removing B shifts the second band down in frequency. Removing both A and B

shows an upward shift in frequency of the main stopband, proving that a much compact circuit is achieved by using the proposed geometry.

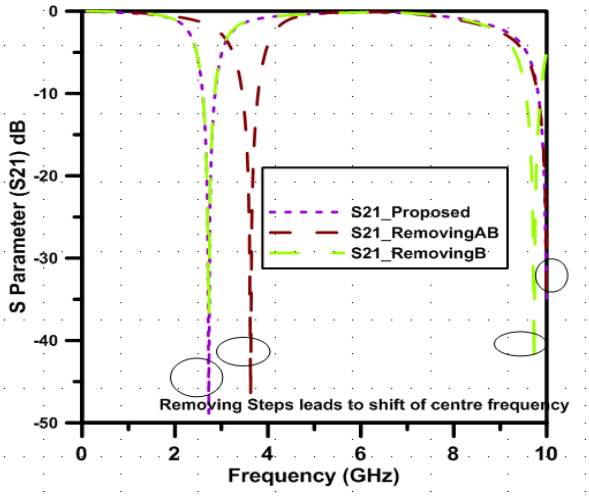

Figure 4-14: Simulated S21 parameter of the proposed filter comparing the effect of slabs A and B.

The proposed filter was fabricated using the substrate RT/duroid 5880 of Rogers with dielectric constant of ε_r =2.2 and thickness of *h*=1.54 mm. The dimension of the filter is 25.8 mm × 4.8 mm. This can be expressed as $0.35\lambda_g \times 0.065\lambda_g$. The circuit is highly miniaturized. Figure 4-15 shows the photograph of the fabricated DMS bandstop filter.

Figure 4-15: Photograph of the proposed bandstop filter structure.

The measured response of the filter is seen in Figure 4-16. The stopband of the measured filter appears at 2.8GHz. The stopband attenuation of the filter is around -50dB, which shows excellent agreement with simulated results. The passband loss is less than -1dB. The filter bandwidth at -25dB is measured to be less than 50MHz. The attenuation achieved is good for many applications where

unwanted distortion signals need to be filtered out. There is a slight shift of the centre frequency of the filter. This is because of fabrication tolerances.

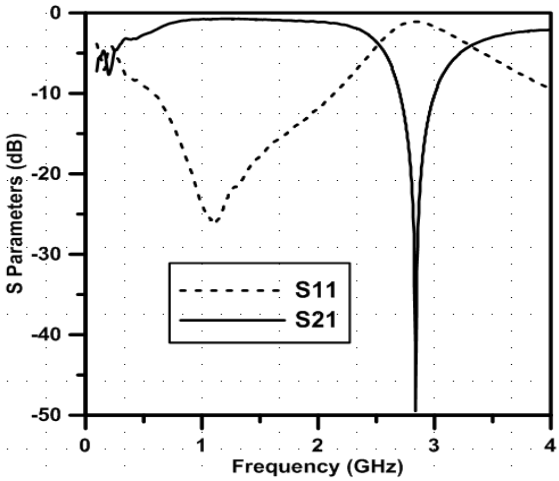

Figure 4-16: Measured S-parameters of the proposed bandstop filter.

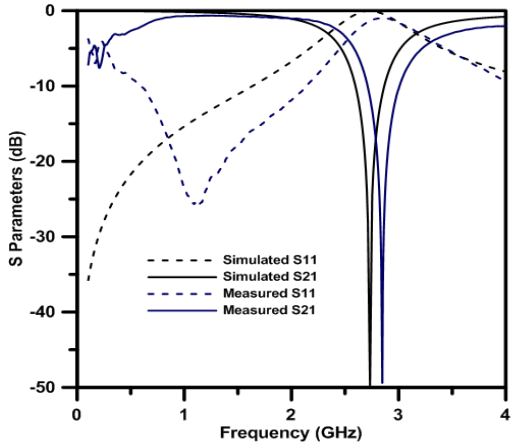

Figure 4-17: Comparison of measured and simulated S-parameters of the proposed bandstop filter.

One such novel fixed bandstop filter was created using a new concept of DMS which showed excellent results. Another example of a bandstop filter is given below which has been designed to be more compact as compared to the previous DMS filter. The filter has a 3dB fractional bandwidth of 10%. The stopband attenuation is around 40dB. The equivalent circuit has been extracted and experimental results are presented. Furthermore the upper spurious response occurs nearly 4 times the fundamental frequency. The filter hence has an extended upper pass band which is beneficial in many applications one of

which is discussed in chapter 5. The configuration of the proposed filter is shown in Figure 4-18.

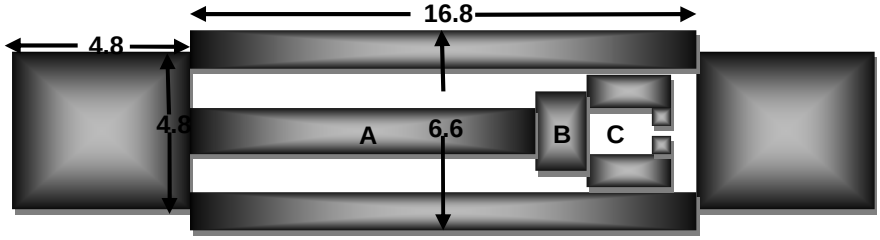

Figure 4-18: Geometric configuration of the proposed filter.

From Figure 4-18, it is seen that on the microstrip line itself, a modified fork shaped pattern is etched which modifies the effective inductance and capacitance of the line by disturbing the current distribution due to the perturbations created. Hence at certain frequencies band gap characteristics are noticed. The slow wave factor which is defined by the ratio of the wavelengths in conventional and slow wave structures is more in a DMS structure as compared to a conventional microstrip line. This is due to the fact that in conventional structures, the phase velocity is governed by the dielectric constant and that value cannot go smaller than a certain amount while in a DMS structure the various perturbations create the possibility of storing the electric and magnetic energies separately giving rise to a slow wave effect .This leads to a reduction in size of the overall filter. The dimension of the etched pattern controls the centre frequency of the structure. The current distribution of the structure is shown in Figure 4-19 at 2.28GHz. It is seen that current is distributed mostly in the etched slots.

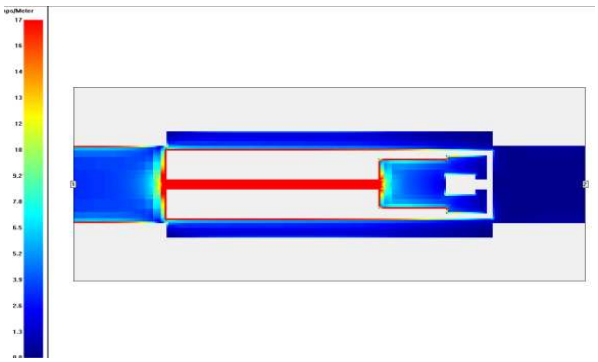

Figure 4-19: Current distribution in the DMS structure.

Section A has dimensions of 10.9 mm by 0.6 mm while Section B has a dimension of 3.5 mm by 3.1 mm. Section C is an open loop structure, where the thinner side arms are 2.1 mm by 1.2 mm. A stepped impedance microstrip line of 16.8 mm by 6.6 mm was used to etch the modified fork shape. The difference between using conventional microstrip line and stepped impedance microstrip line is illustrated in Figure 4-20.

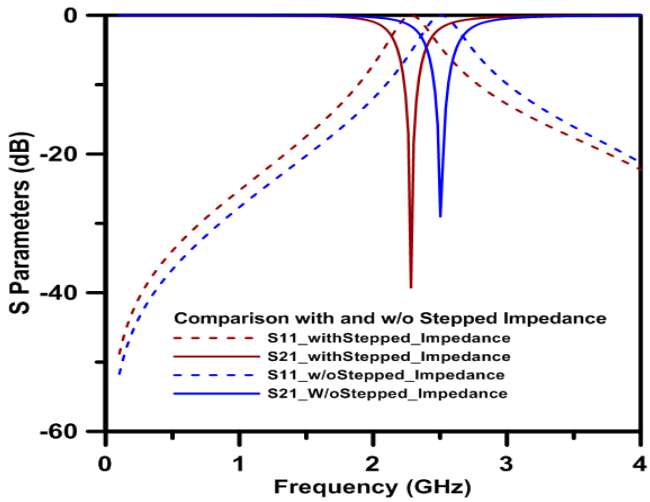

Figure 4-20: Variation of f_o with and without (w/o) stepped impedance.

The structure uses the concept of stepped impedance and hence by using sections A and B having varying dimensions, the ratio of the impedance is adjusted and the desired response is obtained. If a continuous impedance line was used instead of these two sections, the structure would be bigger which is clear from Figure 4-20 above.

The line widths were varied in order to get a good Q response with greater stopband attenuation. The resonance frequency of the filter was at 2.28GHz. In order to investigate the frequency characteristic of the structure, it was simulated using EM Sonnet. The simulated response is shown in Figure 4-21. The response is shown for a range of 0.1GHz-12GHz in order to illustrate the appearance of the first spurious band. It is observed that the first harmonic appears at more than 4 times the fundamental frequency.

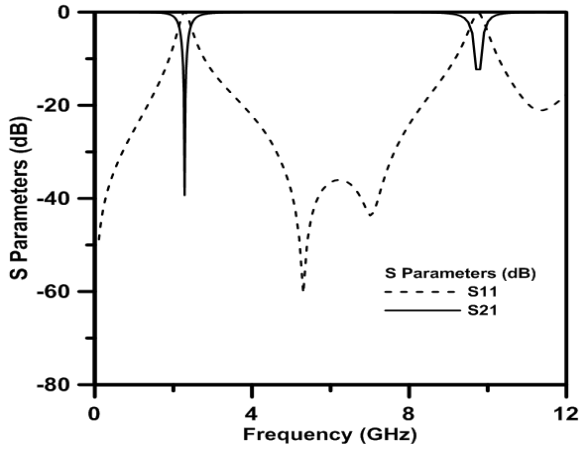

Figure 4-21: Simulated S-Parameter response.

From Figure 4-21, the stopband attenuation is around 40dB. The 3db fractional bandwidth of the simulated response is 13 %. The passband has an insertion loss of less than -1dB. Section B was optimized in order to get a good stopband attenuation level. The effective capacitance was increased when a wider microstrip patch was used as compared to a thinner one. Hence in Figure 4-20, degradation of stopband attenuation is also noticed along with the shift in frequency.

In order to evaluate the DMS filters numerically, modeling and parameter extraction was done using the equivalent circuits of the designed filter. Like DGS, the equivalent circuit of a DMS section is a parallel *LC* circuit. An additional resistor *R* is added in order to model the loss. The equivalent circuit of the modified DMS section is extracted keeping the main DMS section (*RLC* circuit) in mind. The additional gaps are modeled using capacitors C_2 and C_3. While the thin microstrip lines representing inductance L_2 is also taken into account for the final circuit. The initial lumped element values are calculated from the equations as given [4.35].

$$C = \frac{f_c}{4\pi Z_0\left(f_0^2 - f_c^2\right)} \tag{4.1}$$

$$L = \frac{1}{4\pi^2 f_0^2 . C} \tag{4.2}$$

$$R = 2Z_0 \frac{1 - S_{21}(f_0)}{S_{21}(f_0)} \tag{4.3}$$

The parameters f_c, f_0 and S_{21} are the 3dB cut-off frequency, resonant frequency

and the transmission coefficient. Agilent ADS was used in order to extract the final values of the lumped elements as shown in Figure 4-22.

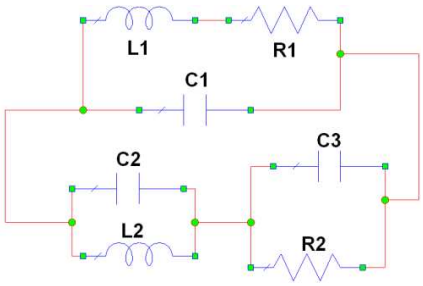

Figure 4-22: Lumped element equivalent circuit.

The extracted parameters of *RLC* have a value of 10Ω, 2.2nH and 2.3pF respectively. The two gaps modelled using the capacitance C_2 and C_3 has a value of 0.4pF and 0.18pF. The parasitic inductance has a value of 2nH. The resistance with the inductance and capacitance are provided to model the losses hence the simulated result below shows the loss in the former of low Q values. The capacitors are used to model the gaps, while the parallel inductance and capacitance model the bandgap feature of the filter.

A parameter extraction model is provided in the form of a flowchart which is shown in Figure 4-23. An iterative process is used in order to come up with the final values of the circuit simulation, while the initial values are calculated by using the equations provided in (4.1), (4.2) and (4.3).

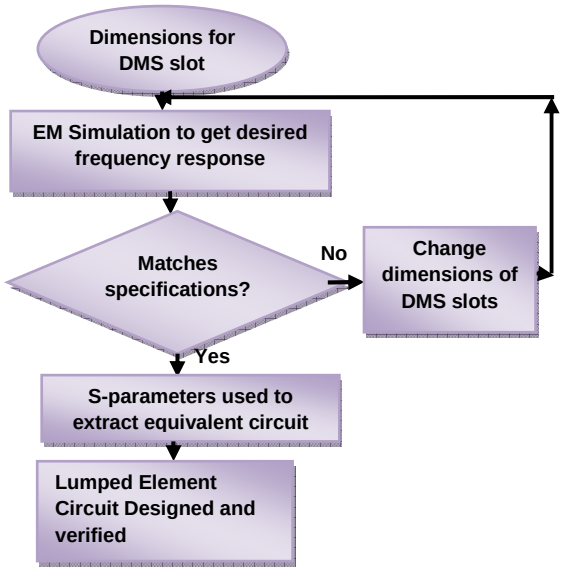

Figure 4-23: Flowchart of the DMS design procedure used.

Figure 4-23 shows the flowchart of the proposed design and analysis of the DMS structure used in this thesis. The flowchart represents the stages of the design of a DMS filter which has been implemented in this thesis. The slot dimensions are first used to simulate the desired structure and obtain an S-parameter response. The desired response is then obtained by varying the dimensions of the DMS etched slots. Once a desired S-parameter response is obtained, it is used to extract the equivalent circuit model for the filter as described above. The EM simulation obtained is compared with the circuit simulation which is obtained from the circuit mentioned in Figure 4-21. It was seen that the response had slightly different 3dB fractional bandwidths as shown in Figure 4-24.

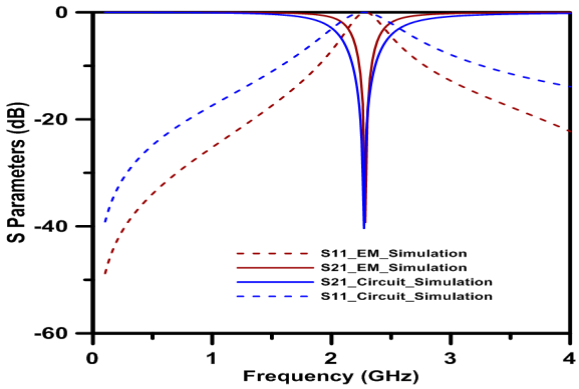

Figure 4-24: Comparison of EM simulation and circuit simulation.

The proposed filter was then fabricated using the substrate RT/Duroid 5880 of Rogers with dielectric constant of ε_r =2.2 and thickness of *h*=1.54 mm. The dimension of the filter is 26.4 mm × 6.6 mm. This can be expressed as $0.28\lambda_g \times 0.068\lambda_g$. Here λ_g is calculated to be 95.68 mm. The circuit is highly miniaturized. It shows a 16 % reduction in area as compared to the previous filter described. Figure 4-25 shows the photograph of the fabricated DMS bandstop filter.

Figure 4-25: Photograph of the fabricated bandstop filter.

The measured response of the fabricated filter is shown in Figure 4-26. The stopband attenuation is around -30dB. The passband insertion loss is less than -1dB. The centre frequency of the filter is at 2.28GHz. The Q factor is measured to be 8. The level of stop band attenuation is slightly lesser than simulated response due to fabrication tolerances and lower Q values. The 3dB fractional bandwidth is 13.9%. The measured data for the fabricated DMS filter shows a good match with EM and circuit simulation.

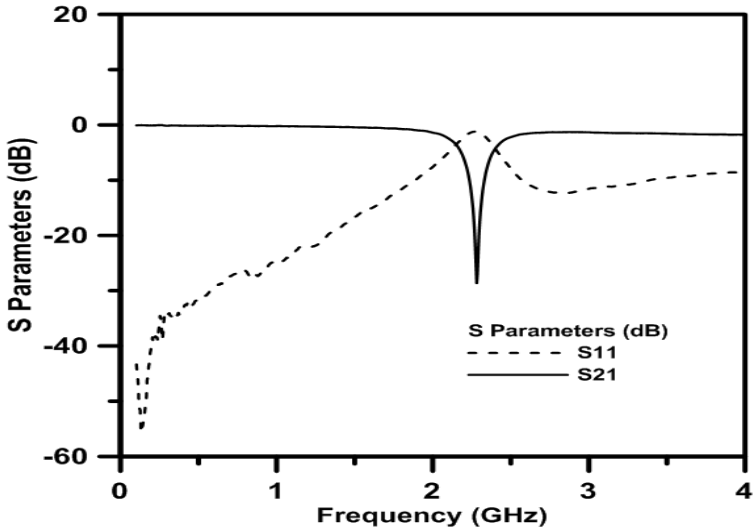

Figure 4-26: Measured response of the fabricated filter.

A fixed single-band filter can only help in interference reduction to a certain extent. This is mainly due to the single stopband appearing at a pre specified location. When there is more than one interfering signal that is when the problem arises with fixed single-band bandstop filter. In such cases, in order to suppress interfering signals, more than one fixed filter is required. This will increase system cost and also take up more space. Hence using single-band fixed filters are not a suitable option. This problem requires more advanced bandstop filters. Hence dual-band filters are introduced where there are two stopband which can help in suppressing more interfering signals. A more advanced filter will be a tunable single-band filter and a tunable dual-band filter discussed in the next section. The following Figure 4-27, shows the layout of the dual-band DMS filter designed.

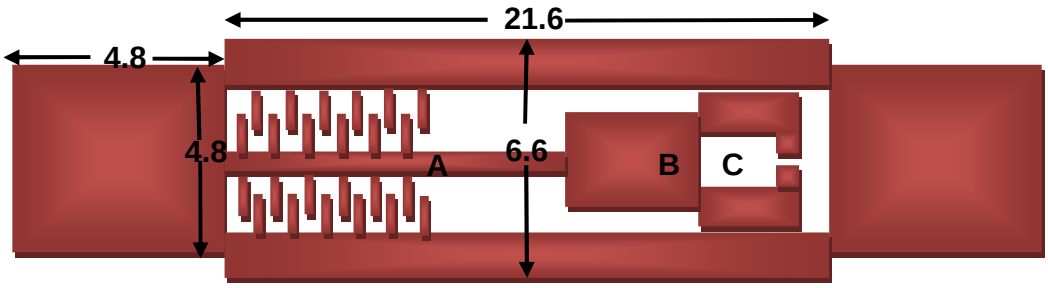

Figure 4-27: Geometry of the proposed dual-band DMS filter.

Comparing Figure 4-18 and 4-27, it is seen that the overall structure of the two filters are similar. The only difference is that in Figure 4-27, there is additional interdigital fingers aligned as shown. The fingers help in providing a much better capacitive coupling. This interdigital structure itself provides with an additional resonant frequency which forms the second stopband of the filter. In order to control the resonant frequency, the finger dimensions and spacing between the fingers needs to be modified. The interdigital fingers can be modelled as a simple combination of interdigital capacitance which is represented by a capacitor in series with an inductor. This is now combined in parallel with another inductance to form the core DMS equivalent circuit.

The dimensions of the filter for structure A is 11.1 mm by 0.6 mm .The section marked as B and C has a dimension of 3 mm by 3.3 mm and 2.1 mm by 1.2 mm respectively. The interdigital fingers are 1.5 mm by 0.3 mm each. There are 12 such fingers on either side of structure A. The overall dimension of the filter is 26.4 mm by 6.6 mm. A Rogers RT/Duroid 5880 substrate dielectric constant of ε_r =2.2 and thickness of h=1.54 mm is used as the substrate. The current distribution of the filter is also noted in Figure 4-28.

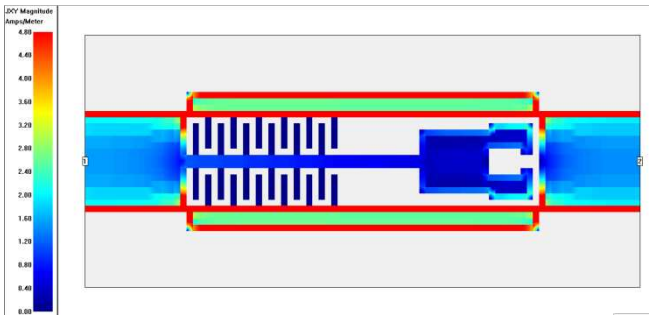

Figure 4-28: Current distribution of the DMS dual-band filter.

When compared with the current distribution in the previous single-band filter, it is noticed that most of the current concentration is at the outer edge instead of the etched pattern on the microstrip line. The change in the current distribution modifies the transverse magnetic field and hence changes the effective inductance. A larger group delay on the other hand introduces a slow wave effect which helps in miniaturizing the circuit further. The simulated response of the structure is given in Figure 4-29.

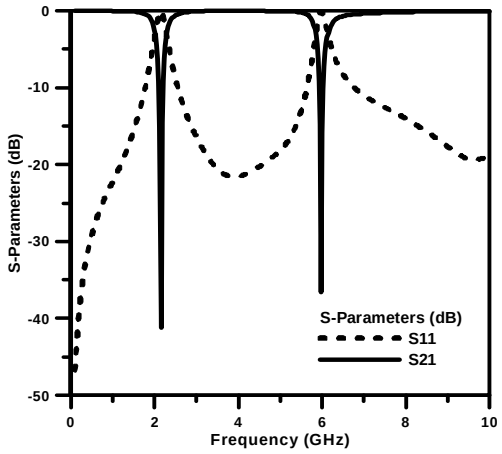

Figure 4-29: Simulated S-Parameter response of the proposed filter.

From Figure 4-29, the two stop bands appear at 2.15GHz and 5.975GHz. The attenuation of the first band is measured as 41.24dB and for the second band it is measured as 36.65dB. The 3db bandwidth measured for the first band is less than 0.25GHz while for the second band it is less than 0.3GHz. The effective centre frequency of the structure is 4.0625GHz. This can be expressed as $0.48\lambda_g \times 0.122\lambda_g$. Here λ_g is calculated to be 53.90 mm. The passband measured is less than -1dB. Hence the designed structure is very compact showing excellent potential for fabrication. The challenge lies in the realisation of the interdigital fingers accurately as sometimes due to inaccuracy in fabrication process, the finger dimension can vary resulting in a distorted output.

4.4 Tunable DMS Bandstop Filter Design

In recent years, there has been an increase in filters which are tunable or reconfigurable. Tunability enables the filters to be more flexible. Hence instead

of the use of multiple fixed filters, a tunable filter can be used to serve the same purpose. For example, WLAN signal appearing at 5GHz is an interfering signal for UWB applications whose range is from 3.1GHz to 10.6GHz which is further divided into lower and upper range to avoid the WLAN signal. Hence a filter with a fixed stopband can only suppress the WLAN. In case of another interfering signal, another fixed filter will be required. A more suitable option would be to use a tunable filter whose centre frequency can be electronically tuned to match the frequency of the interfering signal and suppress it. In this section, a few such novel tunable bandstop filters using DMS is designed and fabricated. Fixed filters which were discussed in the previous section have been modified to implement tunability as discussed.

In the previous section, in Figure 4-10, a fixed DMS filter was introduced. The same filter was modified further in order to make it tunable using varactor diodes placed to achieve a tuning range of 20% from 2.26GHz to 2.75GHz. The proposed filter has been further tested for distortion effects due to the presence of nonlinear varactor diodes. Good result was obtained in both cases. In order to achieve electronic tunability for the DMS filter, it was necessary to make some slight modifications in the filter structure. The transmission line for etching the modified T shape was increased by a few more mm for the ease of fabrication and soldering. The varactor used was NXP BB179 in order to achieve tunability. The filter was still compact and the simulated results obtained were good. Figure 4-30 shows the modified geometry of the tunable filter.

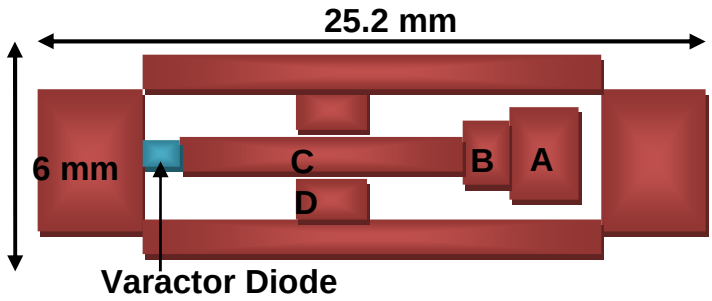

Figure 4-30: Geometry of the proposed filter using varactor diode.

The dimensions of the filter are slightly changed. The increase in the width of the transmission line from 4.8 mm to 6 mm has resulted in a lesser line length of 25.2 mm as compared to the previous value of 25.8 mm. The gap kept for the varactor diode is 0.9 mm by 1.2 mm. Dimension of A has been kept the same. Dimension of B, C and D are 0.9 mm by 2.4 mm, 7.8 mm by 1.2 mm and 2.4 mm by 1.2 mm respectively.

The filter was fabricated using substrate RT/Duroid 5880 of Rogers with dielectric constant of ε_r =2.2 and thickness of *h*=1.54 mm. The photograph of the filter is given in Figure 4-30 which shows the varactor connected in the small gap. The overall dimension of the filter is 25.2 mm×6 mm. This is also equivalent to $0.34\lambda_g \times 0.082\lambda_g$.While applying the reverse bias voltage ranging from 0 V to 30 V two resistors of 3.3 kΩ was used in order to achieve sufficient RF isolation. Hence additional DC bias circuitry was not required.

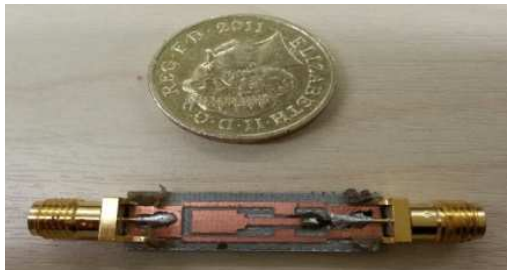

Figure 4-31: Photograph of the proposed tunable bandstop filter.

Figure 4-32 below shows the measured filter response. A good tuning range is achieved from 2.26GHz to 2.747GHz (20 %) tuning range. The stopband attenuation suffers a bit of degradation but it is maintained constant over the whole range at about -18dB. A capacitance range of 20 pF to 2 pF corresponded to the 0V to 30 V reverse bias voltage. The voltages were provided in steps of 8V. The bandwidth of the filter is near constant for the whole tuning range. Overall a good response is obtained with passband less than – 1dB as shown.

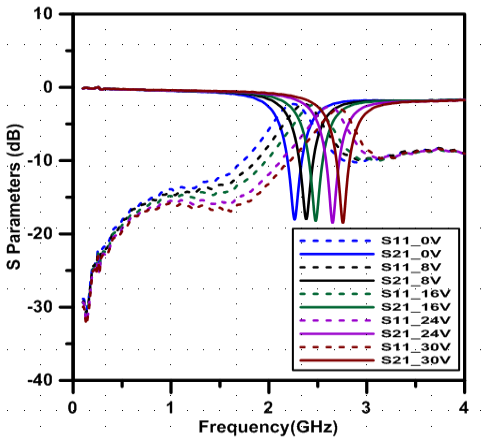

Figure 4-32: Measured tunable filter response for various reverse bias voltages.

The filter designed is for applications requiring devices with excellent characteristics. These filters are used to get rid of additional distortions. Hence it is vital to measure the distortion characteristics of the filter itself. Due to the use of varactor diodes in the tunable filter which has inherent nonlinear transfer function, distortion measurement becomes vital. Here the distortion is measured using experimental test set-up as shown in Figure 4-33.

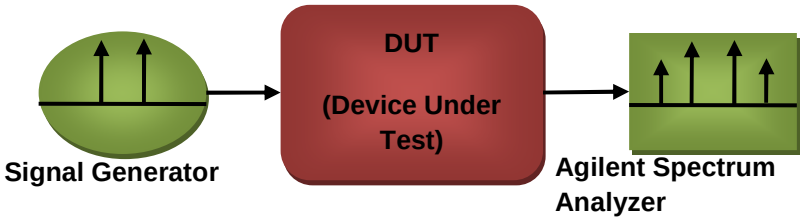

Figure 4-33: Experimental set-up used to test distortion in the filter.

A two tone set up was used in order to determine the distortions. The two fundamental tones are at 2.3495GHz and 2.3505GHz and the lower and upper third order intermodulation distortions are at 2.3485GHz and 2.3515GHz respectively. The distortion was measured for 0V and 30 V at a centre frequency of 2.35GHz. Figure 4-34 shows the measured results. The filter is highly linear and hence can be used in any applications which require it.

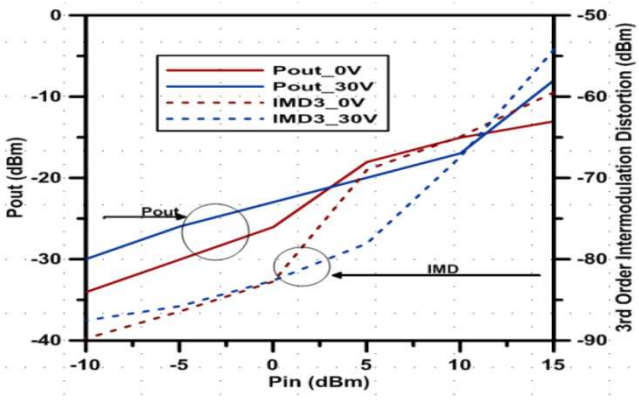

Figure 4-34: Measurement of distortion of proposed tunable filter using two tone signals for Pout vs P_{in} and IMD vs P_{in}.

The measured results for intermodulation distortions shows that for the highest input power of 10dBm the filter has a relative distortion of around 45dB. The result also shows that at higher input power level the IMD for 0V is lower than that for 30V state. Figure 4-35 shows the spectrum showing the third order intermodulation product indicated by marker 2.

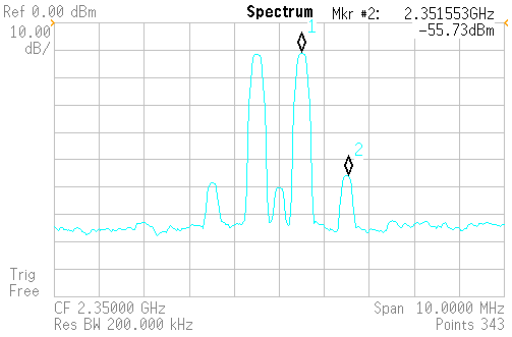

Figure 4-35: Spectrum showing the nonlinear distortion measurement.

From the above results it is evident that the tunable filter designed has excellent characteristics with good linearity. It should be noted that both the above figures shows an apparent loss of a few dB in P_{out}. This is due to the fact that the two tone test is done on a bandstop filter having an attenuation of nearly 20 dB. Hence when maximum Pin of 10 dBm is used, the Pout is measured to be around -10 dBm. Another such filter was further designed using the same structure as Figure 4-18 where a small gap of 0.6 mm by 0.6 mm is kept to solder the varactor diode NXP BB179. The equivalent circuit of the

varactor diode given in chapter 3 is used in order to simulate the filter structure. The following Figure 4-36 shows the geometry of the designed tunable filter.

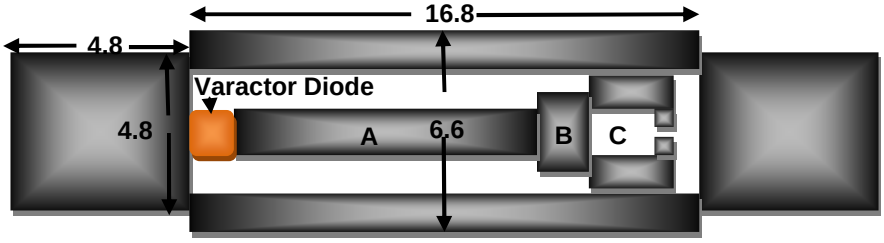

Figure 4-36: Geometry of the tunable DMS filter.

The dimensions of the filter are given for Section A as 9.6 mm by 0.6 mm while Section B has a dimension of 4.2 mm by 3 mm. Section C is an open loop structure, where the thinner side arms are 2.1 mm by 1.2 mm. A stepped impedance microstrip line of 16.8 mm by 6.6 mm was used to etch the modified fork shape. The filter was simulated and the S-parameters are shown in Figure 4-37.

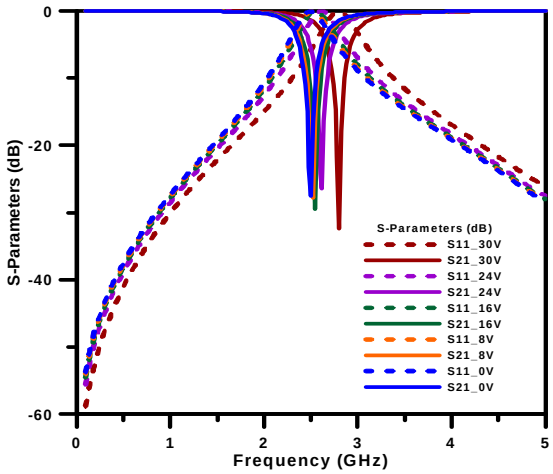

Figure 4-37: Simulated S-parameters of the tunable filter for various reverse bias voltages.

From Figure 4-38, the lower stopband for 0V appears at 2.5GHz while the upper stopband for 30V reverse bias voltage is at 2.8GHz which is 12 % tuning range. A capacitance range of 20 pF to 2 pF corresponded to the 0V to 30 V reverse bias voltage. The 3dB bandwidth of the filter is constant at 0.36GHz. The attenuation for the stopband varies with different voltages being -32.36 which is

the maximum at 30V. The stopband attenuation for all other reverse bias voltages is more than -25dB. The passband of the filter is noted to be always less than -1dB showing excellent results.

The filter was designed using substrate RT/Duroid 5880 of Rogers with dielectric constant of ε_r =2.2 and thickness of *h*=1.54 mm. The overall dimension of the filter is 26.4 mm×6.6 mm. This is also equivalent to $0.321\lambda_g \times 0.080\lambda_g$. This shows that the filter size for the tunable DMS mentioned in Figure 4-35 is better than the filter in Figure 4-30. This filter can be further fabricated and tested for distortions.

The third tunable filter which is discussed in this section is that of a dual-band tunable filter. Tunable dual-band filters have a much wider application when compared to single-band tunable filters. The main reason for that is that a lot more flexibility and control is given to the user. In the previous section, an example of the fixed dual-band filter was given in Figure 4-27. The same filter was modified in order to incorporate a tuning element, a varactor in this case. A varactor model NXP BB179 was used in order to electronically tune the stopbands. Figure 4-38 shows the geometry of the tunable dual-band DMS filter.

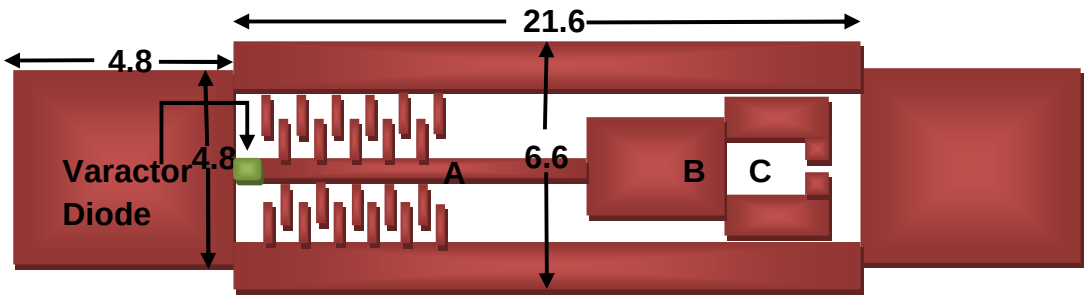

Figure 4-38: Geometry of the proposed tunable dual-band DMS filter.

The filter dimensions undergo a slight modification in order to incorporate the varactor diode. A gap of 0.6 mm by 0.6 mm is kept for the varactor diode as shown in Figure 4-38. The interdigital fingers are changed from twelve to eleven in number. This leads to the change in the resonant frequency of the second band. The dimensions of the filter for structure A is 10.5 mm by 0.6 mm .The section marked as B and C has a dimension of 3 mm by 3.3 mm and 2.1 mm by 1.2 mm respectively. The interdigital fingers are 1.5 mm by 0.3 mm each. The

following Figure 4-39 shows the simulated S-parameters of the tunable dual-band filter for different reverse bias voltages.

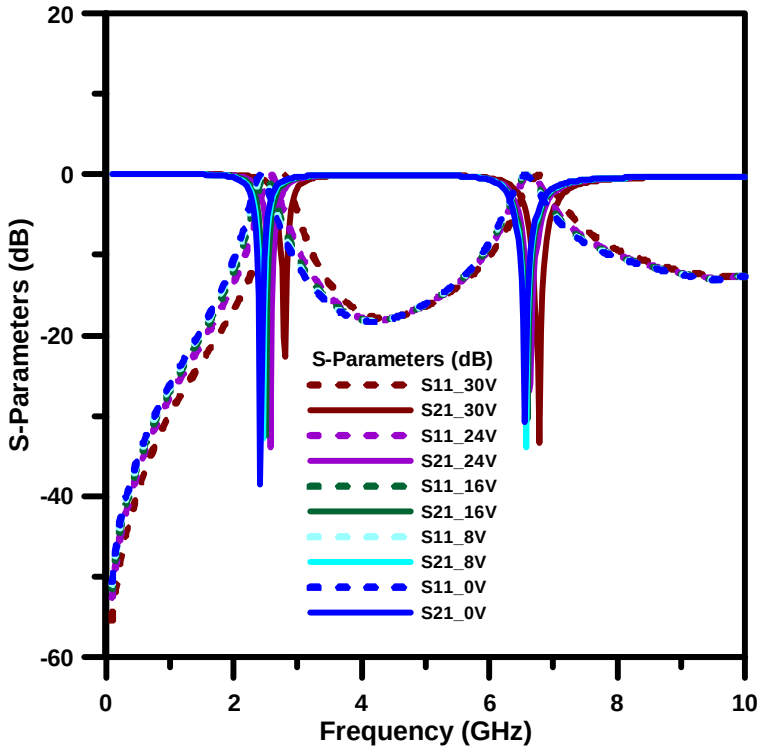

Figure 4-39: Simulated S-parameters of the tunable dual-band filter for various reverse bias voltages.

The simulated result of Figure 4-39 shows the tunability of the filter. The lower stopband has a tuning range from 2.425GHz to 2.8GHz (15%) while the upper stopband shows a tuning range from 6.55GHz to 6.775GHz (3%). The low tuning range for the upper stopband is as expected. A closer look at the structure shows that the varactor diode placed in the gap as shown in Figure 4-37 controls the lower stopband resonant frequency only. The upper stopband resonant frequency is controlled by the interdigital fingers. The slight variation of the upper stopband is due to the modification of the geometry of the DMS filter to incorporate the varactor and also due to the overall effect of a tuning element.

The stopband attenuation of the lower stopband for all reverse bias voltages is more than -20dB. The upper stopband attenuation for all reverse bias voltages is around -30dB and varies slightly. This again shows that the overall effect of the varactor is very less for the upper stopband. The passband is

maintained at less than -1dB. A constant 3dB bandwidth of around 0.275GHz is maintained for the lower stopband for all reverse bias voltage. The upper stopband has a constant 3dB bandwidth of around 0.3GHz.

The filter was designed using substrate RT/Duroid 5880 of Rogers with dielectric constant of ε_r =2.2 and thickness of *h*=1.54 mm. The overall dimension of the filter is 26.4 mm×6.6 mm. This is also equivalent to $0.56\lambda_g \times 0.14\lambda_g$. The effective centre frequency is calculated by taking average of the first band and the second band and then averaging the two which comes to 4.6375GHz. The following Table 4-1 shows the comparison of the work done in this thesis with other filters available in literature.

Parameters\Ref.	**[4.36] 2007**	**[4.37] 2011**	**[4.38] 2011**	**This Work [4.39]**
Permittivity	2.33	3.55	2.65	2.2
Substrate thickness (mm)	0.787	0.81	1.6	1.54
Mid-band frequency (GHz)	1.164	2.53	5.2	2.75
Etched size (mm x mm)	-	$0.422\lambda_g$ x $0.634\ \lambda_g$	$0.857\lambda_g$ x $0.117\ \lambda_g$	**$0.35\lambda_g$ x $0.065\ \lambda_g$**
Etched Size (without including line lengths for connectors) (mm by mm)	$0.074\lambda_g$ x $0.298\ \lambda_g$	-	-	**$0.203\lambda_g$ x $0.065\ \lambda_g$**

Table 4-1: Comparison of filter size for the fixed DMS filters.

When comparing the fixed dual-band filter with other works found in literature, it shows an excellent result when compared to [4.40] which has a dimension of $0.75\lambda_g$ by $0.06\lambda_g$. The work presented here has a dimension of $0.48\lambda_g \times 0.122\lambda_g$ which is much better. A few other dual-band filters are compared with the work done in this thesis such as [4.41] which has a dimension of $0.566\lambda_g$ by $0.490\lambda_g$, [4.42] having a dimension of $0.368\lambda_g$ by $0.313\lambda_g$, [4.43] with a dimension of $0.468\lambda_g$ by $0.668\lambda_g$, [4.44] having a dimension of $0.247\lambda_g$ by $0.250\lambda_g$. Hence a much compact filter is presented here which can be used in several applications.

4.4 Conclusion

This chapter gives an overview of the microstrip bandstop filter and briefly discusses the relevant applications. The importance of the BSF lies in the suppression of interfering signals in this thesis. A brief summary of conventional microstrip bandstop filter is given along with a few examples which include single-band and dual-band bandstop filters as well as tunable filters.

Defected microstrip structure being a new way of designing bandstop filter is discussed and a brief literature review is provided. Several different structures of bandstop filter using DMS is presented. Two such novel fixed single-band bandstop filters were presented along with experimental verification. The filters were highly miniaturized with excellent stopband attenuation and passband characteristics. A novel dual-band fixed bandstop filter is also presented which had attenuations of more than -30dB for both bands.

Tunable bandstop filters using DMS are also provided. One such filter was fabricated and tested for further distortions. Tuning element used for the filter was a varactor having inherent nonlinear properties. Hence the filter was measured for distortion and good linearity was observed. An example of a novel tunable dual-band filter was also provided. The filters presented in this thesis were highly miniaturized and the size was further compared with other such filters available in literature.

4.5 References

[4.1] R.L. Sleven A. J. Anselmo, D. S. Levinson, J.J. Taub and N. Worontzoff, "Bandstop Filter Design for Ultra-Low Loss and High Power," *Microwave Conference, 1973. 3rd European*, vol.1, no., pp.1, 4, 4-7 Sept. 1973.

[4.2] L. Young, G.L. Matthaei and E.M.T. Jones, “Microwave Bandstop Filters with Narrow Stop Bands”, *PGMTT National Symposium Digest* vol: 62, no: 1, pp: 46 – 51.

[4.3] E.G. Cristal, L. Young, B.M. Schiffman and D.B. Weller, “Bandstop Filter Formulas (Correspondence)," *Microwave Theory and Techniques, IEEE Transactions on*, vol.15, no.3, pp.195, 195, March 1967.

[4.4] P.A. Dupuis, E.G. Cristal, "Folded-Line and Hybrid Folded-Line Bandstop Filters," *Microwave Symposium Digest, 1974 S-MTT International*, vol.74, no.1, pp.162, 164, 12-14 June 1974.

[4.5] R.E. Pearson, "Novel microstrip bandstop filter," *Electronics Letters*, vol.13, no.19, pp.561, 562, September 15 1977.

[4.6] R. N. Bates, "Design of microstrip spur-line band-stop filters," *Microwaves, Optics and Acoustics, IEE Journal on*, vol.1, no.6, pp.209, 214, November 1977.

[4.7] P. Guillon, S. Mekerta and Y. Garault, "Microstrip bandstop filter using a dielectric resonator," *Microwaves, Optics and Antennas, IEE Proceedings H*, vol.128, no.3, pp.151, 154, June 1981.

[4.8] S. Amari and U. Rosenberg, “Direct synthesis of a new class of bandstop filters,” *IEEE Trans. Microwave Theory Tech.*, vol. 52, pp. 607-616, February 2004.

[4.9] R.J. Cameron, Ying Wang and Ming Yu, "Direct-coupled realizations for microwave bandstop filters," *Microwave Symposium Digest, 2005 IEEE MTT-S International* , vol., no., pp.4 pp.,, 12-17 June 2005.

[4.10] L. Cheng-Jung, K. M K H Leong, and T. Itoh, "Metamaterial Transmission Line Based Bandstop and Bandpass Filter Designs Using Broadband Phase Cancellation," *Microwave Symposium Digest, 2006. IEEE MTT-S International*, vol., no., pp.935, 938, 11-16 June 2006.

[4.11] D. R. Jachowski, “Passive Enhancement of Resonator Q in Microwave Notch Filters” *IEEE MTT-S*, *Digest,* 2004.

[4.12] D. R. Jachowski, “Compact Frequency-Agile, Absorptive Bandstop Filters” *IEEE MTT-S*, *Digest,* 2005.

[4.13] D.R. Jachowski and A.C. Guyette “Sub-Octave-Tunable Microstrip Notch Filter*” IEEE International Symposium on Electromagnetic Compatibility*, 2009.

[4.14] D. R. Jachowski, "Cascadable lossy passive biquad bandstop filter." In *Microwave Symposium Digest, 2006. IEEE MTT-S International*, pp. 1213-1216. IEEE, 2006.

[4.15] A. C. Guyette, I. C. Hunter, D. P. Roger, and D. R. Jachowski. "Perfectly-matched bandstop filters using lossy resonators." In *Microwave Symposium Digest, 2005 IEEE MTT-S International*, pp. 4-pp. IEEE, 2005.

[4.16] F. Frezza, L. Pajewski, and G. Schettini. "Fractal two-dimensional electromagnetic bandgap structures." *Microwave Theory and Techniques, IEEE Transactions on* 52, no. 1 (2004): 220-227.

[4.17] J. D. Joannopoulos, S. G. Johnson, J. N. Winn, and R. D. Meade *Photonic Crystals Moulding the Flow of Light* , Princeton, 2008.

[4.18] L. Pajewski and G. Schettini, "Photonic Band-Gap Structures with Periodicity Interruptions: Theory and Applications," *Transparent Optical Networks, 2007. ICTON '07. 9th International Conference on*, vol.2, no., pp.88, 91, 1-5 July 2007.

[4.19] F. Frezza, L. Pajewski and G. Schettini, "Periodic defects in 2D-PBG materials: full-wave analysis and design," *Nanotechnology, IEEE Transactions on*, vol.2, no.3, pp.126, 134, Sept. 2003.

[4.20] H.C.C. Fernandes, A.R.B. Rocha and A. Teixeira, "Analysis of antennas with PBG substrate," *Microwave and Optoelectronics Conference, 2003. IMOC 2003. Proceedings of the 2003 SBMO/IEEE MTT-S International* , vol.1, no., pp.207,209 vol.1, 20-23 Sept. 2003.

[4.21] W. Y. Leung, R. Biswas, S. D. Cheng, M. M. Sigalas, S. McCalmont, G. Tuttle, and K.-M. Ho, “Slot antennas on photonic band gap crystals,” *IEEE Trans. Antennas Propagat.*, vol. 45, pp. 1569–1570, Oct. 1997.

[4.22] S. T. Chew and T. Itoh, “PBG-excited split-mode resonator bandpass filter,” *IEEE Microwave Wireless Comp. Lett*., vol. 11, pp. 364–366,Sept. 2001.

[4.23] P. Dansas, N. A. Paraire, and S. Laval, “Feasibility of optical filters and switches using plastic photonic bandgap structures”, *Proc. SPIE*, vol.3135, pp. 219–229, 1997.

[4.24] J. G. Maloney, M. P. Kesler, B. L. Shirley, and G. S. Smith, “A simple description for waveguiding in photonic bandgap materials,” *MicrowaveOpt. Technol. Lett.*, vol. 14, pp. 261–266, Apr. 1997.

[4.25] X. Wang, B.Wang, H. Zhang, and K.J.Shen, “A Tunable Bandstop Resonator Based on a Compact Slotted Ground Structure”, *Microwave Theory and Techniques, IEEE Transactions on*, vol.55, no.9, pp.1912-1918, Sept. 2007.

[4.26] D. Ahn, J. Park, C. Kim, J. Kim, J. Qian and T. Itoh, "A design of the low-pass filter using the novel microstrip defected ground structure," *Microwave Theory and Techniques, IEEE Transactions on* , vol.49, no.1, pp.86-93, Jan 2001.

[4.27] D. Woo, T. Lee, J. Lee, C. Pyo and W. Choi, "Novel U-slot and V-slot DGSs for bandstop filter with improved Q factor," *Microwave Theory and Techniques, IEEE Transactions on* , vol.54, no.6, pp.2840-2847, June 2006.

[4.28] S.Huang and Y.Lee, "A Compact E-Shaped Patterned Ground Structure and Its Applications to Tunable Bandstop Resonator," *Microwave Theory and Techniques, IEEE Transactions on,* vol.57, no.3, pp.657-666, March 2009.

[4.29] G. Chaudhary, Y. Jeong, J. Lim, C. Kim, D. Kim, J. Kim and J. Park,“ DMS harmonic termination load network for high efficiency power amplifier applications, "*Microwave Conference (Emu), 2010 European* , vol., no., pp.946-949, 28-30 Sept. 2010.

[4.30] J.Chen, Q.Xue, J.Wang, W.Shao and L.Xue, “Compact microstrip lowpass filter based on defected ground structure and compensated microstrip line," *Microwave Symposium Digest, 2005 IEEE MTT-S International* , vol., no., pp. 4 pp., 12-17 June 2005.

[4.31] H.W. Liu, J.C. Zhang, S.Wang, L.Zhu, X.H.Guan, J.S. Lim and D.Ahn, "Compact dual-band bandpass filter using defected microstrip structure for GPS and WLAN applications," *Electronics Letters* , vol.46, no.21, pp.1444-1445, October 2010 .

[4.32] J J.A.T. Mendez, H.J. Aguilar, F.I. Sanchez, I.G. Ruiz, V.M. Lopez and R.A. Herrera, “ A proposed Defected Microstrip Structure (DMS) behaviour of for reduced Rectangular Antenna size” *Microwave Optical Tech. Letters,* vol.43, no.6, pp. 481-484, Dec. 2004.

[4.33] J. Wang; H. Ning; L. Mao and M. Li; , "Miniaturized dual-band bandstop filter using defected microstrip structure and defected ground structure," *Microwave Symposium Digest (MTT), 2012 IEEE MTT-S International* , vol., no., pp.1-3, 17-22 June 2012.

[4.34] M. K. Mandal, and S. Sanyal, “A novel defected ground structure for planar circuits,” *IEEE Microwave Compon. Lett*., vol. 16, No. 2, pp. 93–95, 2006

[4.35] C. S. Kim, J. S. Park, D. Ahn, and J. B. Lim, “A novel 1-D periodic defected ground structure for planar circuits,” *IEEE Microw. Wireless Compon. Lett.*, Vol. 10, no. 4, pp. 131–133, Apr. 2000.

[4.36] W. Tong and Z. Hu, “Left-handed L-band notch bandstop filter with significantly reduced size,” *IET Microw. Antennas Propagation*, vol.1, no. 1, pp. 45–49, 2007.

[4.37] M. Naghshvarian-Jahromi and M.Tayarani, "Defected ground structure bandstop filter by semi complementary split ring resonators", *IET Microw. Antennas Propagation*, vol.5, no. 11, pp. 1386–1391, 2011.

[4.38] D. La, Y. Lu, S. Sun, N. Liu and J. Zhang," A Novel Compact Bandstop Filter using Defected Microstrip Structure", *Microwave and Optical Technology Letters*, vol.53, no.. 2, pp. 433–435, 2011.

[4.39] K. Chakrabarty and D. Budimir, "Compact tunable bandstop filters using Defected Microstrip Structure for multi-standard wireless systems," *Microwave Conference (EuMC), 2013 European*, vol., no., pp.1031, 1034, 6-10 Oct. 2013.

[4.40] H.W. Liu, Z.C. Zhang, S. Wang, L. Zhu, X.H. Guan, J.S. Lim and D. Ahn, "Compact dual-band bandpass filter using defected microstrip structure for GPS and WLAN applications," *Electronics Letters* , vol.46, no.21, pp.1444,1445, October 2010.

[4.41] Z. Ma, K. Kikuchi, Y. Kobayashi, T. Anada, and O. Hagiwara, "Novel Microstrip dual-band bandstop filter with controllable dual-stopband response," *Proc. Asia-Pacific Microw.Con*, pp. 1177-1180, December 2007.

[4.42] K.S. Chin, J.H. Yeh, and S.H. Chao, "Compact dual-band bandstop filters using stepped-impedance resonators," *IEEE Microw. Wireless Compon. Lett*., vol. 17, no. 12, pp. 849-851, December 2007.

[4.43] X. Hu, Q. Zhang, and S. He, "Dual-band-rejection filter based on split ring resonator (SRR) and complimentary SRR", *Microw. Opt. Technol. Lett*., vol. 51, no. 10, October 2009.

[4.44] V. K. Velidi, and S. Sanyal, "Compact planar dual-wideband bandstop filters with cross coupling and open-ended stepped impedance resonators", *ETRI Journal*, vol. 32, no.1, February 2010.

Chapter 5 Compensation of Nonlinear Distortion using Novel Bandstop Filters

Compensation techniques for nonlinear distortion suppression varies according to the type of distortions produced. Hence it is important to understand the various types of distortions in RF circuits. As discussed previously in chapter 2 and 3, in a simple wireless transceiver, the presence of certain components adds to the distortions along with several other things. Cross-modulation and interference between different channels are a recurring problem. In recent years, with the introduction of multi-standard systems, it has become imperative to design systems with almost no interference; otherwise the whole point of multi-band and multi-standard systems which operates simultaneously in different frequency bands fails.

Hence in this chapter the problems of distortion due to such cross modulation and interferences are discussed. Examples of such systems are provided with mathematical analysis. Methods of compensation are briefly described and one such method using novel bandstop filter is used. The suppression results due to this particular technique are proven mathematically. Extensive experimental verification is then carried out to see if the method is suitable for distortion suppression. It was found that almost 15dB of improvement can be achieved in such cases, hence proving the validity of the method and its scope for further improvement and research.

5.1 Nonlinear Distortion due to Interfering Signals

This section describes some examples of different situation in a real wireless communication system where interfering signals can produce additional distortions affecting the final output spectrum by introducing unwanted terms. Three main scenarios are described and shown here. The effect of the interfering signal is illustrated along with the effect of the compensation technique in Figure 5-1. Here Tx is the main channel, while Tx1 acts as an

interfering signal to Tx. Now, due to the presence of nonlinear circuit in the transmitter Tx, intermodulation products such as IM2 and IM3 are formed very close to the Tx frequency due to the combination of Tx and Tx1 signals. When a compensation technique which is a bandstop filter in this case is used, the Tx1 interfering signal is minimised subsequently and as a result the IMD2 and IMD3 are also greatly reduced.

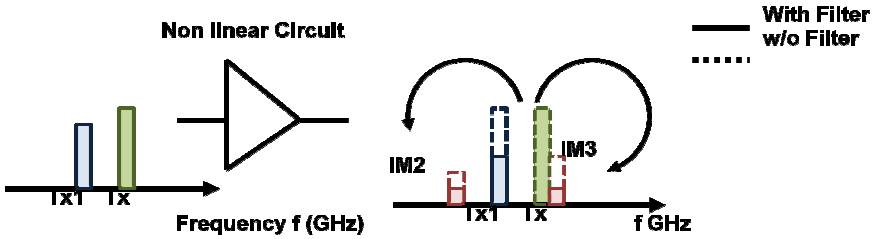

Figure 5-1: Block diagram of a multi band transmitter system showing Tx1 and IM3 suppression by a bandstop filter.

In Figure 5-2, the unwanted intermodulation product such as (2^{nd}, 3^{rd}, 5^{th}, 7^{th} …) of two wanted signals from transmitter can be detected at receiver. The figure illustrates a problem which is seen frequently in a transceiver system. The two wanted signals in the Tx band (930-960MHz) which lies at 930 and 950MHz produces intermodulation distortion products at 910 and 970MHz. These are the third order intermodulation distortion products which fall in the passband and has considerable amount of power to distort the signals. The produced intermodulation product at 910MHz now forms distortions products with the upper Tx band signal at 950MHz. They produce third order intermodulation products which fall again at the RX band at 890MHz as illustrated.

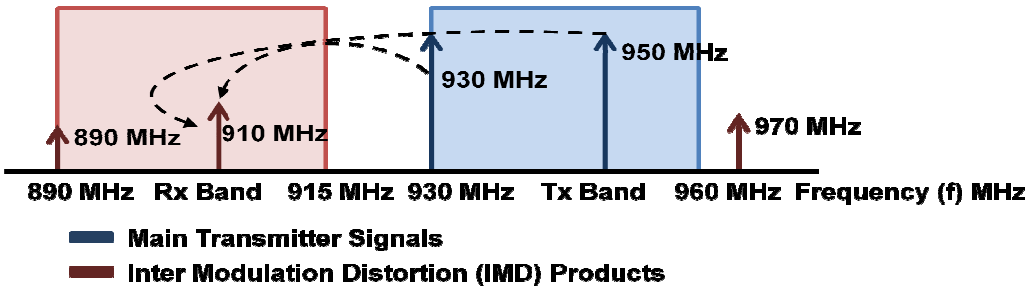

Figure 5-2: IMD products in receiver band due to transmitter.

Another event that generally occurs in the receiver side is that of transmitter signal leakage. This then combines with a continuous wave (CW) tone and forms intermodulation products inside the receiver band. An example in [5.1] and [5.2] shows that code division multiple access (CDMA) system being on the same frequency band as advanced mobile phone system (AMPS) and time division multiple access (TDMA) system causes a similar problem. Signal bandwidths in both AMPS and TDMA are very less hence acting like a CW tone to the CDMA. Hence any transmitter signal leakage will cross-modulate with the CW tone and the cross-modulated products will creep into the receiver band. A diagrammatic representation is shown in Figure 5-3.

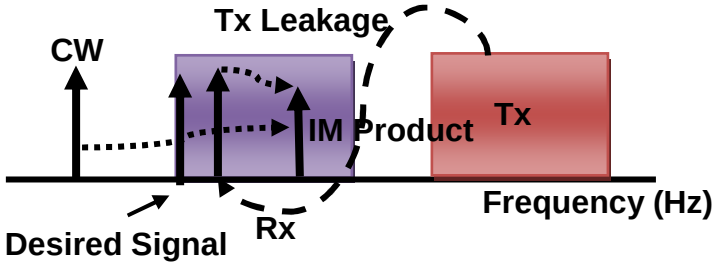

Figure 5-3: IMD product in receiver due to CW and transmission leakage.

The above scenarios lead to spurious effects and unnecessary distortions in the output spectrum. Mathematical analysis is shown here to understand the effect of distortions. To simply the problem, two tone signal is taken, one being the wanted signal and the other one being the unwanted interfering signal. From a general nonlinear series [5.3], the following equation is used.

$$V_0(t) = a_1 * V_i(t) + a_2 * V_i^2(t) + a_3 * V_i^3(t) + \cdots + a_n * V_i^n(t) \quad (5.1)$$

Where, V_0 = Output Voltage and V_i =Input Voltage. The input signal V_i (t) is taken as a combination of wanted and unwanted signal. The unwanted signal can be the Tx leakage or the interfering signals from other bands etc. Therefore,

$$V_i(t) = A_{wanted}\cos(\omega_1 t) + A_{unwanted}\cos(\omega_2 t) \quad (5.2)$$

Where, ω_1 and A_{wanted} is the carrier frequency and amplitude of wanted signal Tx respectively and ω_2 and $A_{unwanted}$ is the carrier frequency and amplitude of the unwanted signal Tx1 respectively. Replacing the input signal in the series which is given in Equation (5.1), it is going to yield an equation as shown in Equation (5.3).

$$V_0(t) = a_1 * [(A_{wanted} * \cos(\omega_1 t)) + (A_{unwanted} * \cos(\omega_2 t))] + a_2 * [(A_{wanted} * \cos(\omega_1 t)) + (A_{unwanted} * \cos(\omega_2 t))]^2 + a_3 * [(A_{wanted} * \cos(\omega_1 t)) + (A_{unwanted} * \cos(\omega_2 t))]^3 + \cdots + a_n * [(A_{wanted} * \cos(\omega_1 t)) + (A_{unwanted} * \cos(\omega_2 t))]^n \quad (5.3)$$

In this case, the first three terms are the most important because of the fact that these intermodulation products appear in the passband or in the vicinity of the passband, the first three power term are evaluated separately for the ease of calculation. The second term $a_2 * [(A_{wanted} * \cos(\omega_1 t)) + (A_{unwanted} * \cos(\omega_2 t))]^2$ can be expanded using simple trigonometric equation where the final result is as in Equation (5.5).

$$V_i^2(t) = a_2 * [(A_{wanted} * \cos(\omega_1 t)) + (A_{unwanted} * \cos(\omega_2 t))]^2 \quad (5.4)$$

$$= a_2 * \left[\left(\frac{A_{wanted}^2}{2} + \frac{A_{unwanted}^2}{2} + \frac{A_{wanted}^2}{2} * \cos(2\omega_1 t) + \frac{A_{unwanted}^2}{2} * \cos(2\omega_2 t)\right) + (\boldsymbol{A_{wanted} A_{unwanted}}(\cos((\omega_1 - \omega_2)t)) + \cos((\omega_1 + \omega_2)t))\right]$$

$$= a_2 * A_{wanted}^2 \left[\left(\frac{1}{2} + \frac{\beta^2}{2} + \frac{1}{2} * \cos(2\omega_1 t) + \frac{\beta^2}{2} * \cos(2\omega_2 t)\right) + (\boldsymbol{\beta}(\cos((\omega_1 - \omega_2)t)) + \cos((\omega_1 + \omega_2)t))\right] \quad (5.5)$$

Where, $\beta = \frac{A_{unwanted}}{A_{wanted}}$, the ratio of the amplitudes of the unwanted and wanted signal. Hence from this, the effect of the amplitude of the unwanted signal on the 2nd order intermodulation products which occurs at $\omega_1 - \omega_2$ and $\omega_1 + \omega_2$ can be seen. If the amplitude of the unwanted signal is zero, then β is zero. When unwanted signal is high, β is also high. The value of β is greater than one when the amplitude of the unwanted signal exceeds the amplitude of the wanted signal. Now similarly evaluating the third term $a_2 * [(A_{wanted} * \cos(\omega_1 t)) + (A_{unwanted} * \cos(\omega_2 t))]^3$ the following results can be obtained as in Equation (5.7) and (5.8).

$$V_i^3(t) = a_3 * \left[\left(\left(\frac{3 * A_{wanted}^3}{4} + \frac{3 * A_{wanted} A_{unwanted}^2}{2}\right) * \cos(\omega_1 t)\right) + \left(\left(\frac{3 * A_{unwanted}^3}{4} + \frac{3 * A_{unwanted} A_{wanted}^2}{2}\right) * \cos(\omega_2 t)\right) + \left(\left(\frac{A_{wanted}^3}{4} * \cos(3\omega_1 t)\right) + \left(\left(\frac{A_{unwanted}^3}{4} * \cos(3\omega_2 t)\right) + \left(\left(\frac{3 * A_{unwanted} A_{wanted}^2}{4}\right) * (\cos((2\omega_1 - \omega_2)t)) + \cos((2\omega_1 +\right.\right.\right.\right.\right.$$

$$\omega_2)t))\Big) + \Big((\frac{3*A_{wanted}\,A_{unwanted}{}^2}{4}) * (\cos((\omega_1 - 2\omega_2)t)) + \cos((\omega_1 + 2\omega_2)t)\Big)\Big] \quad (5.7)$$

$$= a_3 * \frac{3*A_{wanted}{}^3}{4}\Big[((1 + 2\beta^2) * \cos(\omega_1 t)) + ((\beta^3 + \beta) * \cos(\omega_2 t)) + \Big((\frac{1}{3} * \cos(3\omega_1 t)\Big) + \Big((\frac{\beta^3}{3} * \cos(3\omega_2 t)\Big) + \Big((\beta(\cos((2\omega_1 - \omega_2)\,t)) + \cos((2\omega_1 + \omega_2)t))\Big) + (\beta^2(\cos((\omega_1 - 2\omega_2)t)) + \cos((\omega_1 + 2\omega_2)t))\Big] \quad (5.8)$$

Where, $\beta = \frac{A_{unwanted}}{A_{wanted}}$, the ratio of the amplitudes of the unwanted and wanted signal. Hence, clearly the effect of the amplitude of the unwanted signal on the 3rd order intermodulation products which occurs at $2\omega_1 - \omega_2$, $2\omega_1 + \omega_2$, $\omega_1 - 2\omega_2$, $\omega_1 + 2\omega_2$ can be seen. With further increase in the complexity in order, there are other intermodulation products appearing at the output. The intermodulation distortion power in terms of the equation shown here is significantly high when the amplitude of the interfering signal is higher because of the effect of the factor β.

5.2 Compensation Techniques for Distortion Suppression

There are various types of linearization techniques available in literature. It is imperative to find a solution to the existing problem and conduct additional research in areas which are not well developed. Compensation techniques can be briefly classified into seven main categories such as the following [5.4]-[5.10]

1. Feedback
2. Feed forward
3. Pre-distortion
4. Injection method
5. Envelope elimination and restoration (EER)
6. Linear amplification using nonlinear components (LINC)
7. Filtering

The feedback linearization technique is a broader term for many different types of feedback linearization such as RF feedback [5.11], modulation feedback [5.12], polar loop [5.13] and Cartesian loop [5.14]. In its simplest form, the feedback linearizer works by feeding back the distorted output signal which is then passed through a voltage divider with a particular gain, the result from this is then compared to the input signal forming the error signal. The main goal is to correct the input signal as much as possible hence providing a linearized output. The feedback system suffers from problems such as stability issues and a reduction in the overall system gain. Several methods have been proposed in order to get rid of it as in [5.15].

To do away with the disadvantages of the feedback method, feed forward linearization technique is introduced. The fundamental concept of feed forward lies in having two separate loops one for signal cancellation and the other for error cancellation. The main input signal is passed through the nonlinear power amplifier and is subtracted from a delayed version of itself, hence obtaining the IMD products. These obtained distortion products are amplified to the required level and then subtracted from the original signal thus obtaining a distortion free linearized output signal. This takes place in the error loop [5.16]-[5.17]. The problem with the feed forward system is the use of another Class A linear amplifier, which sometimes can be high in cost and contribute to the overall complexity of the system.

The concept of predistortion technique involves both analogue [5.18] and digital [5.19] predistortions. The underlying concept lies in the introduction of a previously inversed PA output which when combined with the real distorted signal, gives a linearized output. The main difference between analogue and digital predistortion technique lies in the fact that the former is used in the RF or IF domain while the latter is used in the digital domain. While analogue predistortion suffers from power loss due to additional RF components, digital predistortion techniques can be extremely complex due to the lack of memory effect consideration leading to an increase in circuit cost and size. In [5.20], an adaptive digital predistortion technique is proposed with improved memory effects.

Another common type of distortion suppression technique is the injection method [5.21]-[5.23]. Injecting particular frequency components back into the

original circuit can cancel out the 3rd or 5th order harmonics according to the components injected. This is mostly done with the frequency difference component such as $\cos(\omega_1 - \omega_2)\, t$ and the second harmonic component $\cos(2\omega_1 t)$.These when mixed with the fundamental tone $\cos(\omega_1 t)$, forms additional third order intermodulation products at $\cos(2\omega_1 - \omega_2)\, t$This can be then amplitude and phase adjusted to cancel out the third order distortion product already produced. Hence a linear output can be achieved. The major drawback of such techniques is the inability of the phase and the gain to be accurately adjusted leading to further problems. Additional low amplitude distortion products formed can also distort the output signal in some cases.

The envelope elimination and restoration method [5.24] comprises of the input signal being divided into two parts, one of which is passed through an envelope detector forming the AM part and the other a limiter, forming the PM part. The AM part is subsequently amplified by a baseband amplifier while the PM part is amplified by a RF amplifier. The final envelope restoration happens when the AM signal is used to modulate the final RF signal. The limiter helps in getting rid of the AM/PM distortions and hence a linearized output is obtained. Few possible disadvantages of the EER method are nonlinearity of the baseband amplifier, envelope detector etc., and delays in the path and reduced efficiency of the system [5.25].

Another linearizer concept is the linear amplification using nonlinear components [5.26]-[5.27]. This type of linearizer uses nonlinear components to achieve a linear output. The main task involved is to split the incoming signal into two parts of phase modulated signal having constant envelopes using an AM-PM modulator. Each individual part is then amplified using highly efficient power amplifiers, and added at the output. This signal has a linear relationship with the input signal thus eliminating distortions and giving a linearized effect. There are many drawbacks of this system including complexity, realization of a AM-PM modulator and phase and gain imbalance of the two branches using identical power amplifiers [5.28]-[5.29].

The filtering concept has been explained in [5.30] and [5.31] where filtering is used both before and after the power amplifier in order to get rid of distortions. Filtering can be done either by a bandpass filter or a bandstop filter.

The BPF has resonators which resonate in the passband. These can however induce transmission loss due to the resistance of the resonators. A steep phase change response is seen due to resonance which can also contribute to the loss. On the other hand, the BSF has resonators which resonate in the stop band. These have lower transmission loss and variation in group delay as compared to BPF. In cases where a BSF is used after the power amplifier, a dual-band filter is required in order to filter out both sides of distortions. Such filters needs to be designed with the power requirements in mind. In cases where interfering signals are present, these can further contribute to nonlinearity as mathematically shown in the next section. Such cases require inter-stage bandstop filters as in [5.2].

5.3 Mathematical Analysis showing Interference Suppression using Novel Bandstop Filter

As previously mentioned in Section 5.2, using a bandstop filter for distortion suppression due to interfering signals is the most convenient method in terms of implementation, size and cost. In order to have an initial proof of theory mathematical expressions were derived which showed that filters could be a possible way of interference reduction and hence an overall reduction in distortions in the output spectrum can be achieved. This will be proved in this section and in the next. This section mostly deals with the proof of theory and mathematical derivations along with both simulation and experimental verification using a nonlinear power amplifier as DUT.

The proposed method shown has been developed and tested using a PA as the DUT. Operating the power amplifier in the saturation region has become vital with the onset of 4G LTE systems which provides excellent data rates and faster communication. This will result in higher efficiency for the amplifier but with reduced linearity. Correction of such IMD products in wireless transmitters is therefore a necessity [5.20].

High power interfering signal along with the main signal can make the intermodulation distortion much worse and can distort the output spectrum considerably. Different methods of PA linearization can be used to overcome

such problem. Such methods require complex circuitry which can prove to be a disadvantage. This chapter presents a simpler compensation technique of minimizing nonlinear distortion produced due to high power interfering signals at the input of the PA. A bandstop filter is used to suppress the additional frequency components. This technique is simple in its architecture and can be flexibly adjusted to suit the requirements of the system where interfering signals are a major issue. This theory is further supported by simulation and experimental verifications.

A wireless system consisting of power amplifiers, reconfigurable/tunable RF circuits can present a persistent problem due the distortion effects produced because of the elements inherent nonlinear nature. It is imperative that new methods are devised for varactor based tunable filters and PIN based reconfigurable filters in order to improve nonlinear distortion performance. In this context, a simple method which is capable of compensating nonlinear effects produced due to the unwanted high power signals at the input of a particular communication system is discussed. The block diagram of the proposed approach is illustrated in Figure 5-4. The bandstop filter is cascaded with the power amplifier which acts as the nonlinear device. Nonlinear device such as reconfigurable/ tunable RF circuits can also be used in place of the nonlinear power amplifier. The power amplifier used has a gain of G_{amp} and an intercept point at I_{amp}. The bandstop filter has a passband loss of $L_{filter1}$ and stopband attenuation of $L_{filter2}$.

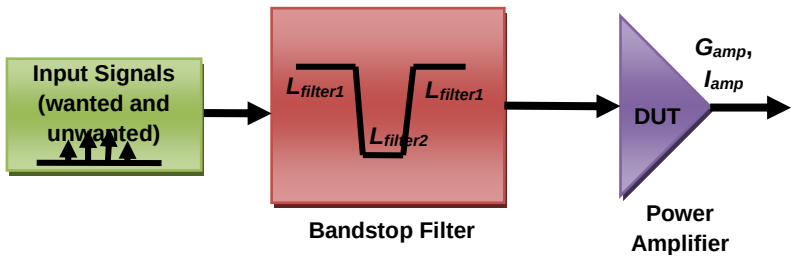

Figure 5-4: Block diagram of the proposed system.

The Figure 5-4 above uses a bandstop filter to filter out the effects of nonlinearity which occurs due to unwanted signals at the input. The concept of the system can be explained as follows. Interfering signals appearing at the input of a nonlinear device causes nonlinear distortions which can affect the

clarity of the output signal. Thus when a bandstop filter designed at the same centre frequency as the unwanted signals is used; the distortions can be filtered out. The stopband attenuation of the designed filter will determine the amount by which the IMD distortions get reduced [5.31]. To calculate the nonlinear distortion of the nonlinear device, such as a power amplifier in this case, the block diagram in Figure 5-4 can be used, which shows a bandstop filter with $L_{filter2}$ as the stopband attenuation and $L_{filter1}$ as the passband attenuation, the power amplifier has a gain G_{amp1} and third order intercept (TOI) point I_{amp1}.

The interfering signals of power level P_{in} dBm combines with the wanted signals producing intermodulation components as the system has nonlinear blocks. Due to the placement of the bandstop filter where the interfering signals falls in the stopband and the input signal (wanted signal) is assumed to be in the passband of the system, the distortions are greatly reduced. The output power level of the IMD signals at the output is calculated for both cases. The case to be considered is when no bandstop filter is used. Nonlinear distortion products produced due to the amplifier will have an output power level as follows:

$$P_{W/o} = 3 * P_{in} - 2 * I_{amp1} + G_{amp1} - L_{filter1} \tag{5.9}$$

Where, $P_{w/o}$ = 3rd order IMD power without bandstop filter, P_{in} = unwanted input signal power, I_{amp1} = 3rd order intercept point and $L_{filter1}$ = passband attenuation of the bandstop filter which is negligible, G_{amp1} = gain of PA. Similarly the case where bandstop filter is used can be now considered. The equation (5.10) shows the power level of the IMD when filter is used. This is now expanded to give equation (5.11).

$$P_{w/filter} = 3 * \left(P_{in} - L_{filter2}\right) - 2 * I_{amp1} + G_{amp1} \tag{5.10}$$

$$P_{w/filter} = 3 * P_{in} - 2 * I_{amp1} + G_{amp1} - 3 * L_{filter2} \tag{5.11}$$

Where, $P_{w/filter}$ = 3rd order IMD power after using filter, P_{in} = unwanted input signal power, I_{amp1} = 3rd order intercept point and $L_{filter2}$ = stopband attenuation of the bandstop filter, G_{amp1} = gain of PA.

When the above results are compared , it is clearly seen from equation (5.9) and equation (5.11) that for the reduction of third order intermodulation power, the bandstop filter plays a major role. The two expressions can be written in terms of each other as in equation (5.12).

$$P_{w/filter} = P_{w/o} + L_{filter1} - 3 * L_{filter2} \quad (5.12)$$

As can be seen from equation (5.12) $P_{w/o} > P_{w/filter}$; where $P_{w/o}$ denotes the IMD power without filter and $P_{w/filter}$ denotes the IMD power with bandstop filter.

5.4 Experimental Verification of the Concept using Bandstop Filter

In a real transmitter system, there are several components which contribute to interfering signals. A mixer can be one such component which creates additional unwanted signals due to its own nonlinearity. Hence a simulation setup was used where interfering signals were emulated by using a mixer which produced additional distortion components. A nonlinear power amplifier was again used as a DUT. In order to verify the system, ADS simulations are performed with a nonlinear power amplifier model, a bandstop filter and a mixer. The later is capable of emulating real life unwanted input signals. The frequency for the 4G (LTE) band of 758MHz-768MHz has been used here. A two tone simulation is done with harmonic balance simulator in order to see the third order IMD products clearly. The mixer is set up in such a way so as to produce two main tones at f_1 which is 761MHz and f_2 which is 763MHz as the main input signal. Due to the mixer's nonlinearity, IMD products are formed at $2f_1$-f_2 at 759MHz and $2f_2$-f_1 at 765MHz which acts as additional interfering signals at the input of the power amplifier. Two scenarios are considered and discussed, one for which the bandstop filter is not used and the other where the bandstop filter is used. This way the two outputs can be compared at the end of the power amplifier and difference due to the bandstop filter can be noted. For the first case, where the filter is not used, the following Figure 5-5 shows the schematic of the system:

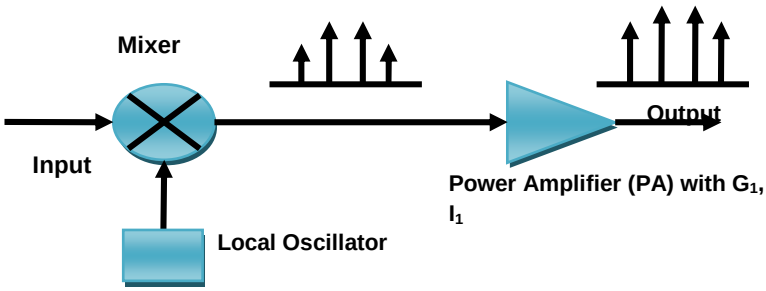

Figure 5-5: Block diagram of the mixer-amplifier system without using bandstop filter.

The emulated interfering signal at the input of the PA produces IMD products which distorts the main output signal by falling in the passband. The power level for such distorted products is quite high as shown below in the simulated results. The input power is varied from a range of -10dBm to 10dBm. The following Figure 5-6 shows the result at the output of the power amplifier for P_{in} = 10dBm, where the IMD product is considerably worse.

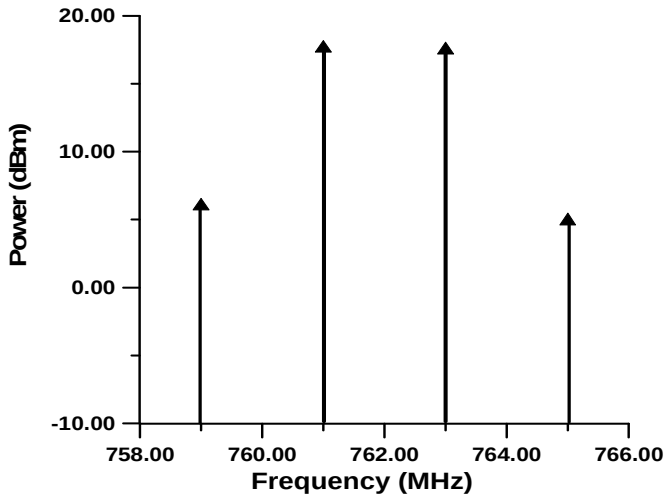

Figure 5-6: Simulated two-tone output spectrum of the Tx without BSF.

From Figure 5-6, it is noticed that the output power of the fundamental tones gets saturated at 17.6dBm. This is mainly due to the fact that the power amplifier goes into saturation beyond a point. The third order intermodulation products occurring at $2f_1$-f_2 and $2f_2$-f_1 (759 and 765MHz) have significant power levels measured to be 6dBm. The difference in the two levels (output power and distortion power) or the relative distortion can be measured as 11.6dB approximately. This is clearly not a good response and the distortion level

needs to be further improved. Hence in the next simulated case, a bandstop filter with centre frequency same as the interfering tones are used, which in this case are 759MHz and 765MHz.

The utility of the inter-stage bandstop filter lies in the fact that it can block unnecessary signals which in turn can minimise the IMD product to a large extent. This particular example case requires a dual-band bandstop filter due to the appearance of multiple unwanted signals. The centre frequencies of both bands are chosen so as to attenuate the unwanted signals falling in the stopband. The stopband attenuation is chosen to be 30dB. The following shows the response of the bandstop filter block used. It has two bands with centre frequencies located at 753MHz and 771MHz. The choice of centre frequency is critical as it has the capability to minimise other interfering signals that may occur in that particular band.

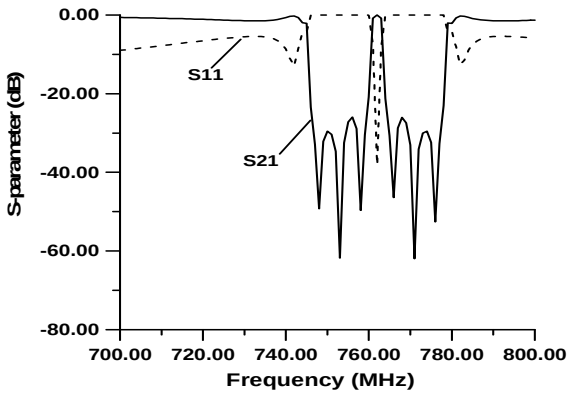

Figure 5-7: Simulated S-parameters of the bandstop filter.

From Figure 5-7, it is clear that the characteristics of the dual-band bandstop filter are critical. Here a narrow bandwidth (approximately 30MHz) is used in order to minimise distortions. The solid line represents the S21 response, while the dotted line shows the S11 response of the filter. From equation (5.12) above, the power of the intermodulation distortion product will be considerably reduced when the interferers fall in the stopband of the filter. The main signal at the input of the power amplifier passes unscathed due to its placement in the passband of the filter. Figure 5-8 shows the simulation setup used.

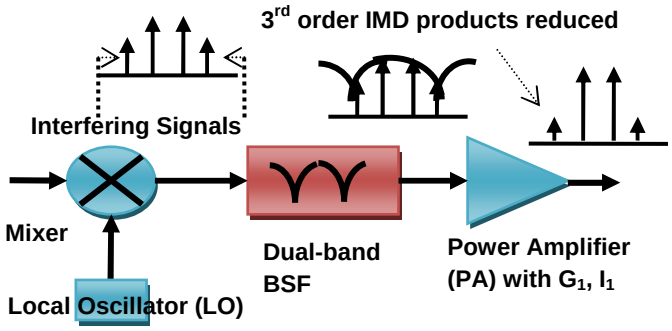

Figure 5-8: IM3 suppression by bandstop filter.

Figure 5-8, shows the cascade of a mixer, a dual-band bandstop filter and the nonlinear PA. The response obtained by simulating the above set-up is shown as in Figure 5-9. The input power is taken as 10dBm, in order to see the maximum distortion effects.

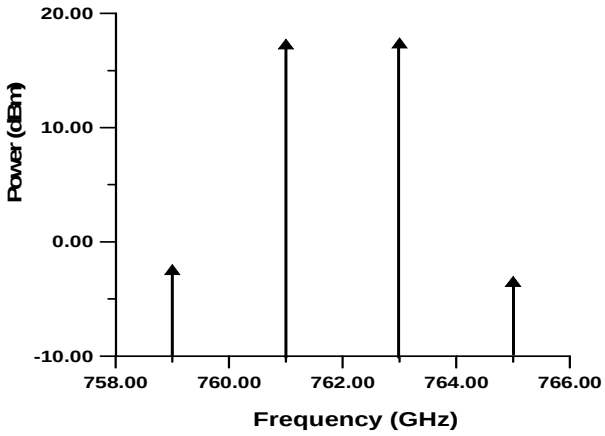

Figure 5-9: Simulated two-tone output spectrum of the Tx with BSF.

Figure 5-9, shows the output of the power amplifier when a bandstop filter is used. The main signal appears at f_1 (761MHz) and f_2 (763MHz) and has a signal level of 17.3dBm. This is similar to the one obtained before in Figure 5-6. Hence this shows that the power efficiency of the amplifier is not compromised by using this method. The third order intermodulation appears at $2f_1$-f_2 (759MHz) and $2f_2$-f_1 (765MHz) having a power level of -3.4dBm. Comparing the above results, it is seen that an overall improvement of 8dB is achieved when the bandstop filter is used as the method of compensation. Nonlinear distortion suppression using this technique was experimentally verified with a 5MHz QPSK signal and a single interfering tone as shown in Figure 5-10.

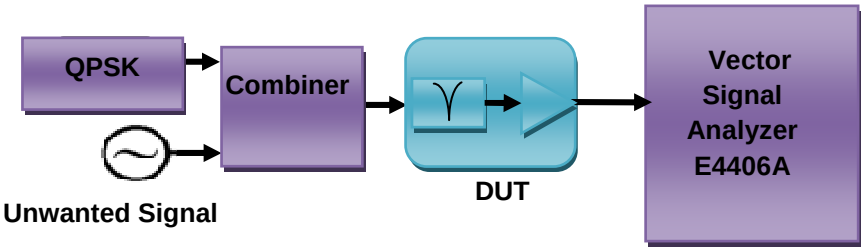

Figure 5-10: Experimental setup for compensation technique.

From Figure 5-10, it can be seen that to emulate the interfering signal and the main signal two differet sources have been used. For the main signal, a 5MHz QPSK digitally modulated signal has been generated at 793.3MHz, while for the interfering signal, a single tone has been generated using Agilent EXG signal generator at 802MHz located very near the main signal. Again, similar to the simulation set-up, two cases were considered, one with the bandstop filter and the other without the bandstop filter. For this purpose a bandstop filter was fabricated having a centre frequency at 802MHz. The experimental result of the filter is shown in Figure 5-11.

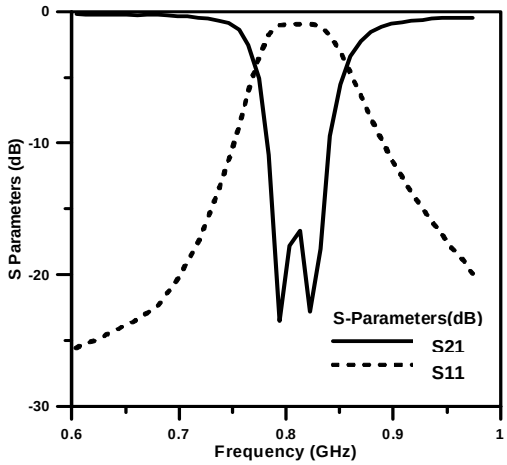

Figure 5-11: Experimental S-parameters of the bandstop filter.

The filter shown has an attenuation of around -20dB and very little passband loss being less than -3dB. The unwanted signal was placed at the centre frequency of the filter , while the main signal was placed in the lower passband of the filter having very little loss. Figure 5-12 shows the measured 5MHz QPSK output spectra before and after using bandstop filter.

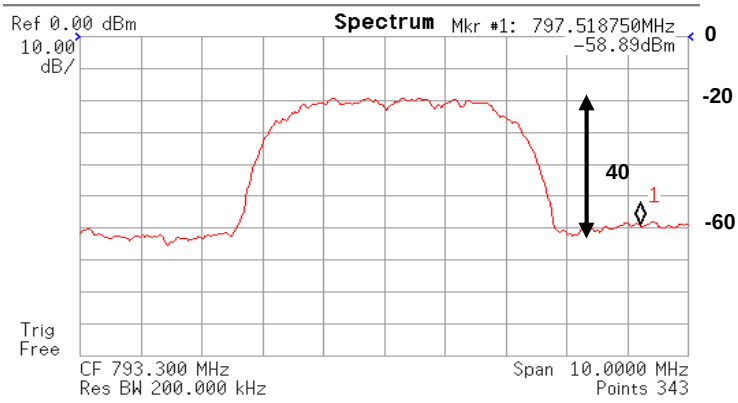

(a)

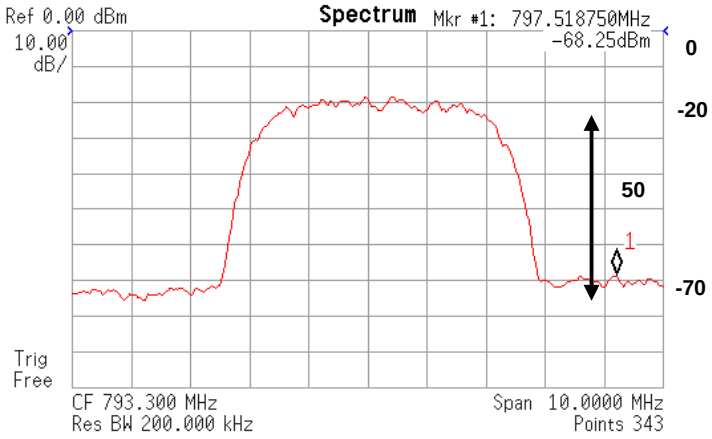

(b)

Figure 5-12: Measured 5MHz QPSK output spectrum of the transmitter (a) without (b) with the bandstop filter.

Figure 5-12 above, shows the comparison between normal output spectrum with interfering signal present at the input and the output spectrum where prior filtering was done to remove the interfering signal. As can be seen from Figure 5-12(a), the relative distortion is 40dB and in Figure 5-12(b), the relative distortion is 50dB. It can be seen clearly that there is a 10dB improvement using the bandstop filter.

Another example using the same bandstop filter is discussed here. Here a digitally modulated signal was used with an interfering tone and simulated with results shown. A different centre frequency for the main signal is chosen and results noted. The main signal at the input of the power amplifier should lie in the passband of the bandstop filter and hence passes unaltered. The following Figure 5-13 shows the schematic used.

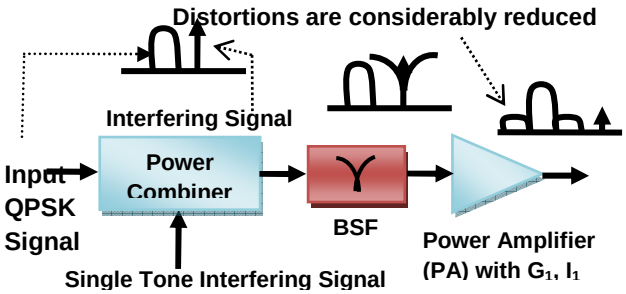

Figure 5-13. Shows nonlinear distortion suppression by bandstop filter.

The 5MHz QPSK signal was generated in ADS and passed through the system along with the interfering tone. The adjacent channel power ratio or the relative distortion is calculated around 20dB without the use of filter. The QPSK signal had a centre frequency of 765MHz. The same setup was used with the filter and responses showed that ACPR was around 30dB. The response obtained by simulating the given circuit is shown in Figure 5-14. An input power of 10dBm was chosen, in order to see maximum distortions.

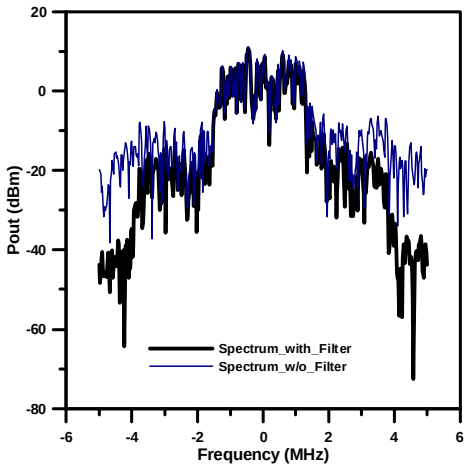

Figure 5-14: Simulated output spectrum comparing the responses of the power amplifier with and without bandstop filter.

Figure 5-14, shows the comparison of the output of the power amplifier in the two cases. The adjacent channel shows that the distortions have been considerably reduced. The power level in the main channel is similar in both cases hence no compromise in the efficiency of the PA is made. It can be seen that there is some improvement in the distortions in the adjacent channel. An improvement of around 10dB was achieved in simulation. Distortion

suppression using this technique was verified experimentally with a 5MHz QPSK signal and a single interfering tone using a similar setup as shown in Figure 5-10. The measurements using the bandstop filter show approximately a 10dB improvement to linearity for the same QPSK input power as shown in Figure 5-15.

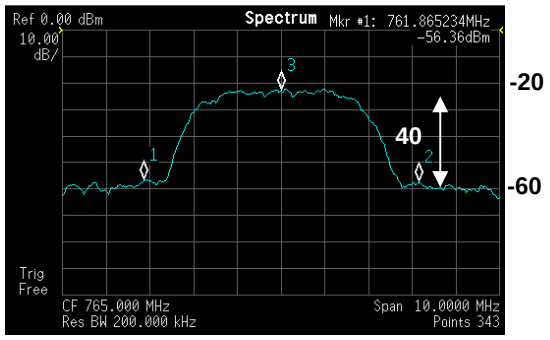

(a)

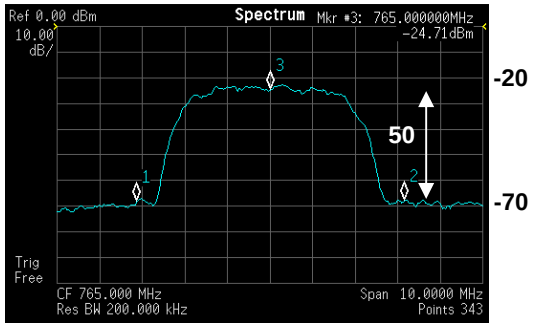

(b)

Figure 5-15: Measured output spectrum of the transmitter (a) without (b) with the bandstop filter.

From the above Figure 5-15, it can be seen that an improvement of 10dB is made. The proposed method using a bandstop filter reduce nonlinear distortion in RF transmitters is simple and low cost. The technique was verified both in simulation and experiments, where the distortion from a single interference tone on a QPSK signal was shown to be suppressed by around 10dB.

The next example shows another proof of theory where a reconfigurable bandpass filter has been used as part of the Tx chain along with a power amplifier. In order to see the nonlinear distortion in the overall Tx, it was important to cascade all the important components contributing to nonlinearity. The device under test comprised of part of the Tx chain. The following Figure 5-

16 shows the setup used where a 5MHz QPSK signal at a center frequency of 2.14GHz was used as the main input signal. The interference tone was located at 2.28GHz. The signals were generated separately and combined with a power combiner. The power amplifier had a gain of 10dB. Hence when interfering signals are present, due to amplification in subsequent stages, the effect of a very strong interfering signal is seen, while in the case where interfering signal is already attenuated by the BSF, very little effect is seen as discussed below.

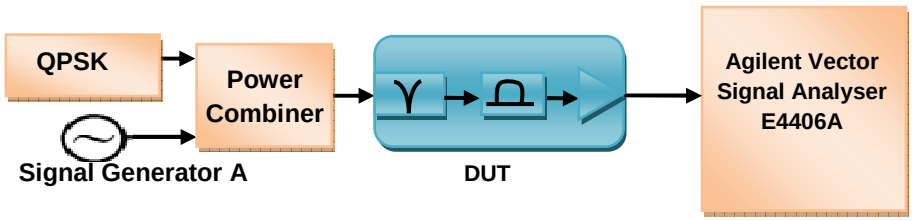

Figure 5-16: Experimental set-up for Tx interference suppresion.

The interfering signal power was hence 20dBm after the amplifier stage. Hence a relative distortion of around 35dB is noticed with the case when no bandstop filter is used. The adjacent channel shows the effect of the strong interfering signal as shown in Figure 5-17. The bandstop filter has a center frequency of 2.28GHz and has a filter response as shown in chapter 4, Figure 4-25. The 5MHz QPSK output spectrum shown for the case where bandstop filter is used has a much better response with a relative distortion of around 51dB. It was noticed that the output power level of the main channel remains the same for both cases with no effect in efficiency of the Tx system. Figure 5-17 below shows the output spectrum for both cases with and without filter.

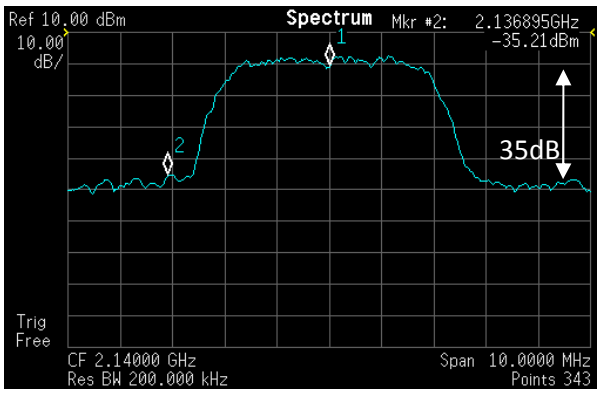

(a)

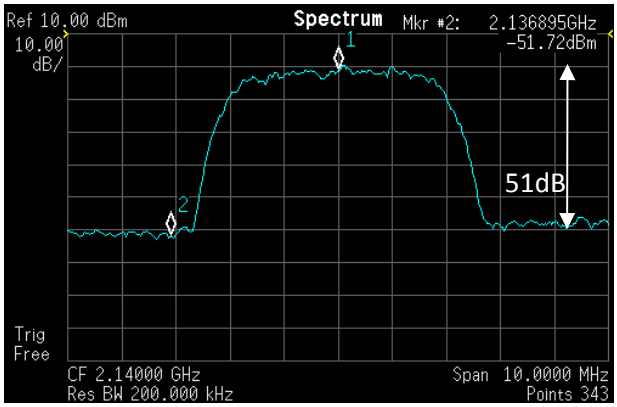

(b)

Figure 5-17: 5MHz QPSK output spectrum (a) without and (b) with bandstop filter.

Hence from Figure 5-17, the relative distortion measured for system with bandstop filter is much higher as compared to the other case without a filter. A difference of nearly 15dB is noticed showing that a much better output is obtained at the Tx when an inter stage bandstop filter is used.

5.5 Conclusion

This chapter summarises the various compensation techniques that can be used for nonlinear distortion suppression in reconfigurable and tunable RF and microwave circuits. The effect of nonlinear distortion due to interfering signals has been presented and various different real life scenarios were explained with examples. Mathematical analysis of nonlinear distortion due to interfering signals is also presented. A method using novel bandstop filter has been used as a technique of compensation and results have been measured for three different scenarios. An experimental setup using a 5MHz QPSK input signal, along with an interfering tone, is passed through the device under test, containing some nonlinear circuit. The output spectrum was measured for both cases with and without using a bandstop filter. It was seen that more than 10dB improvement is obtained when the filter is used as an inter-stage component. The second scenario was similar to the first one but here the main QPSK signal was shifted further away from the interfering signal. It is shown that the interfering signal still had effects on the main signal and a 10dB improvement

was achieved using a bandstop filter. The third scenario tested a combination of a reconfigurable bandpass filter along with power amplifier forming part of the Transmitter system. It was seen that a 15dB improvement was achieved using an inter-stage bandstop filter. This technique of nonlinear distortion compensation shows a good suppression till 15dB. It is superior to other such methods available in literature in terms of cost as very inexpensive microstrip bandstop filters can be designed. This method can directly be used in the RF section of the transceiver without the need of any digital signal processing. This in term reduces complexity and makes the process much simpler.

5.6 References

[5.1] Q. Gu, *RF System Design of Transceivers for Wireless Communications*, Springer *USA*, 2005.

[5.2] T. Ito, M. Kanemaru and A. Matsuzawa, “A 0.8-1.5GHz Multi-Standard WCDMA Receiver with an Inter-Stage Tunable Notch Filter”, *European Microwave Conference*, France, Sept 2010, pp. 1118-1121.

[5.3] W. Eberle, “Wireless Transceiver Systems Design" *Springer USA,* 2008

[5.4] A. F. Mitchell, “A 135MHz feedback amplifier,” *IEE Colloq. Broadband High Frequency Amplifiers: Practice and Theory*, pp. 2/1-2/6, London, Nov. 1979.

[5.5] Y. Yang, and B. Kim, “A new linear amplifier using low-frequency second-order intermodulation component feedforwarding,” *IEEE Microwave and Guided Wave Letters,* vol. 9, no. 10, pp. 419–421, Oct. 1999.

[5.6] S. Chung, J. W. Holloway, and J. L. Dawson, “Energy-efficient digital predistortion with lookup table training using analog cartesian feedback,” *IEEE Transactions on Microwave Theory Tech.* vol. 56, no. 10, pp. 385-392, Oct. 2008.

[5.7] C. S. Aitchison, M. Mbabele, M. R. Moazzam., D. Budimir, and F. Ali, “Improvement of third order intermodulation products of RF and microwave amplifiers by injection," *IEEE Transactions on Microwave Theory and Techniques*, vol. 49, no. 6, pp. 1148-1154, June 2001.

[5.8] F. H. Raab, “Envelope-elimination-and-restoration system concepts,” In *Proc. 1987-RF Expo East, Boston, MA,* pp. 167 - 177, Nov. 1987.

[5.9] D.C. Cox, “Linear amplification with nonlinear components”, *IEEE Transactions on Communication Technology*, vol. 22, no 12, pp 1942-1945, Dec. 1974.

[5.10] C. Rauscher, "Varactor-tuned active notch filter with low passband noise and signal distortion," *Microwave Theory and Techniques, IEEE Transactions on*, vol.49, no.8, pp.1431-1437, Aug 2001.

[5.11] A. F. Mitchell, “A 135MHz feedback amplifier,” *IEE Colloq. Broadband High Frequency Amplifiers: Practice and Theory*, pp. 2/1-2/6, London, Nov. 1979.

[5.12] T. Arthanayake, and H. B. Wood, “Linear amplification using envelope feedback,” *IEE Electronics Letters*, vol. 7, no. 7, pp. 145-146, Apr. 1971.

[5.13] V. Petrovic, and W. Gosling, “Polar-loop transmitter”, *IEE Electronics Letters*, vol. 15, no. 10, pp. 286-288, May 1979.

[5.14] M. Johansson, and L. Sundstrom, “Linearization of RF multicarrier amplifiers using Cartesian feedback,” *IEE Electronics Letters*, vol. 30, no. 14, pp. 1110-1111, Jul. 1994.

[5.15] M. Faulkner, “Amplifier linearization using RF feedback and feedforward techniques,” *IEEE Transactions on Vehicular Technology*, vol. 47, pp. 209-215, Feb., 1998.

[5.16] Y. K. G. Hau, V. Postoyalko, and J. R. Richardson, “Design and characterization of a microwave feed-forward amplifier with improved wide-band distortion cancellation,” *IEEE Transactions on Microwave Theory Tech.* vol. 49, no. 1, pp. 200-203, Jan. 2001.

[5.17] S. P. Stapleton, “Adaptive feedforward linearization for RF power amplifiers,” *55th ARFTG Conference Digest-Spring,* vol. 37, pp. 1-7, Jun. 2000.

[5.18] W. Huang, R.E. Sand, "Novel third-order distortion generator with residual IM2 suppression capabilities," *IEEE Transactions on Microwave Theory and Techniques,* vol.46, no.12, pp.2372-2382, Dec 1998.

[5.19] S. Chung, J. W. Holloway, and J. L. Dawson, “Open-loop digital predistortion using Cartesian feedback for adaptive RF power amplifier linearization,” in *Proc. IEEE MTT-S Int. Microw. Symp. Dig.*, Jun. 2007, pp. 1449–1452.

[5.20] D. Bondar, and D. Budimir, “Digital baseband predistortion of wideband power amplifiers with improved memory effects,” in *Proc. IEEE Radio and Wireless Symposium,* Jan. 2009, pp. 284-287.

[5.21] N. Males-Ilic, B. Milovanovic, and D. Budimir, “Improvement in second harmonics linearization technique for multichannel amplifiers,” *Microwave and Optical Technology Letters*, vol.38, no. 2, pp. 150-153, Jul. 2003.

[5.22] M. R. Moazzam, C. S. Aitchison, “A low third order intermodulation amplifier with harmonic feedback circuitry,” *IEEE MTT-S Int. Microwave Symp. Dig.*, vol.2, pp.827-830, 1996.

[5.23] M. Modeste, et al., “Analysis and Practical Performance of Difference Frequency Technique for Improving the Multicarrier IMD Performance of RF Amplifiers,” *IEEE MTT Symposium on Technologies for Wireless Applications*, Vancouver, pp.53-56, Feb. 1999.

[5.24] L. R. Kahn, “Single sideband transmission by envelope elimination and restoration,” *Proc. of the Institute of Radio Engineers*, vol.40 no.7, pp.803-806, Jul. 1952.

[5.25] F. H. Raab,”Envelope-elimination-and-restoration system concepts,” In *Proc. 1987-RF Expo East, Boston, MA,* pp. 167 - 177, Nov. 1987.

[5.26] D.C. Cox, “Linear amplification with nonlinear components”, *IEEE Transactions on Communication Technology*, vol. 22, no 12, pp 1942-1945, Dec. 1974.

[5.27] X. Zhang, L. E. Larson, “Gain and phase error-free LINC transmitter,” *IEEE Transactions on Vehicular Technology*, vol. 49, no. 5, pp. 1986-1994, Sept. 2000.

[5.28] F. J. Casadevall, and A. Valdorinos, “Performance analysis of QAM modulations applied to the LINC transmitter,” *IEEE Trans. Veh. Technol*., vol. 42, no. 4, pp. 399-406, Nov. 1993.

[5.29] A. Grebennikov, “RF and Microwave Transmitter Design”, *John Wiley & Sons, Inc.*, 2011.

[5.30] H. Uchida, H. Kamino, K. Totani, N. Yoneda , M. Miyazaki, Y. Konishi, S. Makino, J. Hirokawa, M. Ando, "Dual-band-rejection filter for distortion reduction in RF transmitters," *Microwave Theory and Techniques, IEEE Transactions on* , vol.52, no.11, pp.2550,2556, Nov. 2004.

[5.31] J.D. Rhodes and I.C. Hunter, “Synthesis of reflection-mode prototype networks with dissipative circuit elements” *IEE Proc. Microwave Antenna Propagation*, Vol.144, No.6 December 1997, pp.437-442.

Chapter 6 Conclusion

This chapter summarises some of the main concepts of this thesis including a recap of the work done, original contributions made and potential future works that can be carried out. The most important part of this thesis is to develop novel bandstop filters for the use in distortion compensation in RF circuits due to the presence of strong interfering signals in multi-standard wireless system. Prior to that, RF circuits showing nonlinear property was experimentally verified for nonlinear distortion effects using advanced digitally modulated signals.

The thesis aims to address some gaps in research such as the evaluation of nonlinear distortions in RF circuits which includes reconfigurable/tunable filters using digitally modulated signal , creating new tunable bandstop filter using defected microstrip structure, which produces extremely miniaturized circuits due to the inherent properties. A detailed literature review was provided to see these gaps more clearly and problems that needed to be rectified.

A major part of the thesis was to evaluate nonlinear distortions in PIN diodes, varactor diodes and optical switches and filters which use these elements for reconfigurability and tunability. These elements contain inherent nonlinear properties and the amount of nonlinear distortion needs to be tabulated using real life signals. An experimental setup was created where these circuits were used as device under test to test for nonlinearity. Among the digitally modulated signals QPSK, 16 QAM, 64 QAM, 16QAM OFDM and 64 QAM OFDM are extensively used as 3G and 4G signals to give a complete picture of nonlinear distortion measure for PIN diodes, optical switches and reconfigurable filters using PIN diodes and optical switches as reconfigurable elements.

The second most important part of the thesis deals with the development of RF bandstop filters using defected microstrip structure. These can be divided into two parts .The first part deals with the development of novel fixed band filters. A fixed bandstop filter was built using stepped impedance T shaped structure etched on the transmission line. The filter showed excellent stopband attenuation of around 50dB in both simulated and experimental results. The second fixed single-band filter was 16 % reduced in size as compared to the

previous one. This one had a fork shaped structure etched on the transmission line. The measured result showed a 30dB of stopband attenuation. A flowchart was created with design steps clearly mentioned to design a DMS bandstop filter. An equivalent lumped element circuit was developed which showed an excellent agreement with the EM simulation. Another DMS filter having dual-band function was designed. The filter was an extension of the previously designed fixed filter with extra interdigital lines forming the second resonant frequency. This filter showed excellent results with more than 35dB stopband attenuation for both bands.

The second part of the above filter design was extended to create tunable filters. In order to do that, a varactor diode was used as the tuning element. The first filter having the stepped impedance T shaped structure was modified slightly to incorporate the varactor diode in order to make the filter tunable. A 20 % tuning range was achieved and intermodulation distortion was measured in order to establish the linearity of the filter. The second designed filter was found to have a tuning range of 12 %. The dual-band filter was also incorporated with a varactor diode to make the filter tunable. The first band showed a tuning range of 15 % and the second band showed a tuning range of 3%. The varactor was incorporated in such a way so as to tune the first band rather than the second band.

The third major part of the thesis was the implementation of the designed filter in order to compensate for nonlinear distortion due to interfering signals. Various scenarios regarding nonlinear distortion due to interfering signals are discussed along with mathematical proofs. The proof of theory was given by setting up a few experimental setup to emulate the real life scenario with a main input signal and an unwanted interfering signal. The bandstop filter was used to block the interfering signal showing mathematically an improvement in distortions. Three separate cases were considered, one with main signal and interfering signal closer to each other and the second one with main signal and interfering signal further apart. Both cases showed an improvement of 10dB. The third case involved the use of a part of the transmitter consisting of power amplifier, reconfigurable filter where an improvement of 15dB was verified. The next section aims to describe the various contributions to knowledge made.

6.1 Contributions of the Thesis

The original contributions to research are enlisted in the following paragraphs giving a rough overview of the work done in this thesis:

1. Evaluation of nonlinear distortion in reconfigurable/tunable RF circuits such as bandpass filters for multi standard and multi band wireless systems have been done leading to an extension in existing research in distortion mechanism. The nonlinear distortion in RF devices and circuits such as PIN diodes, optical switches, reconfigurable bandpass filters based on PIN diodes/optical switches and power amplifiers were investigated and evaluated.
    - For the first time evaluation of distortion in RF switchable filters has been investigated using LTE standard signals and a summary of findings provided.
    - Digitally modulated signals such as 5MHz QPSK, 16 QAM, 64 QAM, 16 QAM OFDM and 64 QAM OFDM have been used to determine the nonlinearity measure of various switching elements such as PIN diode, optical switch and varactor diodes.
2. A novel microstrip bandstop filter was proposed using defected microstrip structure. For the first time, a tunable defected microstrip Structure has been proposed. Several novel bandstop filters based on this concept was developed including dual-band tunable bandstop filter.
    - Fabrication of DMS fixed band filter using stepped impedance T shaped structure has been done with excellent results.
    - Fabrication of DMS fixed band filter using fork shaped structure had been done with a 16 % size reduction as compared to previous structure
    - Dual-band bandstop filter using DMS structure with extremely miniaturized size was proposed with excellent bandstop responses for both bands.
    - Flowchart for designing DMS bandstop filter structures has been devised.

- Lumped equivalent circuit extraction to match EM simulation results.
- Fabrication of tunable DMS BSF having a tuning range of 20 %.
- Extending both single-band and dual-band filter into tunable filter structures with tuning range greater than 10 %.

3. The novel bandstop filter structures with improved selectivity performance and size reduction for Interference suppression are investigated, designed, fabricated and tested. These filters were further used in the nonlinear distortion compensation technique in RF circuits due to the presence of interfering/unwanted signals in the multi standard and multi band wireless systems. This bandstop filter was capable of compensating the nonlinear distortion for 3.9G/4G systems (LTE, LTE-Advanced and Mobile WiMAX). The extension of proposed technique can be used for beyond-4G wireless systems based on software defined radio due to its adjustable nature. The proposed solution reduces costs and the overall complexity of the subsystem without sacrificing performance of RF circuits (DUTs) for a broad area of potential applications such as next generation high-speed wireless systems.

    - Compensation technique using inter-stage bandstop filter has been described and comparison between simulated and experimental data have been provided with a 10dB improvement in linearity.
    - Implementation and testing of the complete RF subsystem for multi standard and multi band wireless transceiver applications was carried out with an improvement of 15dB in linearity.

6.2 Future Work

Future direction of research for this thesis has some scope of expansion. Even though most of the aspects were covered in the allotted time frame there

can be further improvements made to the overall research. Several points of investigations can be carried out and is presented here briefly.

Nonlinear distortion measurements using digitally modulated signals can be extended to several other switching/tuning devices such as MEMS, liquid crystals etc. in order to provide a wider range of nonlinearity evaluation for switching/tuning devices. A detailed mathematical analysis can be carried out to see the effect of nonlinearity in RF filters.

Bandstop filters using defected microstrip structure can be extended to tri band quad band in order to be more flexibly used in interference suppressions. Bandstop filters with a sharper stopband attenuation level can be designed maintaining miniaturized sizes as mentioned in the thesis. Tunability can be extended by using a varactor stack configuration in order to make a better tunable filter. Reconfigurability can be introduced in the filter by using switches. These switches can help the filter to operate as an all pass filter in the OFF condition and bandstop filter in the ON condition. This can help in situations where the filter needs to be bypassed when no unwanted signals are present.

Compensation techniques such as DPD, injection methods etc. can be used in conjunction with the filter method to achieve further improvement in distortion. These advanced methods could be further tested using reconfigurable/tunable filters. A real life implementation of the whole circuit needs to be created in order to better understand the results and make corrections if needed before production.

Publications

- K. Chakrabarty, L.Athukorala, Z.Golubicic and D. Budimir, “Enhanced Wireless Transmitters using an inter-stage notch filter”, *International Conference in Telecommunication in Modern Satellite Cable and Broadcasting Services (TELSIKS)*, vol.2, pp. 489-492, Oct. 2011
- K. Chakrabarty, L.Athukorala, and D. Budimir, *“*High linearity switchable dual-mode microstrip bandpass filters*”*, *Asia Pacific Microwave Conference Proceedings(APMC),* pp. 1019-1022, Dec. 2011
- K. Chakrabarty, K. Rabbi, C. J. Panagamuwa, J. C. Vardaxoglou, and D. Budimir, “Linearity Evaluation of Optically Reconfigurable UWB Microstrip Bandpass Filter”, *IEEE International Symposium of Antenna and Propagation (APS),* 2013
- K. Chakrabarty and D. Budimir, “Compact Tunable Bandstop Filters using Defected Microstrip Structure for Multi-Standard Wireless Systems”, *IEEE European Microwave Conference (EuMC),* 2013
- K. Chakrabarty, B. Bukvic, N. Mohottige and D. Budimir , “Nonlinear Distortion Evaluation of Reconfigurable RF Circuits in Wireless Communication Systems”, *Microwave & Optoelectronics Conference (IMOC), 2013 SBMO/IEEE MTT-S International*, 2013
- K. Chakrabarty, K. Rabbi, C. J. Panagamuwa, J. C. Vardaxoglou, and D. Budimir, “Evaluation of Nonlinear Distortion in Optically Switchable UWB Filters”, *Microwave and Optical Technology Letters,2014*
- K. Chakrabarty and D.Budimir, “Compensation of Nonlinear Distortion using Inter-stage Compact Bandstop Filter for Multi-Standard Wireless Systems”, *IEEE Mediterranean Microwave Symposium 2014 (accepted)*